INVESTIGATION OF THE JOINT COMMINUTION AND LEACHING PROCESS FOR A GOLD ORE: AN ATTAINABLE REGION APPROACH

NKOSIKHONA HLABANGANA

A thesis submitted to the Faculty of Engineering and The Built Environment, University of the Witwatersrand, Johannesburg, in fulfilment of the requirements for the degree of Doctor of Philosophy in Engineering

Supervisors:

Prof Diane Hildebrandt

Prof David Glasser

Dr M Bwalya

Johannesburg

12 September 2016

DECLARATION

I declare that this dissertation is my own unaided work. It is being submitted for the Degree of Doctor of Philosophy of Science in Engineering in the University of the Witwatersrand, Johannesburg. It has not been submitted before for any degree or examination in any other University.

Signed: …….

Nkosikhona Hlabangana

Abstract

Comminution and leaching unit processes play a major role in extracting valuable minerals from ore. Most of the research reported in the literature has focused on optimising individual unit operations rather than on integrating the whole process. This thesis develops an integrated approach to mineral processing systems and flow sheets and is intended to create a methodology for process synthesis that can be applied throughout the extractive metallurgical industry. This could lead to improved efficiency in the overall process by obtaining optimum recovery and, most important, a reduction in energy and material costs. In order to illustrate the methodology a particular example was chosen, namely optimizing the joint comminution and leaching of a particular gold ore.

In this investigation laboratory scale grinding and leaching profiles for a gold feed sample (1700–850 μm) were measured. In a laboratory mill various combinations of grinding media, filling level and ball size were investigated, and of the three ball sizes used (10, 20 and 30mm) breakage was most pronounced for the 20 mm. Thus for instance it was also established that when using a higher filling (J=30%) and a ball size of 30 mm, more energy was consumed but less liberation occurred, thus a lower amount of gold was extracted during a 24-hour leaching period. Finally, the breakage kinetics of the gold ore was looked at. Using a standard population model the breakage and selection function parameters were successfully calculated.

An investigation into the dissolution kinetics of gold ore in a solution of NaCN was also done. These were found to depend on the stirring rate, reaction temperature, particle diameter and the concentration of the leachant. The rate increased with the

stirring speed, reaction temperature and leachant concentration, but decreased when the particle size was greater. The activation energy for the dissolution was estimated at about 3 kcal/mol. Furthermore, the linear relationship between the rate constant and the reciprocal of the square of the particle size is a strong indication that the gold dissolution process is diffusion-controlled. The experimental results were well-fitted to a shrinking core model.

In attempting to understand the results, the researcher carried out a number of experiments that involved an investigation into the relationship between comminution and leaching in terms of energy usage and particle size, the former to establish the most efficient application of energy, and the latter to identify the degree of fineness that would ensure optimal recovery.

The Attainable Region (AR) method was then used to establish ways of finding the leaching and milling times required to achieve minimum cost (maximise profit). No work on utilizing the AR technique to minimise the cost of milling and leaching on a real industrial ore has previously been published. The investigation aims to show how the AR technique can be used to develop ways of optimising an industrial process that includes milling and leaching. The experimental results were used to show how this method could be successfully applied to identifying opportunities for higher efficiency when performing these operations.

The approach however is general and could in principle be used for any two or more unit operations in determining how the product from one unit should be prepared to feed to the next unit so as to optimize the overall process.

ACKNOWLEDGEMENTS

First and foremost, praises and thanks to God, the Almighty, for His showers of blessings throughout my research work.

I would like to express my deep and sincere gratitude to my research supervisors, Professors Diane Hildebrandt, David Glasser and Murray Mulenga Bwalya, for giving me the opportunity to do research and providing invaluable guidance throughout this study. Their dynamism, vision, sincerity and motivation have deeply inspired me. They taught me the methodology to carry out and to present research work as clearly as possible. It was a great privilege and honour to work and study under their guidance.

I am extremely grateful to my parents for their love, prayers, caring and sacrifices for educating and preparing me for my future especially my mother Esilinah Ngwenya. My special thanks go to my friend Dr G Danha for the keen interest shown to complete this thesis successfully.

Special mention goes to Pippa Lange, Dr Matthew Metzger, and Professor Michael Moys for their helpful suggestions and the numerous corrections to the thesis.

I thank my fellow members in MaPS research group: Dr N Chimwani, Dr P Diale, and Mr N Machobani for the stimulating discussions, for the sleepless nights we were working together before deadlines, and for all the fun we have had in the last three years.

Finally, my thanks go to all the people who have supported me to complete the research work directly or indirectly.

N Hlabangana

TABLE OF CONTENTS

Abstract 3
LIST OF FIGURES 9
LIST OF TABLES 12
1 INTRODUCTION 19
1.1 Motivation 21
1.2 Objectives of this thesis and envisaged contribution 22
1.3 Structure of the thesis 24
2 LITERATURE REVIEW 26
2.1 COMMINUTION 26
2.1.1 Grinding theory 27
2.1.2 The population balance model 32
2.1.3 Grinding mechanisms 41
2.1.4 Factors affecting mill conditions 46
2.2 ANALYTIC ANALYSIS TOOL: ATTAINABLE REGION 56
2.2.1 Background of Attainable Region analysis 56
2.2.2 AR plots 62
3.1 LEACHING 64
3.1.1 Models for predicting the kinetics of mineral dissolution 68
3.1.2 Diffusion through liquid film controls 72
3.2 CHEMISTRY OF GOLD CYANIDATION 77
3.2.1 Factors influencing the rate of dissolution of gold 80
3.3 Milling and Leaching Process Costs 93
4 EXPERIMENTAL SET-UP AND PROCEDURE 101
4.1 MILLING 101
4.1.1 Description of the laboratory grinding mill 101
4.1.2 Mill calibration 103
4.1.3 Milling conditions 106
4.1.4 Feed preparation for laboratory tests 111

4.2 PARTICLE SIZE ANALYSIS 113
4.3 LEACHING 115
4.3.1 Material and methods 115
4.3.2 Feed preparation for leaching tests 117
4.3.3 Leaching test 117
4.4 DATA COLLECTION AND PROCESSING 118
4.4.1 Milling 118
4.4.2 Leaching 118
4.4.3 Experimental repeatability 119
5 A LABORATORY INVESTIGATION OF AN INTEGRATED COMMINUTION AND LEACHING PROCESS. 122
5.1 INTRODUCTION 123
5.1.1 Milling and power usage 124
5.1.2 Leaching 125
5.1.3 The integrated milling and leaching process 125
5.1.4 Numerical Approach 127
5.2 EXPERIMENTAL TECHNIQUE 128
5.2.1 Experimental Energy usage 128
5.2.2 Feed material preparation and milling experimental method 129
5.2.3 Leaching experimental method 129
5.3 RESULTS AND DISCUSSION 130
5.3.1 Milling particle size distributions 134
5.3.2 Leaching results 138
5.4 CONCLUSION 144
6 DISSOLUTION KINETICS OF WITWATERSRAND FAR WEST RAND GOLD ORE IN SODIUM CYANIDE LEACHING 146
6.1 INTRODUCTION 147
6.2 EXPERIMENTAL PROCEDURE 148
6.3 RESULTS AND DISCUSSION 149
6.3.1 Dissolution of gold 149

6.3.2 Kinetics of dissolution 155
6.3.3 Activation Energy 160
6.4 CONCLUSION 163
7 USE OF ATTAINABLE REGION (AR) ANALYSIS TO OPTIMISE JOINT LEACHING AND MILLING PROCESS. 165
7.1 INTRODUCTION 165
7.2 THEORETICAL BACKGROUND 167
7.2.1 Kinetic model 167
7.2.2 Attainable Region approach applied to milling 169
7.3 EXPERIMENTAL TECHNIQUE 170
7.3.1 Material and methods 170
7.4 RESULTS AND DISCUSSION 171
7.4.1 Determination of S function from six monosize fractions 171
7.4.2 Determination of the breakage function parameters 173
7.4.3 Effect of interstitial filling U (Attainable region analysis) 175
7.4.4 Milling and leaching (Attainable region analysis) 178
7.5 CONCLUSION 187
8 CONCLUSIONS AND RECOMMENDATIONS 189
REFERENCES 192
APPENDIX A: LEACHING DATA UNDER DIFFERENT CONDITIONS 205
APPENDIX B: BATCH GRINGING DATA 216
APPENDIX C: AMOUNT OF GOLD ATTAINED DURING THE LEACH DURATION 222
APPENDIX D: MILL ENERGY CONSUMPTION DURING MILLING 224

LIST OF FIGURES

Figure 2.1: First- order reaction model applied to milling normal breakage (after Austin et al., 1984). 35

Figure 2.2: First-order reaction model applied to milling, abnormal breakage (after Austin *et al.,* 1984) 36

Figure 2.3: Mechanisms of breakage: (a) impact or compression, (b) chipping, (c) abrasion 42

Figure 2.4: Motion of charge in a tumbling mill. 43

Figure 2.5: Effects of variation of composition of make-up balls for feed rates between 180 and 222.1m^3/h and ball diameters on the floatable fraction m_2 (Chimwani al., 2015). 54

Figure 2.6: Cumulative particle size distributions with increase in the grinding time for a laboratory ball mill at 92 rotations per minute and 20 % ball loading (Khumalo et al., 2007). ... 61

Figure 2.7: A typical Attainable Region plot of mass fraction of material in size class 2 vs. mass fraction of material in size class 1 (Khumalo et al., 2007). 62

Figure 3.1: Basic sketch of the leaching process. 66

where: J is the amount of substance that diffuses through a surface per time unit, A is the area of the reacting surface, D is the diffusion constant (unit of surface/unit of time) and $dCdx$ is the concentration gradient. 67

Figure 3.2: Concentration of reactant on the surface of solid subjected to leaching (Biomine, 2006). 68

Figure 3.3: According to the un-reacted core models, the reaction proceeds on a narrow front, which moves into the solid particle. The reactant is completely converted as the front passes by (Levenspiel, 1999). 69

Figure 3.4: Representation of concentrations of reactants and products for the reaction for a particle of unchanging size (adapted from Levenspiel). 71

Figure 3.5: Comparison between observed (▲) and calculated values (dash line) of the residual gold concentrations ([Au]s,∞) as a function of the average ore particle size (d^-) de Andrade Lima and Hodouin (2005). 82

Figure 3.6: The effect of pH on gold extraction. Conditions: 20% solids, 0.6 MPa, 300 min-1, 800C, 1% NaCN, 1 hour (Parga et al., 2007). 87

Figure 3.7: Effect of pH on cyanide consumption (Ling et al., 1996). 88

Figure 3.8: Effect of dissolved oxygen concentration on gold conversion (Ling et al., 1996). 90

Figure 3.9: Effect of oxygen addition on cyanidation: pH 11.2, 500 ppm NaCN, 24 hours (Deschênes et al., 2003). 91

Figure 3.10: Effect of cyanide concentration on gold conversion (Ling et al., 1996). 91

Figure 3.11: Effect of cyanide concentration on leaching. Pre-leaching: pH 11.2, 8 ppm O2, 100 g/t Pb (NO3)2, 12 h; cyanide: pH 11.2, 10 ppm O2 (Deschênes et al., 2003). 92

Figure 3.12: Total milling cost difference with optimized and non-optimized liner design (hypothetical case) Dahner and Van Den Bosch (2010). 94

Figure 3.13: Operation of a continuous thickener 99

Figure 4.1: The front and rear view of the Mill equipment set up. 102

Figure 4.2: The calibration section of the mill equipment (Katubilwa, 2012). 103

Figure 4.3: Relationship between voltage and torque for different masses suspended off the mill lever arm. 105

Figure 4.4: Overview of the breakage, leaching and particle analysis stages. 109

Figure 4.5: The 20 mm steel grinding media used in experiments 110

Figure 4.6: Schematic diagram of equipment set-up for the gold leaching process. 115

Figure 4.7: Replicates for class size distributions with J= 5%. Cumulative % passing profile vs. particle size comparisons for 10 mm ball sizes. 120

Figure 4.8: Replicates on effect of sodium cyanide concentration on gold dissolution (experimental conditions: particle size, -150 + 75 µm; temperature, 25^{o} C). 120

Figure 5.1: Simulated charge motion of 19.49 litre mill. 132

Figure 5.2: Variations in the energy used with milling time. 133

Figure 5.3: Class size distribution at (J = 5% d_m = 10mm). (a) Cumulative % passing vs. particle size (b) Grinding profiles of all six class sizes vs. time. 135

Figure 5.4: Class size distribution comparisons. J= 5%. Cumulative % passing profile vs. particle size comparisons for 10 and 20 mm ball sizes. 136

Figure 5.5: Class size distribution comparisons. J= 15%.Cumulative % passing profile vs. particle size comparisons for 10 and 20mm ball sizes. 137

Figure 5.6: Class size distribution comparisons. J =5%, 15% and 30%. Cumulative % passing profile vs. particle size comparisons for 30 and 20 mm ball sizes. 138

Figure 5.7: Leach profiles for milled size classes of a typical Witwatersrand Far West Rand Gold ore. 139

Figure 5.8: Variation in the amounts of gold recovered and milling time, for a 24-hour leach. 140

Figure 5.9: Variation in the amount of gold and energy used for different *J* and d_m values. 141

Figure 5.10: Graph of milling costs USD/ amount of gold g/ton and Energy used vs. milling conditions..... 142

Figure 5.11: Graph of profit USD per ton of mill feed vs. milling conditions. 143

Figure 6.1: Effect of particle diameter on gold dissolution (experimental conditions: sodium cyanide concentration 210 ppm; temperature 25^{o} C). 149

6.2: Effect of agitation speed on gold dissolution (experimental conditions: sodium cyanide concentration 210 ppm; temperature 25^{o} C). 151

Figure 6.3: Effect of sodium cyanide concentration on gold dissolution (experimental conditions: particle size, -150 + 75 µm; temperature, 25^{o} C). 152

Figure 6.4: Effect of temperature on gold dissolution (experimental conditions: particle size -150 + 75µm; cyanide concentration 210ppm). 154

Figure 6.5: Comparison of the researcher's experimental recoveries (a) and those obtained by Marsden and House (b) in 1992. 155

Figure 6.6: Variation of different shrinking core model equations with a leaching time of particles of -300 +150µm diameter. 157

Figure 6.7: Plot of the ash diffusion control model equation applied to different particle sizes as against the leaching time required for gold dissolution (experimental conditions: sodium cyanide concentration 210 ppm; temperature 25^{o} C). 158

Figure 6.8: Plot of ash diffusion control model equation with the leaching time at different temperatures for gold dissolution (experimental conditions: sodium cyanide concentration 210 ppm; particle size -150+75µm). 159

Figure 6.9: Arrhenius plots for gold dissolution in 210 ppm NaCN. 162

Figure 6.10: Dependence of the rate constant on (1/r) and 1/(r^2) for the leaching system ... 163

Figure 7.1: First-order plots for various feed sizes of gold ore ground in a laboratory-scale ball mill..... 171

Figure 7.2: First-order plots for various feed sizes of gold ore ground in a laboratory-scale ball mill..... 173

Figure 7.3: Variation of breakage function values with feed size 174

Figure 7.4: Plot of mass fraction of mass fraction of material in size class 1 (+1700-850µm) versus grinding time..... 176

Figure 7.5: Plot of mass fraction of mass fraction of material in size class (+150-75µm) versus grinding time. 177

Figure 7.6: Attainable Region plot of mass fraction of material in size class 2 (+150-75µm) versus mass fraction of material in size class 1(+1700-150µm). 177

Figure 7.7: Effect of particle size on gold dissolution: (Experimental conditions: pH 11.2; 210 ppm NaCN, 24 hours). 179

Figure 7.8: A 3D plot of recovery vs. leaching time vs. milling time. 180

Figure 7.9: Contour plot showing optimisation for a joint milling and leaching circuit: (values: b = low, c = low). 184

Figure 7.10: Contour plot showing optimisation for a joint milling and leaching circuit: (values: b = high, c = low). 185

Figure 7.11: Contour plot showing optimisation for a joint milling and leaching circuit: (values: b =high, c= high). 186

LIST OF TABLES

Table 3.1: Typical capital cost break down (Stange, W., 1999) 97

Table 3.2: Typical operating cost breakdown (Stange, W., 1999) 98

Table 4.1: Relationship between the torque and voltage for cumulative masses. 105

Table 4.2: Mill conditions. 106

Table 4.3: Feed material characteristics and preparation. 108

Table 4.4: Size classes used 110

Table 4.5: Media conditions used. 111

Table 4.6: Conditions for milling kinetics experiments on varying J (ball filling) on milled material. 112

Table 4.7: Conditions for milling kinetics experiments with varying U (Interstitial filling). 113

Table 4.8: Leaching test parameters for a base case. 116

Table 4.9: Leaching conditions 116

Table 5.1: Results for calculated and measured power values. 131

Table 6.1: Particle size classes used during the leaching experiments. 148

..... 151

Table 6.2: The rate constant k for the ash diffusion control model with the correlated coefficients for gold ore dissolution in a 210 ppm NaCN concentration at different temperatures. 160

Table 7.1: Selection function values for different feed size classes. 172

Table 7.2: Sizes classes used for AR application. 175

Table 7.3: Estimated process operating and capital costs that may be used to calculate b and c 182

Table 7.4: Scenarios for different values of b and c investigated..... 183

Table A. 1: Leaching data for cyanide concentration of 30ppm, particle size, -150 + 75µm; temperature, 25^{o}C. 205

Table A. 2: Leaching data for cyanide concentration of 75ppm, particle size, -150 + 75µm; temperature, 25^{o}C. 205

Table A. 3: Leaching data for cyanide concentration of 210ppm, particle size, -150 + 75µm; temperature, 25^{o}C. 206

Table A. 4: Leaching data for cyanide concentration of 400ppm, particle size, -150 + 75µm; temperature, 25^{o}C. 206

Table A. 5: Leaching data for cyanide concentration of 500ppm, particle size, -150 + 75µm; temperature, 25^{o}C. 207

Table A. 6: Leaching data for stirring speed of 180rpm, cyanide concentration 500ppm, particle size, -150 + 75µm; temperature, 25^{o}C. 207

Table A. 7: Leaching data for stirring speed of 360rpm, cyanide concentration 500ppm, particle size, -150 + 75µm; temperature, 25^{o}C. 208

Table A. 8: Leaching data for stirring speed of 720rpm, cyanide concentration 500ppm, particle size, -150 + 75µm; temperature, 25^{o}C. 208

Table A. 9: Leaching data for stirring speed of 900rpm, cyanide concentration 500ppm, particle size, -150 + 75µm; temperature, 25^{o}C. 209

Table A. 10: Leaching data for stirring speed of 990rpm, cyanide concentration 500ppm, particle size, -150 + 75µm; temperature, 25^{o}C. 209

Table A. 11: Leaching data for temperature 25^{0} C, particle size -150 + 75µm; cyanide concentration 210ppm). 210

Table A. 12: Leaching data for temperature 40^{0} C, particle size -150 + 75µm; cyanide concentration 210ppm). 210

Table A. 13: Leaching data for temperature 80^0 C, particle size -150 + 75µm; cyanide concentration 210ppm). 211

Table A. 14: Leaching data for temperature 100^0 C, particle size -150 + 75µm; cyanide concentration 210ppm). 211

Table A. 15: Leaching data for temperature 120^0 C, particle size -150 + 75µm; cyanide concentration 210ppm). 212

Table A. 16: Leaching data for particle size -1700+850µm, temperature 25^0 C, cyanide concentration 210ppm). 212

Table A. 17: Leaching data for -850+300µm particle size, temperature 25^0 C, cyanide concentration 210ppm). 213

Table A. 18: Leaching data for -300+150µm particle size, temperature 25^0 C, cyanide concentration 210ppm). 213

Table A. 19: Leaching data for -150+75µm particle size, temperature 25^0 C, cyanide concentration 210ppm). 214

Table A. 20: Leaching data for -75+25µm particle size, temperature 25^0 C, cyanide concentration 210ppm). 214

Table A 21: Combined leaching, milling and recovery data for Far west Witwatersrand gold ore 215

Table B.1: Measured particle size distribution for ball size 10 mm, feed size (-1700 +850 µm), U = 0.75, J = 5 %, ϕc = 75 of critical 216

Table B.2: Measured particle size distribution for ball size 20 mm, feed size (-1700 +850 µm), U = 0.75, J = 5 %, ϕc = 75 of critical 217

Table B.3: Measured particle size distribution for ball size 10 mm, feed size (-1700 +850 µm), U = 0.75, J = 15 %, ϕc = 75 of critical 217

Table B.4: Measured particle size distribution for ball size 20 mm, feed size (-1700 +850 µm), U = 0.75, J = 15 %, ϕc = 75 of critical 218

Table B.5: Measured particle size distribution for ball size 30 mm, feed size (-1700 +850 µm), U = 0.75, J = 30 %, ϕc = 75 of critical 218

Table B.6 Measured particle size distribution for feed size -425+300 µm, ball size 20 mm, U = 0.75, J = 5 %, ϕc = 75 of critical. 219

Table B.7: Measured particle size distribution for feed size -600+425 µm, ball size 20 mm, U = 0.75, J = 5 %, ϕc = 75 of critical. 219

Table B.8: Measured particle size distribution for feed size -850+600 µm, ball size 20 mm, U = 0.75, J = 5 %, ϕc = 75 of critical. 220

Table B.8: Measured particle size distribution for feed size -1180+850 µm, ball size 20 mm, U = 0.75, J = 5 %, ϕc = 75 of critical. 221

Table C 1: Total amount of gold attained for ball size 10 mm, feed size (-1700+850µm), U = 0.75, J = 5 %, ϕc = 75 of critical 222

Table C 2: Total amount of gold attained for ball size 20 mm, feed size (-1700+850µm), U = 0.75, J = 5 %, ϕc = 75 of critical 222

Table C 3: Total amount of gold attained for ball size 10 mm, feed size (-1700+850µm), U = 0.75, J = 15 %, ϕc = 75 of critical 223

Table C 4: Total amount of gold attained for ball size 20 mm, feed size (-1700+850µm), U = 0.75, J = 15 %, ϕc = 75 of critical 223

Table D 1: Energy used for grinding with 10mm media (J=5%) 224

Table D 2: Energy used for grinding with 20mm media (J=5%) 224

Table D 3: Energy used for grinding with 10mm media (J=15%) 225

..... 225

Table D 4: Energy used for grinding with 20mm media (J=15%) 226

LIST OF SYMBOLS

K_r Grinding rate constant from Rittinger's law

E_r Specific energy input (energy input per unit feed mass).

K_k Rate constant from Kick's law

E_K Kick's energy per unit volume (specific energy required to reduce the feed particles of size x_f to product particles of size x_p.

E_B Bond's specific grinding energy

W_i Bond's Works Index

S_i Selection function or rate of disappearance of particles of material in size class *i*

$w_i\ (t)$ *W*eight fraction of the mill hold-up that is of size i at time t;

a_T Selection function parameter which is mainly a function of milling Conditions

α Selection function parameter which is material-dependent

μ Index allowing for a decrease in the value of the selection function with increasing particle size

$Q(x_i)$ Correction factor (taken as unity for lower size intervals, that is, $x_i \ll d_{ball}$);

^ Positive number that shows how rapidly the rates of breakage fall as size increases.

b_{ij} Primary breakage distribution function of a particle of size *j* breaking into size *i*

B_{ij} Cumulative breakage function

$P_i(t)$ Cumulative fraction by mass in the mill less than size x_i at time t

β Breakage function parameter characteristic of the material used. Its values generally range from 2.5 to 5

γ Breakage function parameter which is material-dependent. Its typical values lie between 0.5 and 1

Φ_j Fraction of fines produced in a single fracture event. It is dependent on the material being crushed

U Slurry filling or ratio of volume of slurry loaded to the volume of ball interstices available within the static bed of grinding media

f_c Fractional volume filling of the mill by powder based on a formal porosity of 0.4 for powder and ball bed.

J Ball filling or fraction of mill volume occupied by grinding balls at rest including interstices

c Volume fraction of solids in a mixture, see Equation (2.19)

J Number of molecules per unit time that pass through the product layer, see Equation (3.1)

A Area of the reacting particle, see Equation (3.1)

D Diffusion constant (unit of surface/unit of time)

$\frac{dC}{dx}$ Concentration gradient.

N_A Number of molecules of A, see Equation (3.2)

C_s Concentration of A on the core surface, see Equation (3.2)

C_{bulk} Concentration of A on the bulk surface, see Equation (3.2)

ρ_B Density of the solid B (core), see Equation (3.3)

τ Time for complete conversion, see Equation (3.9)

X_B Conversion for the reaction, see Equation (3.12)

R Gas constant, see Equation (3.15)

N_A Avogadro's number, see Equation (3.15)

D Diffusion coefficient of a spherical particle, see Equation (3.15)

a Radius of particle, see Equation (3.15)

T Absolute temperature, see Equation (3.15)

ABBREVIATIONS

AR	Attainable Region
ESKOM	Electricity Supply Commission
CAPEX	Capital expenses
OPEX	Operation expenses

CHAPTER 1

1 INTRODUCTION

Mineral processing plants can consist of a quite complex array of units placed together in a flowsheet. In technical terms we call this a system. Traditionally each of the units has been optimized separately. Unfortunately a set of optimized units does not necessarily lead to an optimum system. It is the purpose of this thesis to try to begin to look at the system rather than units. What this means is that we no longer apply a rigid specification for the output from one unit for entry to the next unit. For instance we no longer say that the output from a mill is $x\%$ below a certain size. We say that the output from the mill must be such that we have the best final output namely the optimum system.

The Attainable Region method has been shown to be a very powerful method for the optimization of systems of chemical reactors and it is believed its use can be extended to mineral processing systems. In order to develop the approach for this situation a relatively simple case study has been chosen namely to optimize a joint milling and leaching process. No longer will we place a specification on the output from the milling process, its value will result from the overall optimization. The emphasis of this thesis will be to show how this can be done on a specific ore using simple but credible models, based on experiments, for both the milling and the leaching.

Comminution and leaching are important unit operations for size reduction and downstream processing of valuable minerals in the mining industry. The primary reason for milling materials down to smaller particle sizes is to liberate valuable components dispersed in the host matrix. Once the material has been reduced to a size small enough to give sufficient liberation, the valuable components are then separated from the host matrix by downstream processes such as leaching. It is therefore necessary that mill products are tailored to the leaching requirements. For this reason, milling has to be comprehensively investigated to enable the determination of the trade-off between milling itself and leaching in order to optimize the complete process.

Therefore a joint leach and comminution approach is advantageous as it strikes a balance between both process expenses.

Besides some rigorous mathematical modelling, Khumalo *et al.* (2006–2008) proposed an analytic tool known as the Attainable Region (AR) technique for the study of ball milling. The tool, first introduced for optimising chemical reaction networks with complex kinetics, has been successfully applied in chemical reactor engineering for choosing and optimising the best reactor configurations (Glasser and Hildebrandt, 1997). The AR has been used in batch milling (Khumalo, 2007; Khumalo *et al.*, 2006–2008; Metzger, 2011; Metzger *et al.*, 2009 & 2012; Katubilwa *et al.*, 2011. One really interesting simulation finding has been that the addition of a classification unit to milling led to a 95% reduction in energy consumption (Khumalo *et al.*, 2008). If this finding transcends laboratory boundaries to actually apply to industry, the implications could be huge considering the inefficiency of ball mills.

For this reason a methodology that uses the AR technique for the minerals industry would be valuable to develop. It is postulated that the technique has the potential to determine operating conditions and circuit configurations that will suggest efficient use of energy and improved mineral recovery. Ultimately, the AR technique is expected to assist in the formulation of appropriate recommendations for the industry.

1.1 Motivation

Very little has been done to investigate a joint milling and leaching system in general from an AR point of view in particular. However, bridging this gap is relevant to the minerals industry and should be regarded as the ultimate goal in the development of this aspect of the AR technique.

Of importance to industry will be the proposition of a more holistic way of analyzing, designing, and optimising flow sheets subject to more stringent requirements ranging from technological and energy constraints to environmental and economic considerations.

The anticipated success of such an undertaking could give an edge to the South African industry and will help reinforce its global position in the area of mineral processing. The AR has revolutionised the way complex systems involving various process units are designed in the chemical industry. It is hoped that the development of this tool for industry can be a valuable asset.

It is generally agreed that finer grinding leads to faster leaching as predicted by the leaching models as value material gets more liberated hence requiring less time to leach however the cost in terms of energy and hence money goes up. Thus the question is how fine should one grind to make the most profit?

Thus optimising the milling stage is one way of improving the efficiency of such processing circuits. In order to optimise the milling stage, requirements of the leaching in terms of particle size have to be fully understood first.

- A number of researchers have suggested that bigger balls are needed to break (shatter) larger particles faster but a finer product is achieved by using smaller balls (Khumalo, 2006; Katubilwa *et al.*, 2011). However, the use of small balls is believed to promote abrasion and attrition which are energy inefficient breakage mechanisms (King, 2001).
- Less powder and fewer grinding balls are needed to incur more effective grinding (Metzger *et al.*, 2011); however, some researchers have suggested mills with high ball loading J and powder filling U close to unity (that is $U \cong 1$) (Tangsathitkulchai, 2003).

1.2 Objectives of this thesis and envisaged contribution

For the past few years, the energy crisis has been so acute in South Africa that the price of electricity has been spiraling. Any idea that is put on the table to make the mining industry more competitive is undoubtedly welcome. This is true especially when one considers the fact that this industry is a very big consumer of electricity.

Ball milling is specifically known to be one of the main operations putting the industry in this uncomfortable position (Austin *et al.*, 1984; Napier-Munn *et al.*, 1996). It is therefore crucial to invest time and resources in the research and development of better milling circuits and operations.

Many researchers have studied the effect of degree of liberation or particle size on leaching kinetics and have just selected different particle sizes or size classes and used them to get the optimum required class by observing size that gives the highest gold recovery (Hlabangana et al. 2016).

The objectives associated with achieving the aim of the research are:

- explore the effect of grinding media fill level, grinding media size and grinding time on the resulting size distribution which can be used to successfully control and optimise the performance of a milling circuit, with the leaching requirement in mind;
- determining the breakage and selection function parameters of a gold minerals ore
- leach the milled product ground for different time durations and find a model that best fits the data; and
- determine energy consumption of the process

The resulting particle sizes would then be processed in a batch leaching apparatus in order to leach gold from each of the size classes. This vital information would be used to determine the optimal size for maximum gold recovery as a function of operation time (for grinding and leaching), energy consumption and other operational variables.

1.3 Structure of the thesis

The thesis is in two major sections, literature review and experimental work that involved both grinding and leaching experiments designed to generate data for evaluation.

CHAPTER 1: Introduction to the leaching and comminution problem and establishing why investigation of the two processes is necessary.

CHAPTERS 2 AND 3: Review of the comminution and leaching process with the view of providing the framework for the research provided in the thesis. This section also includes the discussion of the analytic tool called Attainable Region analysis (AR).

CHAPTER 4: Both milling and leaching experiments conducted under various conditions are presented to obtain the laboratory scale results that form the basis of discussion in the subsequent chapters.

CHAPTER 5: Presented here are the results of laboratory scale grinding and leaching profiles for a feed sample in a laboratory mill. Various combinations of grinding media, fill level and ball size were investigated and the energy requirements.

CHAPTER 6: A study of the dissolution kinetics of gold ore in a solution of NaCN is undertaken. The dissolution kinetics is examined in terms of the stirring rate, reaction temperature, particle diameter and the leachant concentration.

CHAPTER 7: The selection and breakage function parameters are determined for the Far West Witwatersrand ore using four mono-size class feeds 1700–1180 µm, 1180–850 µm, 850–600 µm and 600–425 µm of a gold ore. The AR is then used to optimise milling and leaching and thereby reduce overall costs.

CHAPTER 8: The chapter reviews the work reported in the previous ones and shows that objectives set out initially were successfully accomplished. The researcher also gives recommendations on how the milling and leaching circuit can be improved. A foundation is laid for future work which should focus on devising ways of validating all the laboratory findings on an industrial scale.

CHAPTER 2

2 LITERATURE REVIEW

Because of the historical background and technical context of this thesis, the writer has divided the literature review into two separate chapters. The first deals with comminution, the prerequisite process that prepares the ore for leaching with a short section on the Attainable Region methodology used in the chapters that follow. Chapter 3 deals with leaching in general, and goes on to gold recovery through cyanidation (a leaching process) and finally milling and leaching costs

2.1 COMMINUTION

The comminution process is highly energy intensive, consuming 3% to 4% of the electricity generated worldwide. For example, it accounts for up to 70% of all energy consumed in the cement industry (Fuerstenau et al. 1999). The process operates at low efficiencies when the input energy is compared to the breakage achieved. Schonert (1979) estimated the energy consumption for the grinding processes was as much 3% of the electricity generated in the industrialized countries of the world. In a typical mineral processing plant, comminution can account for 55%–70% of its total power consumption. It follows that any intervention that can reduce energy utilization while operating efficiently will be welcomed in the industry, as it will increase profitability (Cohen, 1983; Lynch and Narayanan, 1986).

During the last few years there have been considerable improvements in comminution efficiency. These can be attributed not only to the development of new machines that are capable of using energy more efficiently, but also to the work done by researchers on optimising the design of grinding circuits and operating variables so that the performance of existing machines can be improved (Oner, 1999).

The major objective of the process of comminution is to:

- achieve a certain particle size to liberate valuable materials for the downstream operations, like leaching and flotation;
- achieve a certain particle size for end use, for example in cement and gravel processes; and
- reduce the size of material for easier transport and processing.

2.1.1 Grinding theory

The size reduction of solids and minerals by mills and crushers is an important industrial operation. The power used for the process can take a variety of forms: kinetic, microwave and/or chemical energy. Since ball mills are widely used in the industrial grinding circuits, a vast amount of research has been directed towards modelling ball mill performance (Rumpf, 1973; Lynch, 1977; Austin et al., 1984). Since comminution is basically a process of creating a new surface area, there was a strong incentive in the early years of ball mill modelling to use some form of empirical energy/size relationship. The first theory of comminution was proposed by Rittinger in 1857 (Austin, 1973). He

postulated that the energy input required to reduce a solid to a particle is proportional to the new surface area produced, according to equation 2.1.

$E_r = K_r$ [new surface area – old surface area] (2.1),

where K_r is the grinding rate constant and E_r is the specific energy input (energy input per unit feed mass).

This theory provides the basis for calculating the minimum specific energy required to break the bonds that existed between the two new surfaces.

In 1967 Rose, after carrying out experiments in comminution that involved careful measurement of the energy balance in the mill during operation, reported that the surface energy consumes only a small fraction of the energy input to the mill. His research findings showed that energy to the mill appears as heat, sound, or energy of phase transformation, while the energy required for generating a new surface is less than 1% of the power supplied to the mill. As a result, the specific energy predicted by the equation above cannot be taken as a control variable in designing plant scale-ups, because surface energy represents so small a percentage of the whole. Rittinger's theory does not take into account the fact that particles absorb energy elastically before they reach the yield point.

Kick (1885) proposed a theory that supposes that the energy used is directly related to the reduction ratio $\frac{x_f}{x_p}$ (where x_f and x_p are feed and product particle sizes respectively).

Therefore equivalent amounts of energy should result in equivalent geometrical changes in the sizes of the pieces a solid is broken into. For example, if one unit of energy reduced a number of equal-sized particles to particles of one half the size, then the same amount of energy applied to the particles resulting from the first test should result again in a size reduction of one half, or a size one quarter the original size. The Kick concept may be expressed as follows in equation 2.2:

$$E_K = K_k \log\left(\frac{x_f}{x_p}\right) \qquad (2.2)$$

where: K_k is the rate constant; and E_K is Kick's energy per unit volume (that is, the specific energy required to reduce the feed particles of size x_f to product particles of size x_p.

The theory Kick formulated focused on the stress and strain of cubes under compression. However, because the applied stress is proportional to the volume of material, this theory fails to describe the effect of surface energy, as described by Rittinger, and consequently under-predicts the mill's energy requirements.

Rittinger's law is mainly applicable to the part of the process in which new surface is being created, and is most accurate in fine grinding, where the increase in surface per unit mass is large. Kick's law, on the other hand, relates the energy required to cause elastic deformation before fracture occurs, and is more accurate than Rittinger's for coarse grinding, where the amount of surface produced is considerably less.

Bond (1952) later postulated a third theory of comminution. The theory is an empirical equation based on analysis of data from laboratory and industrial mills. He stated that the useful energy applied in breaking a stated weight of material is inversely proportional to the square root of the diameter of the product particles (see the equation below). The hypothesis suggests that work input is used in the deformation of the particles, and that this is released as heat. Local deformations beyond the critical strain result in the formation of a crack, which propagates and results in breakage. The strain energy levels depend on the volume of the particle, while the expansion of the crack results in the creation of new surface areas. As should be apparent, Bond's postulation combines those of Rittinger and Kick.

The mathematical form of this third comminution theory estimates mill power per ton of 80% passing screen size of feed and product and is given as:

$$E_B = W_i \left(\frac{10}{\sqrt{x_p}} - \frac{10}{\sqrt{x_f}} \right) \qquad (2.3)$$

where: E_B is the specific grinding energy, x_f is the size, in microns, which 80% of the feed passes, x_p is the size, in microns, which 80 % of the product passes; and W_i is Bond's Works Index

The Work Index is defined as the kilowatt-hours (KWH) required to reduce one ton of ore from infinite feed size to 80% passing 100 microns. The Bond theory has been

extensively applied in comminution systems for the quantitative definition of the resistance of solid particles to breakage.

The advantages of the Bond sizing method (Austin *et al.,* 1984) are:

I. its simplicity;

II. its capacity to work in many different circumstances to a reasonable accuracy, as it is based on plant measurement.

There are two disadvantages to use of this sizing method.

I. the specific energy required to take a feed with a certain 80% passing size to a product with a certain 80%-passing size cannot be the same for a batch test, the standard Bond locked cycle test, or a steady state continuous mill with a real mill residence time distribution.

II. it groups all the grinding sub-processes into a single work index term, and it also expresses the particle size distribution in terms of the amount passing a single size, rather than using multiple parameters to describe the distribution. This limits its application.

These theories of comminution are empirically based, which imposes constraints on their usefulness to the engineer designing comminution systems. For example, they cannot be applied to a wide size distribution, the sub-processes of transportation, normalization of the distribution of breakage products, and selectivity. Serious limitations of these empirical approaches in accurate prediction, simulation and control of the grinding mill performance have been reported (Blaskett, 1970; Herbst and Fuerstenau, 1980; Austin and Brame, 1983). These have been identified as knowledge

about the various comminution micro-processes and the energy transfer patterns in the mill.

The modern ball mill models (Herbst and Fuerstenau, 1980; Austin et al., 1984; Kavetsky and Whiten, 1982) describe the ball mill in terms of three mechanisms. These are:

- a breakage distribution function to describe the product size distribution from a breakage event;
- a breakage rate function to describe the size-dependent rate at which the particles of various sizes will break in a ball mill; and
- a material transport function to describe the size-dependent material transport through and out of the mill.

The population balance model described below was developed by Bass in 1954 to address the shortcomings of the empirical models, to provide a matrix that can be applied to the many different aspects of comminution and it can also be used for quantitative modelling.

2.1.2 The population balance model

It is noted that repetitive actions of breakage in the mill causes size reduction. The feed and the product size distribution are related. Fragments after first breakage have a wide range of different particle sizes and chances of further breakage will depend on machine design and initial particle size. Two processes are therefore occurring in the

mill, that is the selection of the particle for breakage, and breakage which results in distribution of fragment sizes (Gupta and Yan, 2006).

2.1.2.1 Selection function

The mill can be likened to a chemical reactor in that knowledge of rates at which material breaks enables the engineer to calculate how rapidly the particles disappear. However, unlike what happens in a chemical reaction such as $A \rightarrow B$, the fragmentation of a single size produces a wide range of product sizes. If we split a size range into a number of intervals, the fraction of material broken down from a fixed size that falls into a smaller size interval can be considered a product. The probability that further breakage will be required depends on the machine design and the desired particle size. Knowing how quickly a size breaks, and the size ranges in which the products appear, gives a clear understanding of the milling process. This matches the elemental description of the size-mass or population balance of a reactor (Austin 1984).

When the material in the mill is being subjected to a variety of breakage actions, we represent the size distribution in the mill by means of size intervals defined by screen intervals and separated by sequences of $\sqrt{2}\ or\ \sqrt[4]{2}$. The rate of disappearance of particles per unit time and unit mass is proportional to the mass fraction of that size is given by:

Rate of disappearance of size i due to breakage $\alpha\ w_i(t)W$

Rate of breakage of size $i = S_i\ w_i\ W$

where S_i is the specific rate of breakage and w_i is the weight fraction of unbroken material of size i in the mill at time t. W the total material charge in the mill.

The equation for a batch process becomes:

$$\frac{dw_i}{dt} = -S_i.w_i(t) \qquad (2.4)$$

For efficient particle breakage events (normal breakage), the size reduction process is assumed to be first order, in other words it is assumed that S_i does not change over time. This equation can be solved to give:

$$logw_i(t) - logw_i(0) = -S_i t/2.3 \qquad (2.5)$$

where $w_i\ (t)$ is the weight fraction of the mill hold-up that is of size i at time t, S_i is the specific rate of breakage; and t is the grinding time.

The formula proposed by (Deniz, 2004) shows that the specific rate of breakage does not vary with grinding time over a range of particle sizes (that is, an average rate of breakage S is assumed over a total grinding time).

The disappearance of a given size fraction of material usually obeys a first-order breakage pattern (Austin 1984).

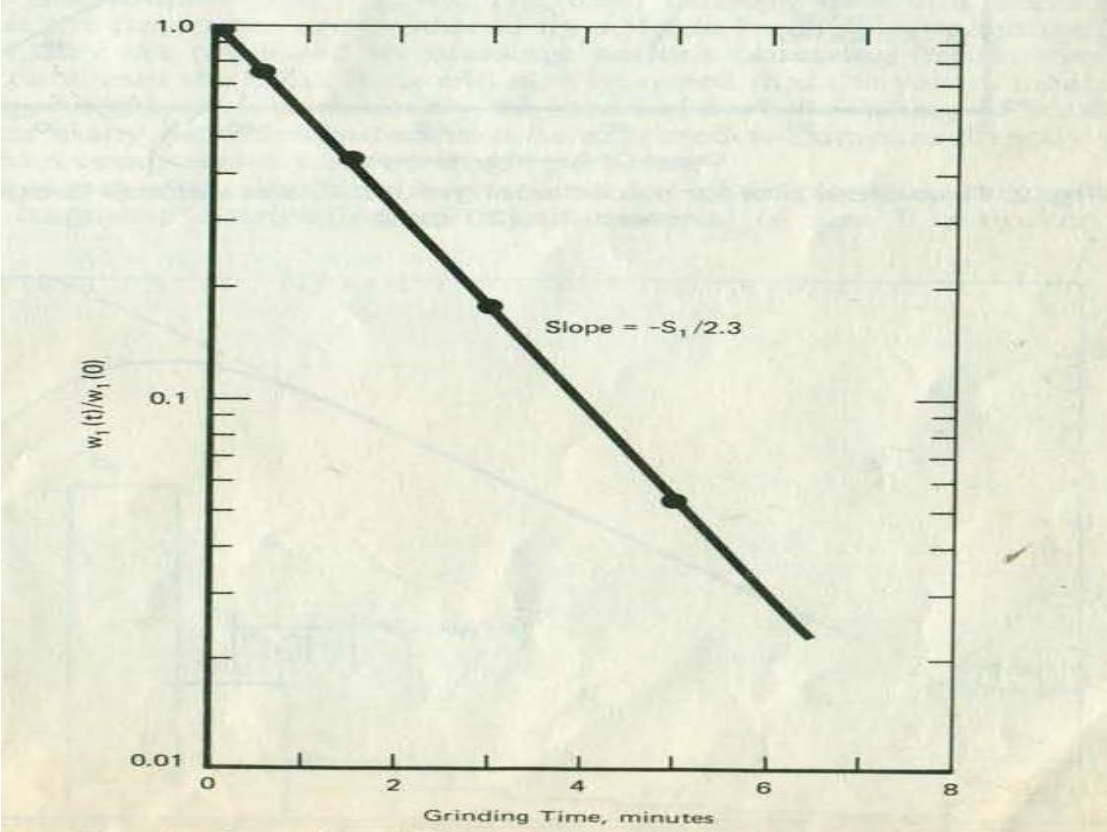

Figure 2.1: First- order reaction model applied to milling normal breakage (after Austin et al., 1984).

Figure 2.1 shows the first-order breakage law for a given material. However, some deviations from this law have been noted in the case of coarse materials (Austin *et al.* 1976). In this instance, breakage is said to occur in the abnormal region as illustrated in Figure 2.2.

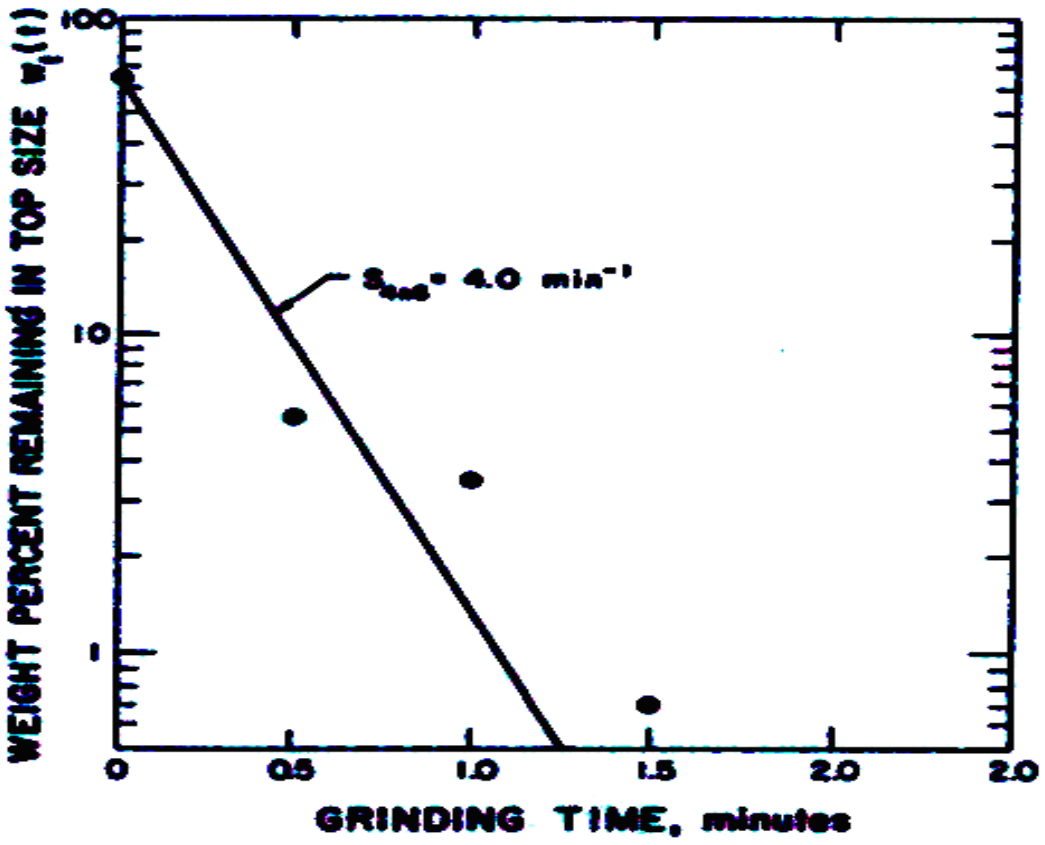

Figure 2.2: First-order reaction model applied to milling, abnormal breakage (after Austin *et al.*, 1984)

To determine the variations in specific rate of breakage S_i with particle size, Austin et al. (1984) used the following model;

$$S_i = a_T x_i^{\alpha} Q(x_i) = a_T x_i^{\alpha} \left(\frac{1}{1+\left(\frac{x_i}{\mu}\right)^{\wedge}} \right) \qquad (2.6)$$

where: x_i is the upper limit of the size interval indexed by i, mm; a_T and α are model parameters which are dependent on material properties and the grinding conditions; α is a positive number, which is characteristic of the material (providing the test conditions

are in the normal operating range), but the value of a_T varies with the mill conditions; μ is an index allowing for a decrease in the value of the selection function with increasing particle size; $Q(x_i)$ is a correction factor (taken as unity for lower size intervals, that is, $x_i \ll d_{ball}$); ^ is a function of Q_x and is a positive number that shows how rapidly the rates of breakage fall as size increases. The higher the ^ value, the more rapidly the selection function value decreases and this value is a characteristic of the material; and for finer materials, $Q(x_i)$ approximates to 1.

At this point the equation becomes:

$$S_i = a_T \, x_i^{\alpha} \qquad (2.7)$$

The above formula was proposed by Austin et al. (1984) for the variation of the specific rate of breakage S_i with particle size.

On drawing a log-log scale a straight line is obtained with the slope α and breakage rate a_T at a standard particle size taken as 1mm.

Increasing a_T and S_i increases the effective breakage rate of the original particle in size class i to undersize. A greater value of a_T means that there is faster grinding. α is a positive number normally in the range 0.5 to 1.5 and is a material property which is independent of mill conditions such as ball load, ball size and mill hold up (Austin and Brame 1984).

2.1.2.2 Cumulative progeny fragment distribution

If a material of size class i is broken up, the weight fraction of the products that occurs in the interval j is given by b_{ij}. The matrix of numbers b_{ij} is needed to describe the general fragmentation into all sizes of interest. The rate of production of size class i material is equal to both the product of the fraction of i from j, and the rate of breakage of size j.

Particles of size j are then broken into smaller sizes, with all fragments of sizes contributing to the diminishing scale of particles as comminution proceeds. Therefore the rate of production of size i material equals the sum of the rate of appearance from breakage of all larger size minus the rate of disappearance by breakage. For a general size interval i, a batch size-mass balance equation becomes

$$\frac{dw_i(t)}{dt} = -S_i w_i(t) + \sum_{j=1}^{i-1} b_{i,j} S_j w_j(t) \qquad \text{n > i > j >1} \qquad (2.8)$$

The summation term is the fraction of material broken out of size j that is smaller than the upper sizes of interval i (Tangsathitkulchai, 2003) and n is the sink size. The sink size is the minimum class obtained for a particular breakage process. This nth interval gives a value of $S_n$which equals zero because material cannot be broken out of the final n^{th} interval.

The accumulation of $w_i(t)$ values give the fraction of charge below size j

$$P_j(t) = n \sum_n^j w_i(t) \quad (2.9)$$

On grinding a material for a short time in the mill a set of primary fragments are produced, which would in turn have a probability of being broken. The primary breakage distribution function is defined as the average size distribution resulting from a fracture of a single particle (Kelly and Spottiswood 1990).

These progeny fragments can be described by a cumulative breakage distribution function b_{ij}, obtained from product size distributions.

$$b_{i,j} = \frac{mass\ of\ \ particles\ \ from\ class\ \ j\ broken\ to\ size\ i}{mass\ of\ \ particles\ \ of\ \ class\ \ j\ broken} \quad (2.10)$$

It is conveniently represented as a cumulative primary daughter fragment distribution that is written in the form:

$$B_{i,j} = \sum_{k=n}^{i} b_{k,j} \quad (2.11)$$

B_{ij} is the sum fraction of material less than the upper size of screen interval i obtained from primary breakage of size j material. The following expressions were shown by Austin et. al, (1984) which showed that B_{ij}value from sizes can be estimated from size analysis of the product from grinding of the size j material.

$$B_{ij} = \frac{\log[(1-P_i(0))/(1-P_i(t))]}{\log[(1-P_{j+1}(0))/(1-P_{j+1}(t))]} \qquad i > j \qquad (2.12)$$

where: $P_i(t)$ is the cumulative fraction by mass in the mill less than size x_i at time t. B_{ij} can be fitted to an empirical function (Austin et. al, 1984) for non-normalized B_{ij} values

$$B_{i,j} = \Phi_j \left(\frac{x_{i-1}}{x_j}\right)^{\gamma} + (1-\Phi_j)\left(\frac{x_{i-1}}{x_j}\right)^{\beta} \qquad (2.13)$$

$$\phi_j = \phi_1 [X_i/X_1]^{-\delta} \qquad (2.14)$$

where X_i is the top size, and $B_{i,j}$ is the weight fraction of primary breakage products

β is a parameter characteristic of the material used the values of which generally range from 2.5 to 5.

γ is also a material-dependent characteristic the values of which are typically found to be between 0.5 and 1.5.

Φ_j represents the fraction of fines that are produced in a single fracture event. It is also dependent on the material used.

δ, is a model parameter that depends on the properties of the material.

If $B_{i,j}$ values are independent of the initial size, i.e. dimensionally normalisable, then δ is zero (Austin 1984).

On plotting experimentally determined $B_{i,j}$ values versus X_1 on log scales, the slope of the lower straight line portion of the curve gives the value of γ, ϕ is the intercept of this part of the line extrapolated to X_2 , and β is determined to make the function fit the upper part of the curve. The slope of the lower portion of the $B_{i,j}$ curve can be denoted by γ with smaller values γ showing that once particles of certain size break, this

produces many much smaller progeny fragments. Therefore γ is a convenient and measurable parameter for characterizing material dependent properties (Makhokha, A. and Moys, M.H 2006)

2.1.3 Grinding mechanisms

Milling is the last stage of the comminution process in which particles (ore) are reduced to an optimum size range by a combination of grinding mechanisms and the process occurs through the fracture of the ore. Fracture is defined as a probabilistic process such that a particular lump will be disintegrated when it receives a sufficiently massive impact as it tumbles in the mill.

The degree of grinding of an ore particle depends on the probability of the ore entering a zone between the medium shapes and the probability of some breakage event taking place after entry.

Several mechanisms contribute to the grinding action that takes place inside a mill including impact or compression, due to forces applied almost normally to the particle surface; chipping due to oblique forces; and abrasion due to forces acting parallel to the surfaces (Figure 2.3). These mechanisms distort the particles and change their shape beyond certain limits determined by their degree of elasticity, which causes them to break. These can also be classified in terms of the magnitude of the stress. Austin et al. (1976) showed that if the specific energy of impact is low enough, the size distribution of the breakage products is similar to that expected of an abrasion mechanism. In each size class and material, there is a minimum energy level below which abrasion is

dominant, and above this minimum energy, impact or compression becomes the dominant mechanism.

Chipping fracture is specifically the removal of asperities from irregular feed rock, which leads to rounded pebbles.

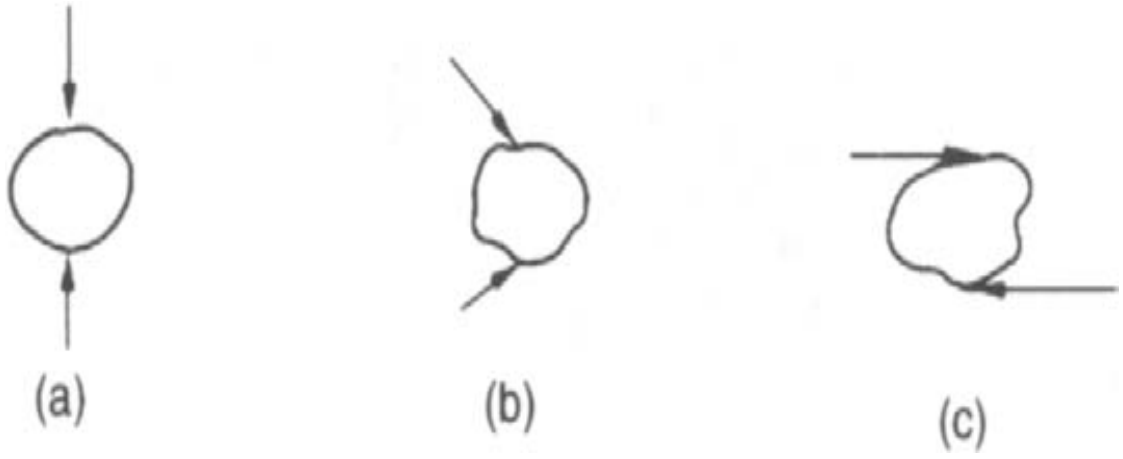

Figure 2.3: Mechanisms of breakage: (a) impact or compression, (b) chipping, (c) abrasion

The kinetics of milling depends on:

(a) Particle presentation to sites/regions where it will be subjected to grinding forces.

(b) The application of forces adequate to effect breakage of particles.

In ball mills, the presentation of particles to grinding forces is affected by the degree of particle mixing with the grinding media.

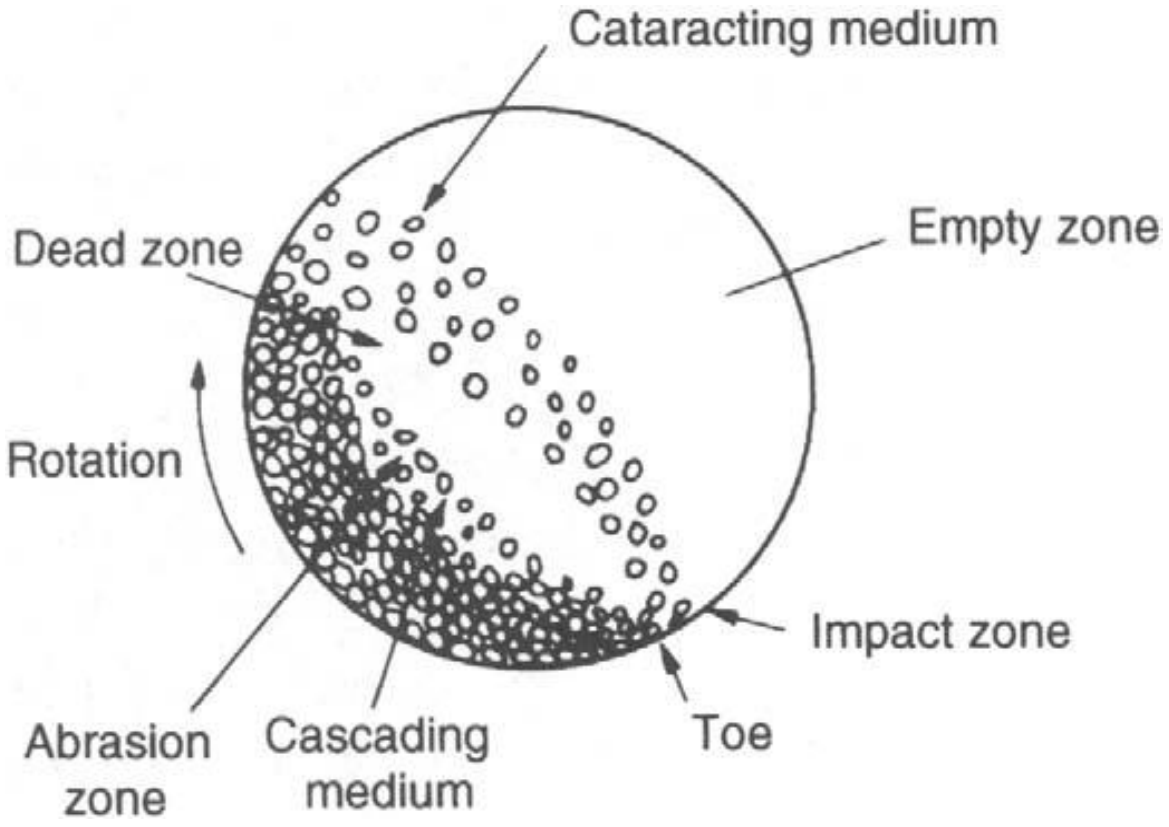

Figure 2.4: Motion of charge in a tumbling mill.

The relative motion between media is responsible to a great extent for the grinding action. Ball media are entrained in a tumbling motion which engenders some interactions (Figure2.4). During these interactions media collide or roll over each other. Depending on the type and the magnitude of the interaction, particles break following a certain pattern. King (2001) argued that in a ball mill particles break primarily by impact or crushing and attrition. It seems however that impact breakage is predominant at coarser particle sizes whilst attrition is the main reduction mechanism at finer sizes. In between the two extremes, breakage is composed of some combination of impact and abrasion.

2.1.3.1 Abrasion breakage

Abrasion is the steady removal of relatively small fragments broken from the lump surface as the rock tumbles in the mill. It is therefore the surface removal of particles due to the rubbing action (when two particles move parallel to their plane of contact) characterized by the production of fines and yet with an identifiable parent particle. Small pieces of each particle are broken or torn off the surface, leaving the parent particles largely intact. It normally occurs when insufficient energy is applied to cause significant fracture of the particle. Rather, localised stressing occurs and a small area is fractured to give a distribution of very fine particles (effectively localised shatter fracture) (Kelly and Spottiswood, 1982).

2.1.3.2 Breakage by attrition

This form of grinding that occurs as a result of rubbing action within the ball mass and between the ball mass and the mill liners when a ball mill is running at low speed. The size reduction depends mainly on the surface areas of the media in interaction (Hukki, 1954). It is caused by the relative movement between powder and individual grinding media components in the mill. In the relative motion of particles and media, very small particles happen to be nipped between large balls or between large balls and mill liners. The rubbing together of the two media or of media and liners will result in the production of a significant number of very fine particles compared to the parent size. For that reason, it would be fair to assume that attrition is largely responsible for the breaking of

particles that have become smaller than the voids between the grinding media and that the stresses induced in the particle nipped between the two media or between the media and the liners are not large enough to cause fracture (King, 2001).

2.1.3.3 Impact breakage

An impact mechanism occurs when the particle is smashed between a ball and the mill shell or between the balls. Particle failure is due to compression resulting in fracture. Product particles display a wide range of sizes with disappearance of the parent particle.

It is also referred to as breakage by compression. King (2001) elaborated on this mechanism of fracture and discovered that it involves shatter and cleavage. Fracture by cleavage occurs when the energy applied is just sufficient to load comparatively few regions of the particle to the fracture point, and only a few particles result. Fracture by shatter on the other hand occurs when the applied energy is well in excess of that required for fracture. Under these conditions many areas in the particle are over-loaded and the result is a comparatively large number of particles with a wide spectrum of sizes. The specific energy of fracture energy decreases as size increases but the rate of decrease reduces as the particle size increases and eventually becomes a constant for larger particles (Tavares et al., 1998). It is found particle fracture energy increases at a rate approximately proportional to the particle mass. For a given impact energy, larger

particles have a smaller probability of being broken since the energy that a particle absorbs from the impact must exceed its fracture energy.

2.1.4 Factors affecting mill conditions

Changing mill conditions could be considered as similar to changing temperature in a chemical reactor. Briefly discussed below are some of the mill conditions that need to be specified in order to address the question of optimisation. Studying the comminution processes and understanding different parameters that affect it has increasingly become of interest to researchers in the field of mineral processing. Milling kinetics (Austin et al., 1984), load behaviour (Liddell and Moys, 1988; Dong and Moys, 2003) and mill power (Yildirim et al., 1998; Morrell, 1993) have been studied as functions of media size; feed particle size distribution, fraction of mill filled with balls and powder, mill diameter, mill speed and other variables affecting them.

2.1.4.1 Powder filling

It is found that for a given ball loading, it is undesirable both to under fill or overfill the mill with powder. At low powder filling much of the energy of the tumbling balls is taken up in the steel to steel contact while at high powder filling the powder cushions the breakage action. Mill filling is expressed as fraction of mill volume filled by feed bed:

$$f_c = mass\ of feed/(feed\ density \times mill\ volume) \times 1.0/0.6 \quad (2.15)$$

For the application of the population balance model, knowledge of the behaviour of the selection and breakage function is of vital importance. By definition U is the fraction of voids between the balls that is filled by ground material. It is represented by the equation below:

$$U = \frac{f_c}{0{,}4J} \quad (2.16)$$

$$J = massofballs/(balldensity \times millvolume) \times 1.0/0.6 \quad (2.17)$$

where f_c and J are the fractional volume filling of the mill by powder and balls, respectively (based on a formal porosity of 0.4 for powder and ball bed).

The effect of powder filling on selection and breakage functions has been investigated by a number of researchers who have reported their results for batch grinding of near mono-sized materials at different powder fillings. Shoji et al (1982) have shown that the slope of the linear part of the selection function had a constant value in a normal range of powder filling (e.g. from 0.3 to 2) and the breakage function was not affected at all by the environment.

Shoji (1982) and Deniz and Onur (2002) studied the effect of powder filling on grinding. A strong correlation between rates of breakage, powder filling (f_c) and ball filling (J) in the mill was found (Shoji 1982). With a ball filling (J) of 20% to 50%, and powder filling

(U) of 50% to 150, the specific rates of breakage for a 0.6m mill internal diameter were found to be well represented by an established empirical correlation:

$$S(f_c,J) = k\left[\frac{1}{1+6{,}6J^{2{,}3}}\right]\exp(-CU) \qquad (2.18)$$

where *C* is 1.2 and 1.32 for dry and wet grinding respectively.

Shoji et al., (1982) discovered that at three levels of powder filling, the selection functions are determined by one size-fraction tests. The selection function was found to decrease rapidly with increasing powder filling. When the powder filling was low, the breakage function appeared to be higher.

In most cases, a low value of powder filling gives a small absolute rate of breakage. On increasing the powder filling, more powder fills the collision space in between the balls and therefore results in a higher value of absolute breakage. A stage is eventually reached when all effective spaces in which collisions between balls are occurring are filled and the absolute breakage rate will be maximum.

Continued addition of the powder increases mill hold up but does not necessarily increase breakage because the collision zones are already saturated. Overfilling will then eventually lead to powder cushioning causing the ball powder bed to expand and result in poor ball-ball powder collisions and thus breakage rate reduces.

2.1.4.2 Media size and filling

The mill power does not vary much with ball diameter, so that the wrong choice of ball diameter causes inefficiency. The efficiency of the grinding process depends on the surface area of the grinding medium and in a ball mill it is affected by contacts between the balls and the ore particles. The right selection of ball sizes is of vital importance and must be made in relation to the largest and hardest particles of the feed. A charge of too small balls leads to slumping of the charge and low power draw plus excessive wear rates of the balls. The optimum choice of ball sizes depends on the feed size distribution, the desired product size, and the balance between energy and steel costs.

The rate of breakage depends on how much of the mill volume is filled with balls. The fractional ball filling, J, is conventionally expressed as the fraction of the mill filled by the ball bed at rest. It is conventional to define constant formal bed porosity for all calculations. Using a formal bed porosity of 0.4

2.1.4.3 Mill speed

Various laboratory studies, pilot plant works, and full-size plant observations showed that the mill speed, which is an operating variable, can affect grinding efficiency to achieve a given output fineness. The normal specific rates of breakage vary with mill speed. There is a critical speed for a mill which is the lowest speed at which the balls are just held against the wall and do not fall. The maximum in power occurs at different fractions of critical speed from one mill to another, depending on the mill diameter, the type of lifters, the ratio of ball-to-mill diameter, and the ball and powder filling conditions. The maximum is usually found within the range of 70–85% of critical speed.

Within the range of speeds near the critical speed there are relatively small changes in the normal specific breakage rates with rotational speed. There is no significant variation in B (Equation 2.13) values with mill speed within this range (Austin 1984).

The change from the cascading to the cataracting pattern (shown in Figure 2.4) is the cause of the peak of the feed size specific rate of breakage S_i under the conditions of ball-filling volume fraction J=0.5 and interstitial filling U = 1 in dry batch grinding of dolomite (Herbst and Fuerstenau, 1980). For these conditions, and with the eight 0.25-in. lifter bars on the 10-in.-diameter shell, the change occurred at a fraction of mill critical speed, c = 75%. Furthermore the change to cataracting is accompanied by a reduction in S_i, and hence, cascading is the major action within the mill for the conditions stated.

2.1.4.4 Slurry density

In the last decade, industrial practice is increasingly moving towards operating at higher slurry densities, for example, greater than 40% ore by volume. Some reasons for this are the higher throughputs realized for given installed equipment capacity at higher percent solids Klimpel (1982/83), the need with certain coals, some industrial minerals and fine chemicals, etc. to grind at as high a slurry density as is possible so as to produce a given quality of product Klimpel (1982).

Austin (1984) defines slurry density as the fraction by weight of solids in the mixture. The rheological properties of slurry are better defined by the volume fraction of solids, c:

$$c = (w_s/\rho_s) \times 1/\{(w_s/\rho_s) + [(1 - w_s)/\rho_l]\} \quad (2.19)$$

where w_s is the weight fraction of solid, $\rho_s and \rho_l$ are the densities of the solid and the liquid. The viscosity of the slurry also depends on the size distribution of the particles and it plays a major role in the size reduction process. Slurry density affects the dynamics, particle breakage effects, material transport and grinding behavior of mill grinding kinetics. A number of researchers have studied the effects and role of slurry density on grinding behavior of grinding mills. Tangsathitkulchai et al. (2002) found that the slurry density of quartz test material determined the distribution of solid charge in the mill, with the migration of particles from the tumbling zone to the mill periphery as solid concentration was increased.

From his results it is clear that slurry density affects the net power draw of the mill. For low concentrations the power decreases first before attaining a constant level. It becomes constant because there is no circulation path change of the mill charge. In this region mill power increases as slurry density increases. At high values of slurry density power draw is low. This indicates there is a decrease in tumbling action of grinding media as the slurry viscosity becomes high.

It is apparent therefore that changes of slurry density, if great enough, might influence the movement pattern of the grinding balls. The change in the circulation regime of the mill charge, and grinding performance, is reflected by a change in mill power consumption.

2.1.4.5 Influence of interstitial filling

The interstitial filling is the fraction of the interstitial spaces between the balls in the ball bed at rest that are filled with powder and is represented by a U. Shoji et al (1982) investigated the effects on the grinding of powder filling, for wet and dry grinding of quartz in a laboratory ball mill. The measured curve of breakage rate versus powder filling at a set ball load was such that at low filling of powder there was a small rate of breakage. As the amount of powder increases, the collision spaces between the balls are filled and higher rates of breakage are obtained. When all the effective space in which collisions between tumbling balls are occurring is filled with powder, the rate of breakage reaches a maximum.

The addition of more powder increases the mill hold-up but does not give increased breakage because the collisions zones are already saturated and further powder just enters a reservoir of powder. A plateau of almost constant breakage rates is obtained. Eventually, overfilling leads to deadening of the collisions by powder cushioning, the ball–powder bed expands to give poor ball–ball powder nipping collisions and the breakage rates decrease. It was concluded that U = 0.6–1 is the optimum filling condition for the maximum breakage rates at all ball loads.

Tangsathitkulchai (2003) investigated the effect of slurry concentration and powder filling on mill power for a small laboratory ball mill, with a constant ball load and rotational speed of the mill. The outcome of tests was that grinding at about U = 1 gave the maximum net mill power.

Deniz (2010) investigated the influence of interstitial filling (U) on breakage parameters for a laboratory ball mill, with a constant ball diameter (25.4 mm) and rotational speed of mill (% critical = 0.75). Dry grinding of different size intervals of gypsum samples

showed that with different interstitial filling grinding followed a first-order breakage law with constant normalized primary breakage distributions. The product of S and f_c is called the ‘‘relative absolute rate of breakage”, and is important because it is proportional to mill capacity. Differentiating $f_c S_i$ with respect to U and setting the value to zero to find the maximum gives the highest capacity. He discovered that a high value that is U = 1.5–2.0 is an effective ratio. This is because the gypsum sample used in the experiments is a material that is easy to grind relative to other materials. Shoji et al. (1982) found the maximum at U = 0.83 for a quartz mineral. Tangsathitkulchai (2003) found that grinding at about U = 1 gave the maximum in net mill power. Deniz and Onur (2002) independently found that an interstitial filling fraction of U = 0.4 is a good powder–ball loading ratio to give efficient breakage in a ball mill for a pumice sample.

2.1.4.6 Ball size distribution

In industry the ball size distribution is used in order to control and optimise the quality of the mill product. Effective milling of different particle sizes in a tumbling mill can be done by using a mix of balls of different diameters. Therefore in a mill each ball size effectively breaks a particular particle size Cho et al. (2013). It is not simple to directly control the ball size distribution in a mill as this depends on makeup charge and the wear rate. The abrasive milling environment is the chief cause of grinding media wear and therefore periodic charging of new grinding balls is required. A number of researchers have suggested make-up charge policies, Austin et al. (1984); Menacho and Concha (1985, 1986); and Bwalya et al. (2014). Bond (1961) suggested feeding a

mono-sized charge to obtain a specific grinding duty whilst Concha et al. (1992) and Cho et al. (2013) went on to optimise the make-up ball policy by combining a grinding circuit and a ball wear model.

Chimwani et al. (2015) went on to investigate effect of ball size distribution which is a function of make-up ball sizes. The objective was to optimise the milling in a grinding circuit in order to maximise the production of the narrowly-sized mill product for floatation (−75 + 9 µm).

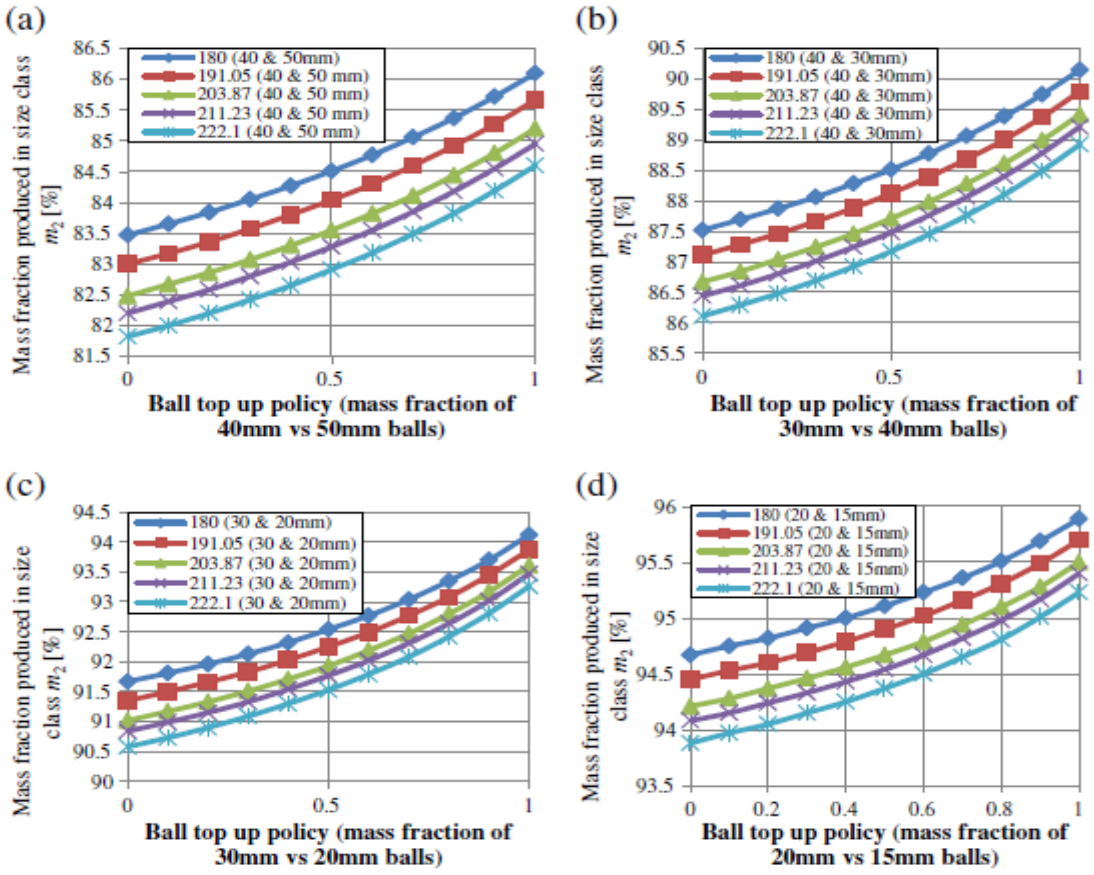

Figure 2.5: Effects of variation of composition of make-up balls for feed rates between 180 and 222.1m^3/h and ball diameters on the floatable fraction m_2 (Chimwani al., 2015).

For (a) the make-up balls consisted of 50 and 40mm ball diameter, (b) 40 and 30mm ball diameter, (c) 30 and 20 mm ball diameter and (d) 20 and 15 mm ball diameter.

Results suggested that the smallest mono-sized balls in the make-up give rise to a ball size distribution that gives the highest amount of the desired size class. They agree with what Bwalya et al. (2014) suggested, that is feeding a mono-sized ball charge. On the other hand, Cho et al. (2013) recommended a mix of two ball sizes as an optimum. The differences in their findings are probably due to the different objective functions of the studies carried out. One's response variables were the breakage parameters whereas other was the maximum production of a desired size range.

2.2 ANALYTIC ANALYSIS TOOL: ATTAINABLE REGION

The Attainable Region (AR) is defined as the set of values of all the output variables that can be achieved by any possible steady state process using a given feed. The output variables (also called state variables) define the space in which the achievable points can be found. The Attainable Region (AR) is a special tool that was introduced initially to optimise chemical reaction networks with complex kinetics. It is now more widely applied, and in this case was used to obtain optimum results for operation of a combined milling and leaching system for a gold ore.

2.2.1 Background of Attainable Region analysis

Horn (1964) devised the AR method in relation to optimizing chemical reactors. He showed that if it was possible to compile a set of possible outputs/outcomes (for instance concentrations) for all possible reactor systems for a given set of kinetics and feeds, finding the optimum configuration would be simple. This set of output concentrations he called Attainable Regions. His idea was to determine all possible outlet concentrations, regardless of reactor configuration, rather than examining a single concentration from a single reactor. This meant that AR is the full set of outcomes that can be achieved by all possible designs (possibly subject to some constraints) of the processing unit in response to the prescribed input. This is why the AR concept could

have a wide scope, and could be used successfully in a number of different contexts. Horn however gave no clear indication of how one construct the AR in general.

The beauty of the approach is that if the AR is known, one can search the region to find the output conditions that optimise a given objective function, for example selectivity or maximum concentration. This technique has two advantages. Firstly, it simplifies optimisation problems, as searching over a defined set for the maximum defined function value is a simple and straightforward process. Secondly, the chosen value of that objective function can be used as a yardstick for purposes of comparison. This idea could be of great help, because if a particular reactor has an optimal objective function that is not equal to the target or the expected value found using AR, the researchers know what improvements it should be possible to make.

However, this tool was not put into practice for 20 years, as Horn and those who followed up on the research were unable to find a systematic method of identifying the AR.

Glasser et al. (1987) and Hildebrandt (1990) adopted a geometric approach to the construction of an Attainable Region, in which the vector description of the fundamental processes of reaction and mixing are used. This geometric interpretation led to their development of necessary conditions for the AR that can be used to test whether a proposed region is a candidate for a complete attainable region.

These conditions for chemical reactors are as follows.

(1) The attainable region includes the feed point/s and initial state/s of the system.

(2) No fundamental process (rate) vector in the boundary of the attainable region points out of the region. In other words, the fundamental process vectors in the boundary must point inward, be tangential to the boundary, or be zero.

(3) If the state variables obey linear mixing rules, and if the fundamental process of mixing is permitted, then the attainable region will always be convex. When working in a space where mixing is not a meaningful process, or one has chosen not to allow it, the requirement that the attainable region be convex falls away.

(4) If mixing is permitted as a fundamental process, it must not be possible to extend a negative rate vector at any point lying outside the region so that it intersects the region. (A CSTR with a feed point within the region can be used to achieve that point).

Hildebrandt and Glasser went on to show that once the AR is found, the optimisation of the problem is straightforward, provided the objective function is an algebraic function of only the system variables. Once the AR is known, a path between the feed point and the optimum point on the AR can be found. In some cases this path could involve a complex combination of mixing and reaction, which in turn could be interpreted as providing a blue print for an optimal reactor structure. Therefore, having obtained the AR, the engineer can design a reactor structure to achieve points in the AR. Hildebrandt and Glasser (1990) also studied three-dimensional problems and provided guidelines on how the AR can be constructed in three-dimensional space.

The technique of AR analysis has been used extensively for the optimisation of reactor networks (Glasser et al., 1987; Hildebrandt and Glasser, 1990). Its greatest advantage is that it focuses on the fundamental processes involved in a system rather than the unit

operations themselves. AR analysis allows us to solve process synthesis and optimisation problems by providing guidelines for the construction of the attainable region, as well as the means (necessary conditions) to check the results.

It has also been found applicable to mineral processing. Khumalo et al. (2007) stated that since a mill can be considered as basically a reactor system where “reacting” large feed particles are converted into smaller product particles, the AR approach can be successfully applied to the field of comminution. In the research reported in this dissertation, AR is used to optimise the size class of choice, for example M2, which is the intermediate size in this research, with a minimum energy input into the grinding mill. In order to determine the candidate region, the researcher has to carry out a set of steps, including:

- selecting the fundamental processes occurring in the system (for example, breakage and mixing in a milling situation);
- choosing the state variables (such as M1—the feed size— and M2, where M3—the fine size is found by mass balance); and
- finding the optimum, that is, the maximum M2 that can be achieved with minimum energy use (Metzger et al., 2007).

In 2006, Khumalo et al. suggested the method of representing PSDs as points in space, allowing connectivity of the points, as a better method for process optimisation purposes than using the traditional approach, where PSDs were shown in terms of cumulative plots (Figure 2.6). The power of this method is that the characteristic equation comprises the required size class (objective function), the feed size class and the

control variable. This reduces the dimensionality of the geometric representation considerably.

Instead of using equipment in parallel, Khumalo proposed that comminution systems should use equipment in series, so that the value of $\bar{E}$ (input energy) could be varied along the circuit. This is desirable because the larger particles break along the available cracks, resulting in stronger and smaller particles with fewer cracks.

The candidate AR, once obtained by Khumalo, was interpreted in terms of pieces of equipment and optimum process conditions. This solved the process synthesis and optimisation problems for comminution systems simultaneously. The optimum conditions obtained from the AR determined the target against which the efficiency of the actual process should be measured.

Khumalo et al. (2007) later validated these assumptions in experiments using silica and quartz feeds, where they showed that the experimental attainable region is convex, as shown in Figure 2.7, where the PSDs are plotted as single points that have been joined together.

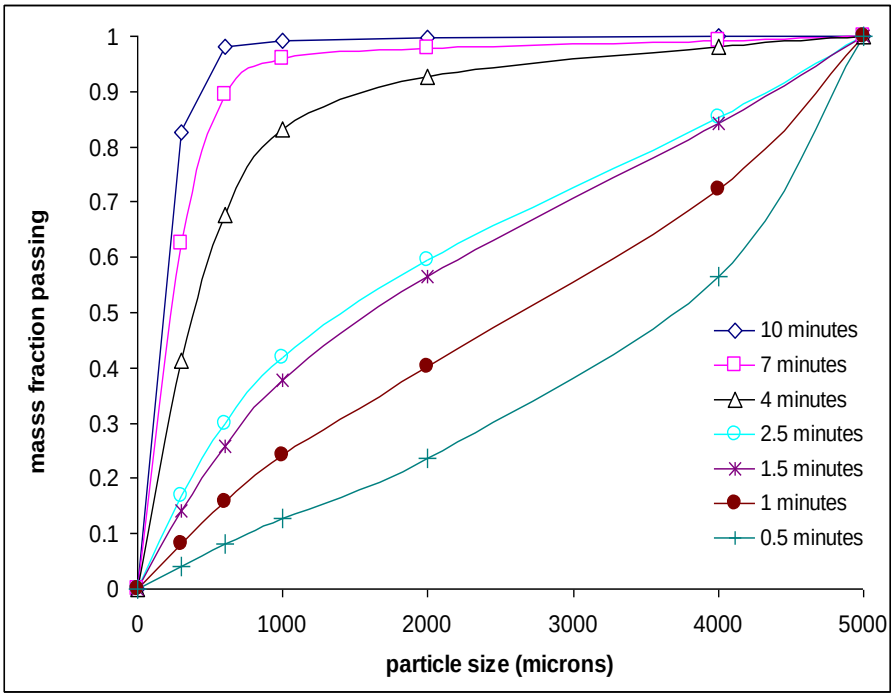

Figure 2.6: Cumulative particle size distributions with increase in the grinding time for a laboratory ball mill at 92 rotations per minute and 20 % ball loading (Khumalo et al., 2007).

Metzger et al. (2009) applied AR analysis to optimise the comminution of silica sand particles in a laboratory mill, and showed that it is a useful tool in determining optimal policies to reduce milling times. Metzger's objective was to produce the greatest amount of size class two by breaking the starting material (size class one) and reducing the production of fines (size class three).

2.2.2 AR plots

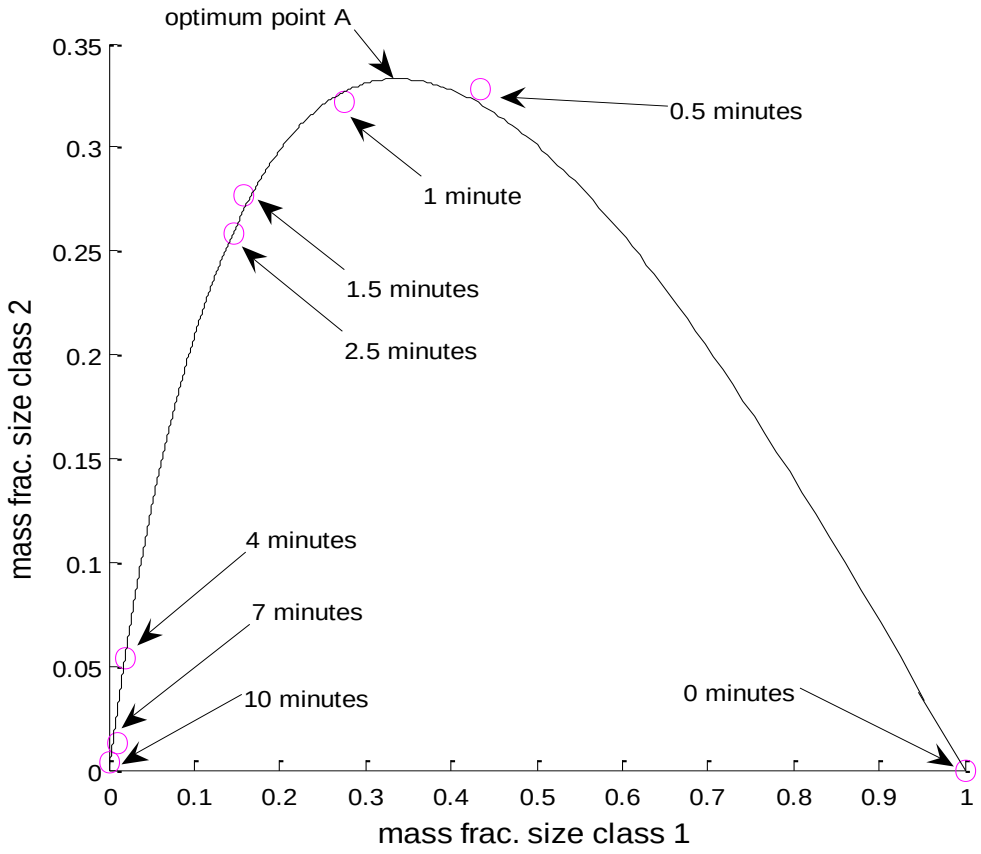

Figure 2.7: A typical Attainable Region plot of mass fraction of material in size class 2 vs. mass fraction of material in size class 1 (Khumalo et al., 2007).

As shown in Figure 2.7, the plot provides a way of representing PSDs in n-dimensional space, using the geometrical approach of the AR technique. This assists engineers when determining control policies, because they can track the change of mass fraction in each size class with a given energy input in an n-dimensional space. The AR approach can be extended to n-dimensional size classes. However, since single points

are used industrially to specify the desired output, the characteristic equation will mostly comprise three size classes.

The size classes are grouped as follows.

(i) The feed size class, taken as the top size class or size class 1 in comminution terminology,

(ii) The middle size class, which is a result of moderate extent of breakage. This is termed size class 2, and could be the desired product (thereby defining the objective function of the breakage system), and

(iii) The fines size class, which is a result of a relatively large extent of breakage. This is termed size class 3, which could also be the objective of the breakage system.

CHAPTER 3

3.1 LEACHING

Crundwell (1997) describes leaching as one of the unit processes that is central to the hydro-metallurgical treatment of ores. It is a downstream operation that is used to recover valuable metals. Leaching is fundamentally a separation process that entails the dissolution of a metal or mineral in a liquid. The particles created by comminution are immersed in usually an aqueous solution to dissolve the desired minerals or compounds in the ground material and cause them to detach themselves from the less valued materials in the solution, and be removed. The waste minerals and compounds in the same solution rejected by the leaching reaction should have a sufficiently low solubility to yield an acceptable separation of valuable and waste minerals during the leach. This process like all other unit processes in extractive metallurgy is simply a means of capturing one component of the ground ore and leaving behind the other.

The choice of the leach acid (lixiviant) and the method used for leaching is entirely dependent on what minerals are to be leached, and the form in which the minerals are present. The leaching process is almost always wedded to a liquid/solid separation plant, in which the solid is an unattached mineral or phase, or a precipitate formed during leaching, or a combination of these.

The solids that are rejected or left as residue contain un-leached values, partly as un-decomposed materials, partly as adsorbed or absorbed components in the precipitates, and partly as entrained in the solution. The presence of adsorbed components or metals in precipitates is due to thermodynamic conditions that partition the leached metal species between the two phases; that is, the solid precipitate and the aqueous solution. An entrained leach solution is attributable to an imperfect liquids/solids separation. All of these represent economic losses to the operation, so any attempt to optimise the leaching process must also consider leaching costs.

Leaching economics, especially the capital costs involved in building a leaching plant, are to some extent dependent on the leaching rates. However, the average leaching rate is not as important as the leaching time necessary for an acceptable level of extraction.

The leaching process will vary with the difficulty depending on the mineralogical texture of the ore. The particles to be leached may be in the following states:

I. free particles (pure substance);
II. middlings (valuable components partially exposed); and
III. dispersed valuable material within gangue matrix that is not accessible to lixiviant.

In (III) the material is regarded as unextractible. An ore or concentrate in this form has to be ground to the extent that the mineral is reduced to minimum form that the leaching agent can access. In (I) and (II), the material can be leached directly.

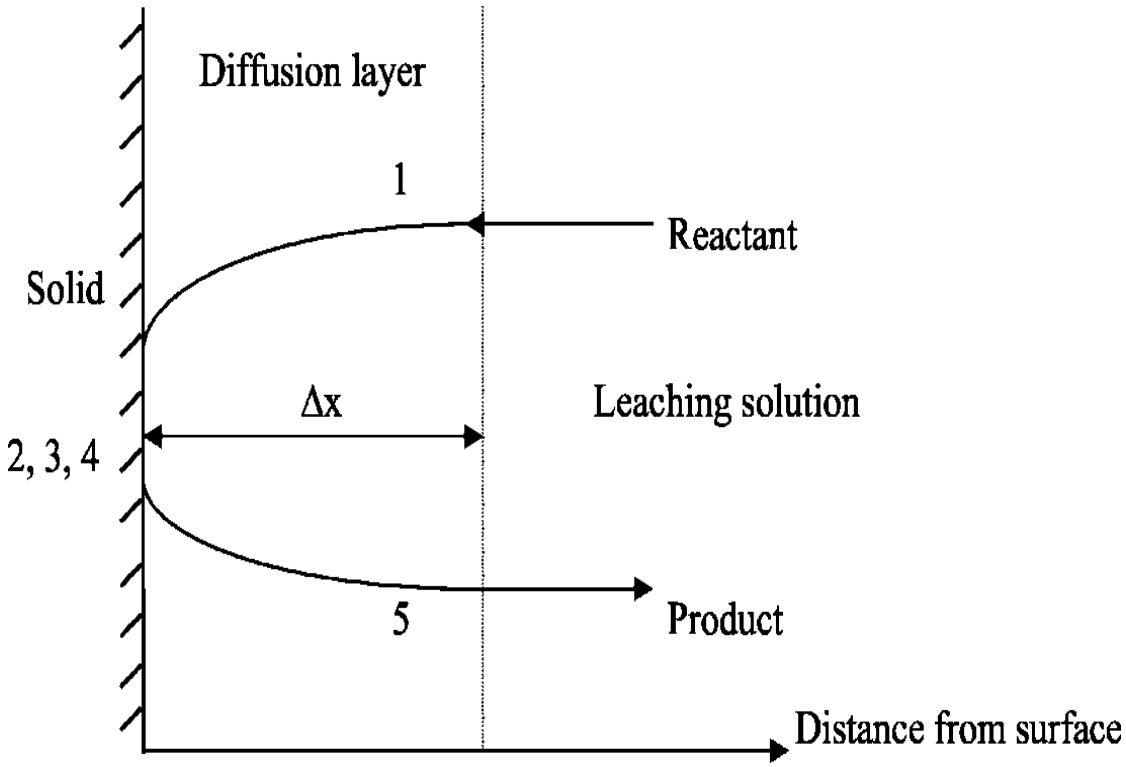

Figure 3.1: Basic sketch of the leaching process.

The diagram in Figure 3.1 shows the sequence of fundamental steps that take place during the leaching process, which can be described as follows:

1. diffusion of the reactant from the bulk of the solution to the mineral surface layer through the diffusion layer (Δx);

2. adsorption of the reactant on the solid;

3. reaction of the leaching agent with the mineral surface to form a soluble species;

4. desorption of the product from the solid; and

5. dispersion of the leached mineral product through the diffusion layer (Δx) away from the solid.

In this simple model the reaction rate will be proportional to the surface area, other factors being equal. In the sequence, 1 and 5 are liquid phase diffusion processes, which are described by steady state flux equations. Fick's Law governs the rate of diffusion in a solution:

$$J = \frac{dn}{dt} = -A.D\frac{dC}{dx} \qquad (3.1)$$

where: J is the amount of substance that diffuses through a surface per time unit, A is the area of the reacting surface, D is the diffusion constant (unit of surface/unit of time) and $\frac{dC}{dx}$ is the concentration gradient.

The leaching rate is thus dependent on the area of the leaching body A, the diffusion coefficient D, and the concentration gradient $\frac{dC}{dx}$.

In addition, the concentration gradient depends on the thickness of the diffusion layer (Δx), which is shown in Figure 3.2.

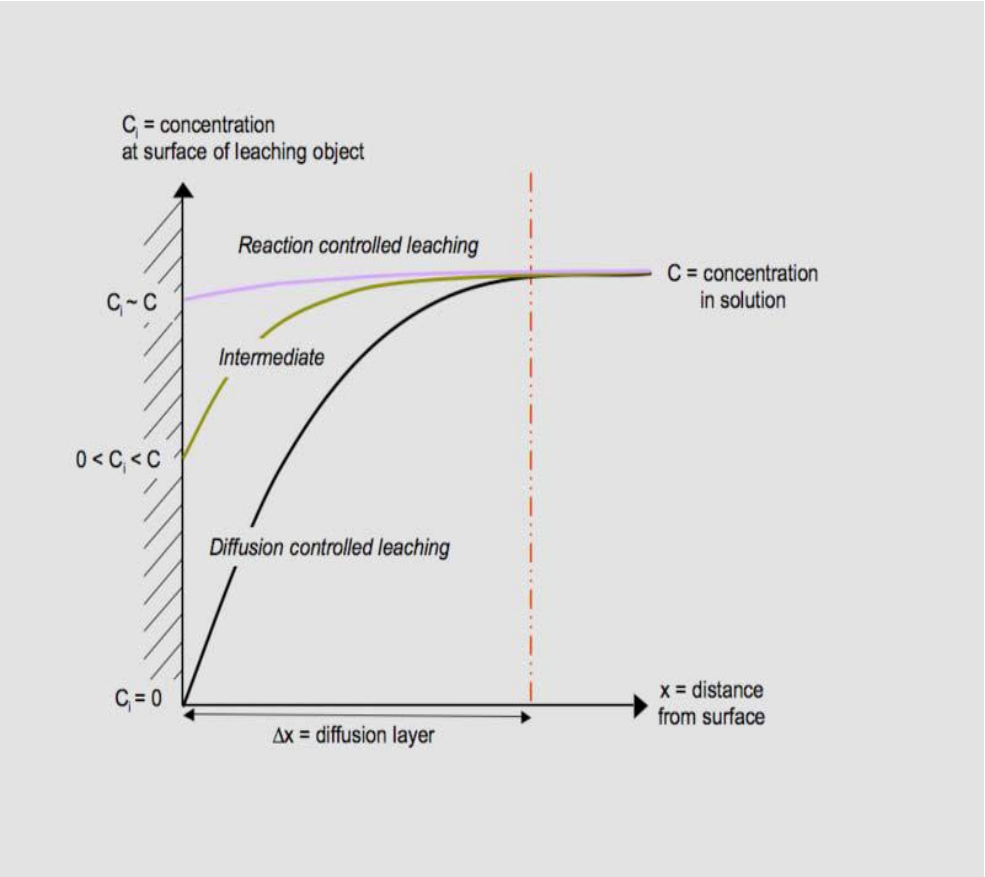

Figure 3.2: Concentration of reactant on the surface of solid subjected to leaching (Biomine, 2006).

3.1.1 Models for predicting the kinetics of mineral dissolution

The models commonly used in the prediction of mineral dissolution are the shrinking core and the shrinking particle models.

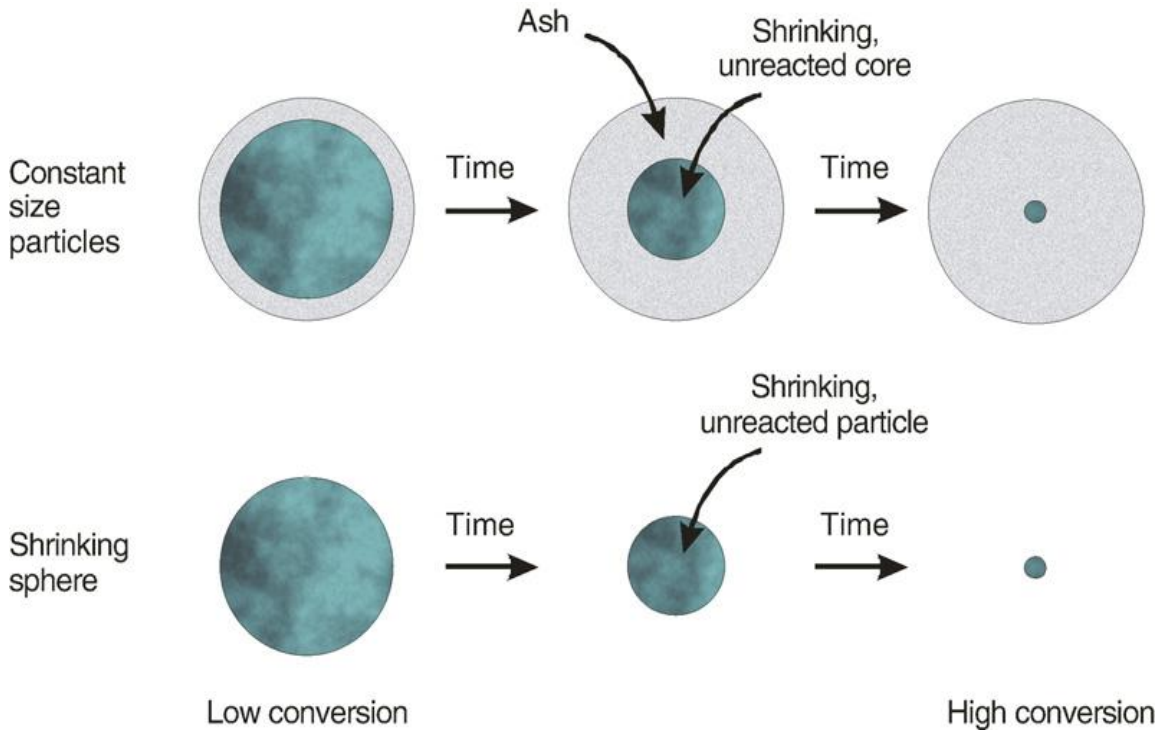

Figure 3.3: According to the un-reacted core models, the reaction proceeds on a narrow front, which moves into the solid particle. The reactant is completely converted as the front passes by (Levenspiel, 1999).

3.1.1.1 Shrinking core model

Yagi and Kuni proposed the shrinking core model in 1955. The solid matrix is taken to be porous and is initially surrounded by a fluid film, through which there is mass transfer between the bulk fluid and the inside of the solid particle. The material of interest dissolves into the lixiviant at an interface of the reacting material, leaving the unreacted

matrix behind. As a result the reacting core shrinks although the overall particle size remains constant; hence it is called the ‘shrinking core/ constant particle size model.

The most widespread application of the shrinking core model is as a means to predict the kinetics of mineral dissolution. The leaching of mineral particles by means of a reagent in solution can be represented by the following equation:

A (fluid) + *bB (solid)* ⟶ *aqueous and solid products*

where A represents the solvent, B represents the soluble component undergoing leaching, and b is the stoichiometric coefficient of B.

The model construction is based on the following assumptions:

I. the solid particles undergoing leaching have a spherical geometry and are porous at the start of, and during, the reaction;
II. the chemical reaction is irreversible and first-order with respect to the liquid reactant;
III. the chemical reaction determines the kinetics of the whole process; and
IV. the concentration of the lixiviant is constant throughout the whole process.

The kinetics are, however, made complex by changes in porosity, pH, and solution concentration. For leaching involving a gaseous phase, for example, oxygen, its diffusion and the subsequent reaction with mineral particles combine to give a non-

steady-state concentration gradient within the ore fragment. This treatment provides a basis for modeling all similar leaching systems.

This formulation, which represents a reaction, is the basis of the shrinking core model, which postulates that as the reaction proceeds, the solid component is converted into a soluble product and some other solid waste material. The latter is left behind as an un-reacted solid, an ash that is porous and inert. The un-reacted core shrinks as the reaction progresses, whilst the overall size of the particles remains constant.

.

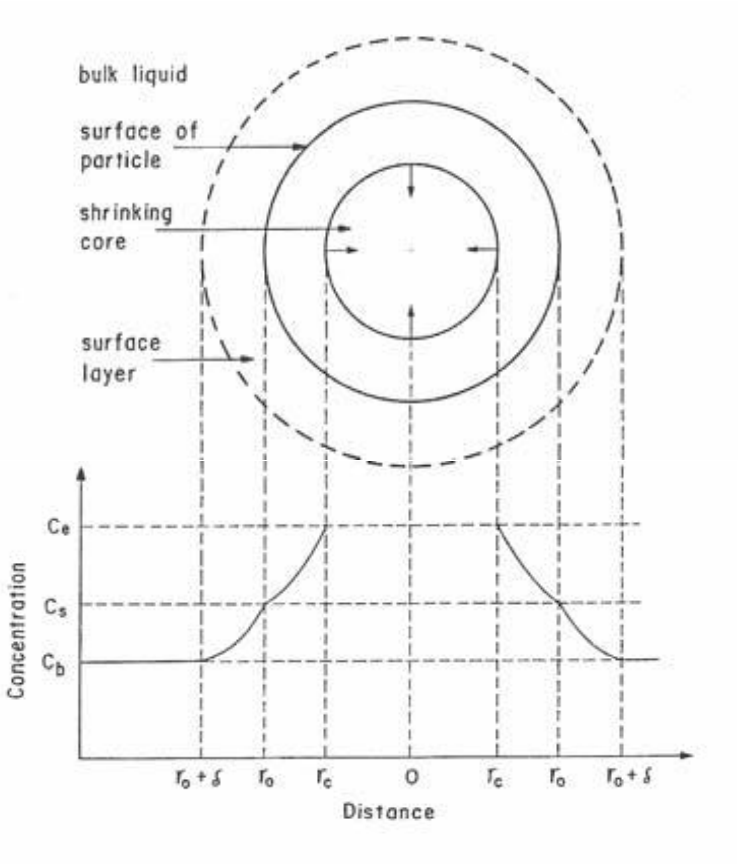

Figure 3.4: Representation of concentrations of reactants and products for the reaction for a particle of unchanging size (adapted from Levenspiel).

Figure 3.4 shows the shrinking-core concept, which is a special case of the general treatment in that it illustrates the different regions inside the mineral fragment. One of three conditions may control the overall reaction rate:

- diffusion through the liquid film;
- diffusion through the ash layer (formed by converted solid or inert material); or
- chemical reaction.

3.1.1.2 Shrinking particle model

As the reaction proceeds, the unreacted core of the particle tends to shrink. The model postulates that no ash layer is formed during the leaching reaction. The solid particles react with the liquid or gas reactant and shrink during the reaction, finally disappearing. The reactions are confined to the surface of the particle, the size of which is reduced by gasification and/or flaking of the solid products.

The chemical reaction controls are similar to those exhibited by the shrinking core model. Any deviation from the equation for diffusion controls depends on whether the particle is large or small.

3.1.2 Diffusion through liquid film controls

The rate of reaction per unit surface area is equal to the molar flux of A from the main body of the liquid to the surface of particle, as expressed by:

$$-\frac{1}{S_{ex}}\frac{dN_A}{dt} = -\frac{1}{4\pi R^2}\frac{dN_A}{dt} = \frac{b}{4\pi R^2} = constant \qquad (3.2)$$

No liquid reactant is present on the surface, and $C_{bulk} - C_s$ becomes the driving force of the reaction.

The equation for the stoichiometry of the reaction is:

$$A(l) + bB(s) \longrightarrow products$$

$$\frac{dN_A}{dt} = -\frac{1}{b}\frac{dN_B}{dt} \qquad (3.3)$$

Combining the above equations (3.2 and 3.3) gives:

$$-\frac{1}{S_{ex}}\frac{dN_B}{dt} = -\frac{1}{4\pi R^2}\frac{dN_B}{dt} = \frac{b}{4\pi R^2}\frac{dN_A}{dt} = constant \qquad (3.4)$$

Letting ρ_B represent molar density of B in the solid in mols/m^3 and V the volume of the particle, the amount of solid B present can be shown as:

$$N_B = \rho_B V = \frac{moles\ B}{cm^3 solid} \qquad (3.5)$$

The decrease in the radius of unreacted core as a result of disappearance of dN_B moles of solid reactant is given by:

$$dN_B = -bdN_A = -\rho_B V = \rho_B\left[\frac{-4\pi r_c^3}{3}\right] = -4\rho_B \pi r_c^2 dr_c \qquad (3.6)$$

Then replacing equation (3.6) by (3.2) will give the rate of reaction in terms of shrinking radius of unreacted core as:

$$-\frac{1}{S_{ex}}\frac{dN_B}{dt} = \frac{\rho_B r_c^2 dr_c}{R^2 dt} = bk_l C_{Al} \qquad (3.7)$$

where k_l is the mass transfer coefficient between the fluid and particle $\left[\frac{m^3}{cm^2 s}\right]$. Rearranging the above, we can find how unreacted core shrinks over time:

$$\frac{\rho_B}{R^2}\int_R^{r_c} r_c^2\, dr_c = bk_l C_{Al}\int_0^t dt$$

On integrating

$$t = \frac{\rho_B R}{3k_l C_{Al}}\left[1 - \left[\frac{r_c}{R}\right]^3\right] \qquad (3.8)$$

and taking r_c = 0 time for complete conversion τ:

$$\tau = \frac{\rho_B R}{3k_l C_{Al}} \qquad (3.9)$$

Dividing equation (3.8) by (3.9) we get:

$$\frac{t}{\tau} = \left[1 - \left[\frac{r_c}{R}\right]^3\right] \qquad (3.10)$$

and writing in terms of fractional conversion, one obtains:

$$1 - X_B = moles\ of\ B\ unconverted = \frac{volume\ of\ unreacted\ core}{total\ volume\ of\ particle} = \left[\frac{r_c}{R}\right]^3 \qquad (3.11)$$

while combining (3.10) and (3.11) yields:

$$\boldsymbol{\frac{t}{\tau} = \left[1 - \left[\frac{r_c}{R}\right]^3\right] = X_B} \qquad (3.12)$$

The reaction given in equation (3.12) represents the relation of time and radius of un-reacted core and the fractional conversion of solid B.

A similar analysis may be carried out for the cases when the rate-controlling step is the diffusion through ash layer controls or the chemical reaction. The corresponding equations for the control regimes are presented in the table below (extracted from Levenspiel, [1999]).

Table 25.1 Conversion-Time Expressions for Various Shapes of Particles, Shrinking-Core Model

		Film Diffusion Controls	Ash Diffusion Controls	Reaction Controls
Constant Size Particles	**Flat plate** $X_B = 1 - \frac{1}{L}$ L = half thickness	$\frac{t}{\tau} = X_B$ $\tau = \frac{\rho_B L}{b k_g C_{Ag}}$	$\frac{t}{\tau} = X_B^2$ $\tau = \frac{\rho_B L^2}{2b\mathscr{D}_e C_{Ag}}$	$\frac{t}{\tau} = X_B$ $\tau = \frac{\rho_B L}{b k'' C_{Ag}}$
	Cylinder $X_B = 1 - \left(\frac{r_c}{R}\right)^2$	$\frac{t}{\tau} = X_B$ $\tau = \frac{\rho_B R}{2b k_g C_{Ag}}$	$\frac{t}{\tau} = X_B + (1 - X_B)\ln(1 - X_B)$ $\tau = \frac{\rho_B R^2}{4b\mathscr{D}_e C_{Ag}}$	$\frac{t}{\tau} = 1 - (1 - X_B)^{1/2}$ $\tau = \frac{\rho_B R}{b k'' C_{Ag}}$
	Sphere $X_B = 1 - \left(\frac{r_c}{R}\right)^3$	$\frac{t}{\tau} = X_B$ **(11)** $\tau = \frac{\rho_B R}{3b k_g C_{Ag}}$ **(10)**	$\frac{t}{\tau} = 1 - 3(1 - X_B)^{2/3} + 2(1 - X_B)$ **(18)** $\tau = \frac{\rho_B R^2}{6b\mathscr{D}_e C_{Ag}}$ **(17)**	$\frac{t}{\tau} = 1 - (1 - X_B)^{1/3}$ **(23)** $\tau = \frac{\rho_B R}{b k'' C_{Ag}}$ **(22)**
Shrinking Sphere	**Small particle** Stokes regime	$\frac{t}{\tau} = 1 - (1 - X_B)^{2/3}$ **(30)** $\tau = \frac{\rho_B R_0^2}{2b\mathscr{D} C_{Ag}}$ **(29)**	Not applicable	$\frac{t}{\tau} = 1 - (1 - X_B)^{1/3}$ $\tau = \frac{\rho_B R_0}{b k'' C_{Ag}}$
	Large particle (u = constant)	$\frac{t}{\tau} = 1 - (1 - X_B)^{1/2}$ **(31)** $\tau = (\text{const})\frac{R_0^{3/2}}{C_{Ag}}$	Not applicable	$\frac{t}{\tau} = 1 - (1 - X_B)^{1/3}$ $\tau = \frac{\rho_B R}{b k'' C_{Ag}}$

3.2 CHEMISTRY OF GOLD CYANIDATION

The dissolution of gold, and in particular the chemistry of dissolution, has been studied extensively over the last three centuries. The cyanidation principle, a metallurgical technique for extracting gold by using cyanide as a lixiviant, has been widely followed since the 19th century because of the relatively low cost of this leaching agent and its effectiveness as a solvent. Even more importantly, it has selectivity for gold over some other metals. Although cyanide is toxic, applying it with care and taking appropriate precautions mitigates any risk its use may pose to human and environmental health.

The French chemist P. J Macquer (1718–1784) discovered potassium ferrocyanide ($K_4(Fe(CN)_6)$) as a product of reaction between the pigment Berlin blue (Prussian blue) with the alkali (KOH). In 1783, another chemist, Carl Wilhelm, heated Berlin blue with dilute sulphuric acid and produced an inflammable gas that dissolved in water. The name hydrogen cyanide (HCN) was given to the gas by Gay-Lussac in 1811.

1n 1783 the Swedish chemist Carl Wilhelm Scheele discovered that gold dissolved in aqueous solutions of cyanide. Bagraton (1843) and J.W. Mellor (1923) also noted the ability of cyanide to dissolve gold. The modern cyanide process was developed in Glasgow, Scotland, in 1887 by John Seward MacArthur, whose research was supported financially by two physicists, Robert and Dr William Forrest. MacArthur and the two Forrest brothers recognised the importance of cyanide leaching of auriferous ore for the production of gold and silver, and MacArthur patented the process in that same year.

A considerable amount of research has been undertaken at laboratory scale into alternatives to cyanide as a lixiviant. Most, if not all, of these have revealed limitations that hinder their widespread adoption in the gold mining industry. Thiourea, for example, despite offering a proven technology and suitability for use with refractory ores, is associated with high detoxification costs, has limited recyclability, and requires process conditions that are difficult to control. Thiosulphate offers the same advantages, but is highly unstable, has limited recyclability and requires expensive detoxification treatment. Thiocyanate, while more stable than the former two reagents, is under researched at present, but it appears that significant obstacles to its use will hinder its eligibility to be considered as a viable alternative to cyanide. Again, halides have proved difficult to handle and control, and are also expensive.

It follows that, in spite of the vociferous opposition to the use of cyanide in the gold mining industry expressed by many environmental activists, cyanide will continue to be the only practical choice of leach reagent in large-scale gold extraction processes. This may change if further research and development finds ways to make one or more of the alternative lixiviants economically competitive. It should be realized, however, that much of the opposition to the use of cyanide in the mining industry is based on a relatively small number of well-publicized pollution incidents, most of which were caused by either poor design or faulty operation of gold extraction processes. Cyanide has been used for over a century in gold mines all over the world, and there is ample evidence that in well-designed and properly-managed mining operations, it can be used safely as a gold leaching reagent that poses no significant risk to human life or the environment.

The oxidant most commonly used in the cyanidation process is oxygen, usually supplied from atmospheric air. This process makes use of potassium cyanide (KCN), sodium cyanide (NaCN), and calcium cyanide ($Ca(CN)_2$) as leaching agents. Potassium cyanide is considered the best of the three solvents, although it is the most expensive. Calcium cyanide has the lowest solubility of the three, although it is the cheapest solvent. According to the relative claims of efficacy and price, it follows that sodium cyanide is most frequently chosen for industrial use.

Metal salts will ionize when dissolved in water to give their respective metal cat-ion and free cyanide ions (CN^-), as shown in equation 3.13 below:

$$KCN^- \longleftrightarrow K^+ + CN^- \qquad (3.13)$$

The cyanide ions will in turn hydrolyze in water to form hydrogen cyanide (HCN) and hydroxyl ions (OH^-), which have a tendency to increase the pH.

$$CN^- + H_2O \longleftrightarrow HCN + OH^- \qquad (3.14)$$

When a pH of about 9.3 is reached, almost half of the total amount of cyanide consists of hydrogen cyanide, while the other half comprises free cyanide ions. At pH values higher than the above, the total amount of cyanide is largely present as free cyanide. Undesirable reactions may occur during the leaching process because both hydrogen

cyanide and free cyanide can be oxidized with oxygen to form cyanate (CNO^-), which has the effect of reducing free cyanide concentration rather than dissolving gold.

3.2.1 Factors influencing the rate of dissolution of gold

Many researchers have examined the effect of different parameters on the dissolution of gold in leach solutions. These include the effect of the pH, temperature, particle size or surface area exposed; the stirring rate or degree of agitation and mass transport, the cyanide and oxygen concentration, and the presence of other metal ions. The effect of leaching duration and of pulp density has also been examined.

3.2.1.1 Particle size

Plant operators have studied the effect of particle size on gold recovery extensively. Most of the literature published on these researches indicates that the recovery increases with the fineness of the ground material (de Andrea Lima and Hodouin, 2005). Other engineers tested various models to describe the effect of particle size on the level of recovery. The disadvantages of finer grinding are that, the longer grinding process requires higher energy plus higher cyanide consumption leading to increased expenses. They become even more when the ore contains sulphide minerals that consume more cyanide (Breuer et al., 2008).

Particle size is the factor that most affects the extraction rate and ultimately the amount of gold recovered. Leaching is different from flotation and other direct concentrating processes in that it requires only the exposure of the minerals, and not their liberation. The dissolution rate is proportional to the exposed surface area of the gold. The amount of exposed area is a function of the particle size distribution and the liberation characteristics of the material, which in turn is affected by the efficiency of the comminution process prior to leaching.

In general, the leaching rate increases with decreasing particle size, due to the increase in liberation. However, this is not always the case, as some ores containing cyanocides may decrease with decreasing particle size. This may be attributed to a higher rate of competing reagent- consuming reactions. In this particular case, an optimum particle size should be found that strikes a balance between gold liberation and cyanide consumption.

From the equations found in the models, the kinetics of leaching is shown as a function of the particle size. In most cases smaller particle sizes yield faster leaching kinetics, therefore

- in chemically-controlled leaching the dependency is proportional to $\frac{1}{r}$; and
- in diffusion-controlled leaching the dependency is proportional to $\frac{1}{r^2}$.

Ling et al. (1996) studied the effect of particle size on gold dissolution, and discovered that smaller particles can improve the gold dissolution rate in that they provide a bigger

surface area to maximize the contact between solid and liquid. de Andrade Lima and Hodouin (2005) proposed residual gold concentration in ore particles as a function of the ore particle size, as shown (Figure 3.5). Results showed that the coarser the particles the higher amount of residual gold concentration that has been un-leached.

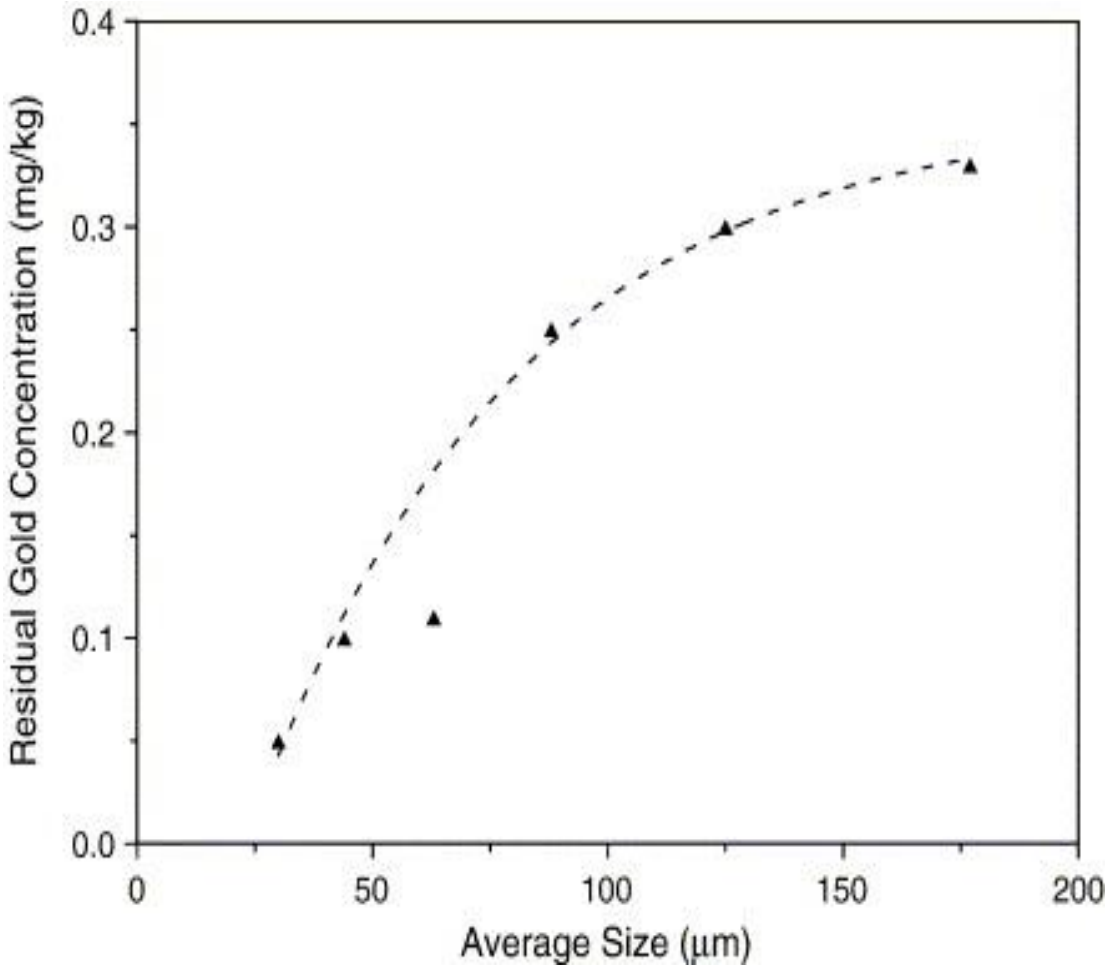

Figure 3.5: Comparison between observed (▲) and calculated values (dash line) of the residual gold concentrations ([Au]s,∞) as a function of the average ore particle size ($\bar{d}$) de Andrade Lima and Hodouin (2005).

3.2.1.2 Temperature

An increase in the leaching temperature should improve the activity and diffusion rates of the reacting species, and hence the solubility of the gold. Heat increases the kinetic energy of the solvent particles so that they collide more frequently, thus speeding up the rate of reaction.

For diffusion-controlled reactions, the effect of a rise in temperature causes the rate to increase more or less linearly. The diffusion constant also increases with the temperature, in accordance with the Stokes–Einstein equation:

$$D = \frac{R.T}{6.\pi.r.\eta.N} \qquad (3.15)$$

In this equation, R is the universal gas constant, r is the radius of the diffusing molecule (assumed to be a sphere), η is the viscosity of the medium, and N is Avogadro's number.

Raising the temperature of the reactants will cause the leaching rate constant to increase exponentially with the temperature, in accordance with Arrhenius' equation:

$$k = A.e^{\frac{-E}{RT}} \qquad (3.16)$$

Ambient temperatures are usually applied to leaching systems because the high costs associated with high temperatures are generally considered unjustified, especially for the low-grade ores. Elevated temperatures are mostly used when treating high-grade ores. In practice these treatments, referred to as intensive cyanidation processes,

frequently require additional cyanide and oxygen reagents, and are carried out in reactors such as the inline leach and the Acacia.

3.1.1.3 Stirring rate

Agitation has the effect of reducing the thickness of the external diffusion layer. Because the process of gold leaching is externally mass transport controlled, the rate of dissolution depends on the thickness of the diffusion layer and the mixing characteristics of the bulk solution.

For diffusion-controlled reactions, the effect of increasing the agitation rate is to raise the reaction rate to a limiting value. To minimise the diffusion layer, we need to maximise the flow rate of the mixing solution. In the treatment of slurries this is achieved by pumping in air or by mechanical agitation. Agitation or stirring improves the homogeneity of the material, and also diminishes the diffusion layer.

Chemically-controlled leaching is not affected by agitation, as the chemical reaction is then much slower than diffusion through the diffusion layer.

The dependency of diffusion in say a leaching vessel can be given by the progressive equations below Habashi (1999):

$$\Delta x = L.N_{RE}^{-0.9}N_{Sc}^{\frac{-1}{3}} \qquad (3.17)$$

where: Δx is the diffusion layer thickness, L is the characteristic length, N_{RE} is the Reynolds number and N_{Sc} is the Schmidt number.

$$N_{RE} = \frac{\rho.N.(2r)^2}{\mu} \quad (3.18)$$

where: μ is the dynamic viscosity, N is the rotational speed of the stirrer, ρ is the pulp density and r is the radius of the stirrer.

$$N_{Sc} = \frac{\mu}{\rho.D} \quad (3.19)$$

For the Schmidt's number, D is the diffusion constant.

3.2.1.4 pH

The leaching process is mostly performed at a pH > 9.4 to prevent loss of cyanide by hydrolysis. The addition of lime (CaO) is typically used to maintain pH in the gold leaching circuit (Ling et al., 1996; Ellis and Senanayake, 2004).

Reducing the pH would favour the conversion of the available cyanide into hydrogen cyanide in solution. In such a situation a loss of cyanide by volatilization of HCN is highly probable. Perry et al. (1999) studied the dissolution of gold at low pH, and found that, while thermodynamics indicate that gold can be leached by using HCN, their investigations showed that HCN does not leach gold sufficiently fast to compete with the rate of leaching with cyanide. They also noted that above a pH of 9.5 the dissolution rate is low, and dependent on the presence of other solution species, ore constituents and the type of alkali used for controlling the pH.

The alkali to be used for pH modification should always be added before the cyanide, to prevent loss of cyanide by hydrolysis. The pH should always be checked throughout the

leaching circuit, especially when the ores being treated contain alkali-consuming reagents. Calcium hydroxide (slaked lime) or sodium hydroxide can be used for pH modification. Slaked lime is cheaper than sodium hydroxide, but is less soluble and produces solutions that readily form salts and scales. Unslaked lime (*CaO*) is less costly than slaked lime, but is less effective. Sodium hydroxide, on the other hand, has higher solubility than slaked lime, which may lead to the dissolution of ore constituents, such as silicates. This in turn can precipitate in a number of unwanted forms that affect downstream processes like gold precipitation and carbon adsorption. In general, therefore, calcium hydroxide is the pH modifier of choice.

Parga et al. (2007) have shown the effect of pH on gold extraction in the diagram in Figure 3.6. This shows that the gold extraction for a high-pressure system reduces when the pH increases.

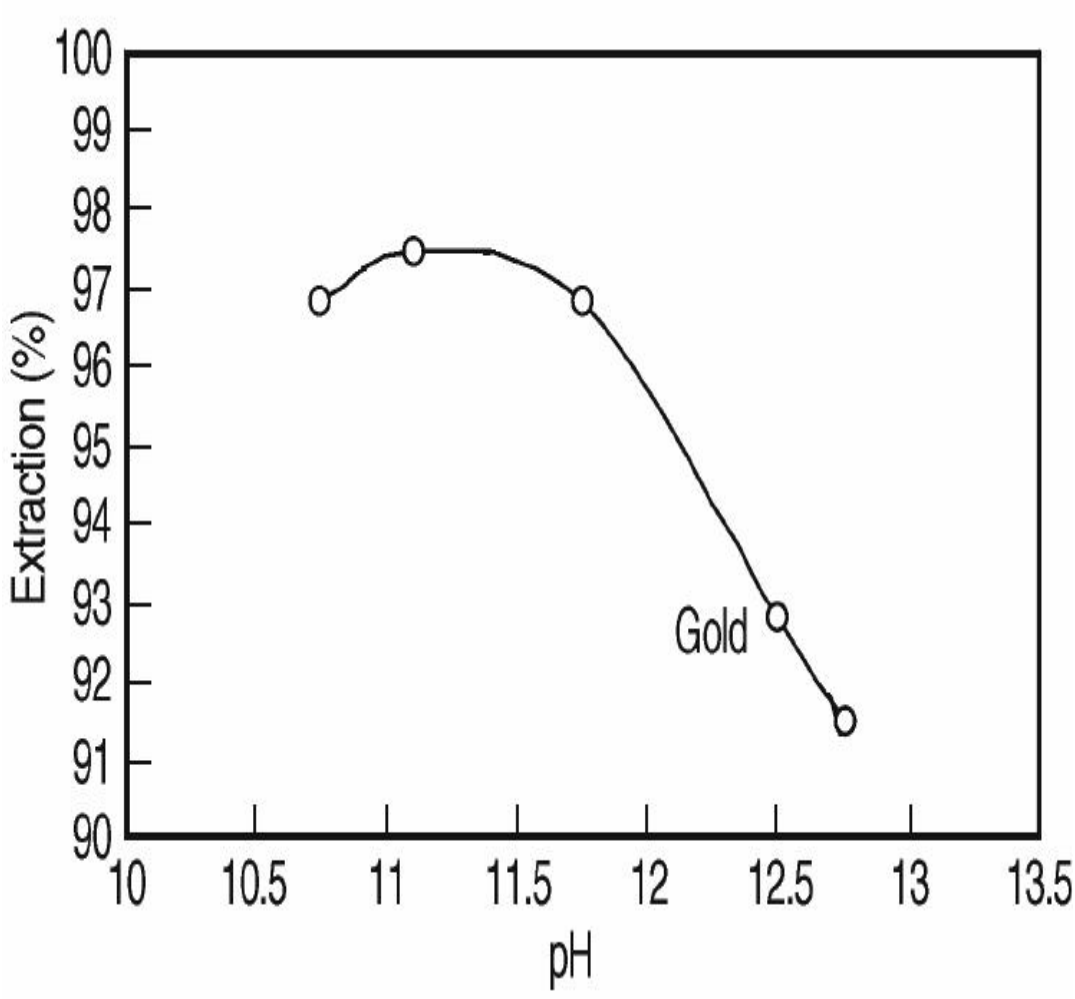

Figure 3.6: The effect of pH on gold extraction. Conditions: 20% solids, 0.6 MPa, 300 min-1, 800C, 1% NaCN, 1 hour (Parga et al., 2007).

However, Ling et al. (1996) found that a high pH level also results in lower cyanide consumption, as shown in Figure 3.7.

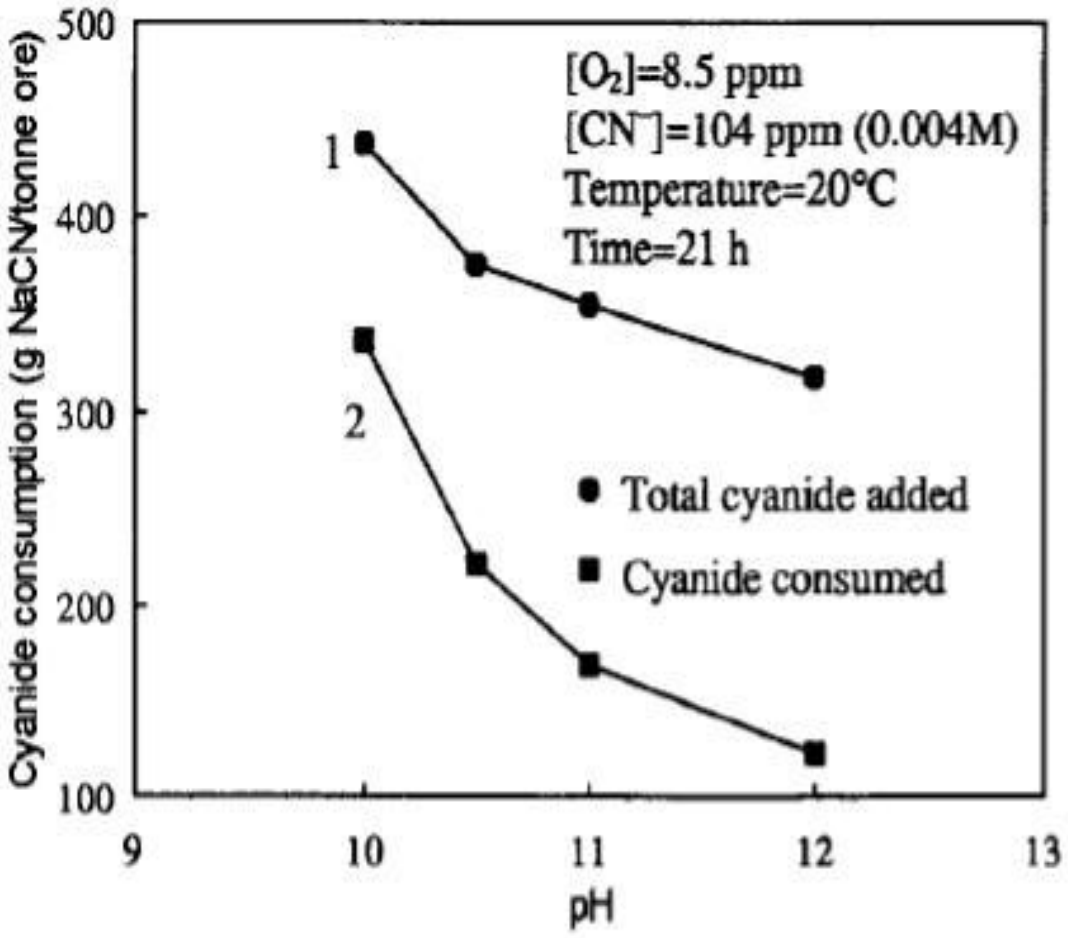

Figure 3.7: Effect of pH on cyanide consumption (Ling et al., 1996).

(Marsden and House, 1992) pointed out that the optimum pH for leaching should be derived independently for each ore type and leaching system.

3.2.1.5 Effect of dissolved oxygen and cyanide concentration

The sole drawback of the cyanide/oxygen leaching chemistry for the dissolution of gold is the low solubility of oxygen in water. Nicol et al. (1987) showed that, under most

conditions, the rate of gold leaching is controlled by diffusion of oxygen to the metal surface. The concentration of oxygen in water therefore, plays a role in the rate of gold dissolution. This, in turn, is a function of air pressure. The solubility of oxygen varies with altitude in the 5–10 mg range for air-saturated solutions. Temperature also plays a role, with oxygen solubility varying inversely with temperature. In other words, a rise in temperature can result in a decline in the rate of gold leaching, even when the diffusivity of the oxygen improves.

There are various ways in which the oxygen concentration can be increased. An option could be to use pure oxygen instead of air to increase the partial pressure of oxygen under atmospheric conditions. Alternatively, a more expensive method would be to employ hydrogen peroxide to supply oxidant to the surface of the gold particle.

Deschenes et al. (2003) conducted a series of experiments with dissolved oxygen. The ore was milled to a size of 37 µm and 0.55kg/t. of 300ppm NaCN was used. They discovered that when they added 100g of lead nitrate per ton to the pre-leach circuit, the gold dissolution process improved, reaching a leaching efficiency of 96%.

The results obtained by Ling et al. (1996) are presented in Figure 3.8. Ling and his co-researchers reported that high amounts of dissolved oxygen did not have a noticeable effect on the gold dissolution rate at the cyanide concentration level of 104 ppm.

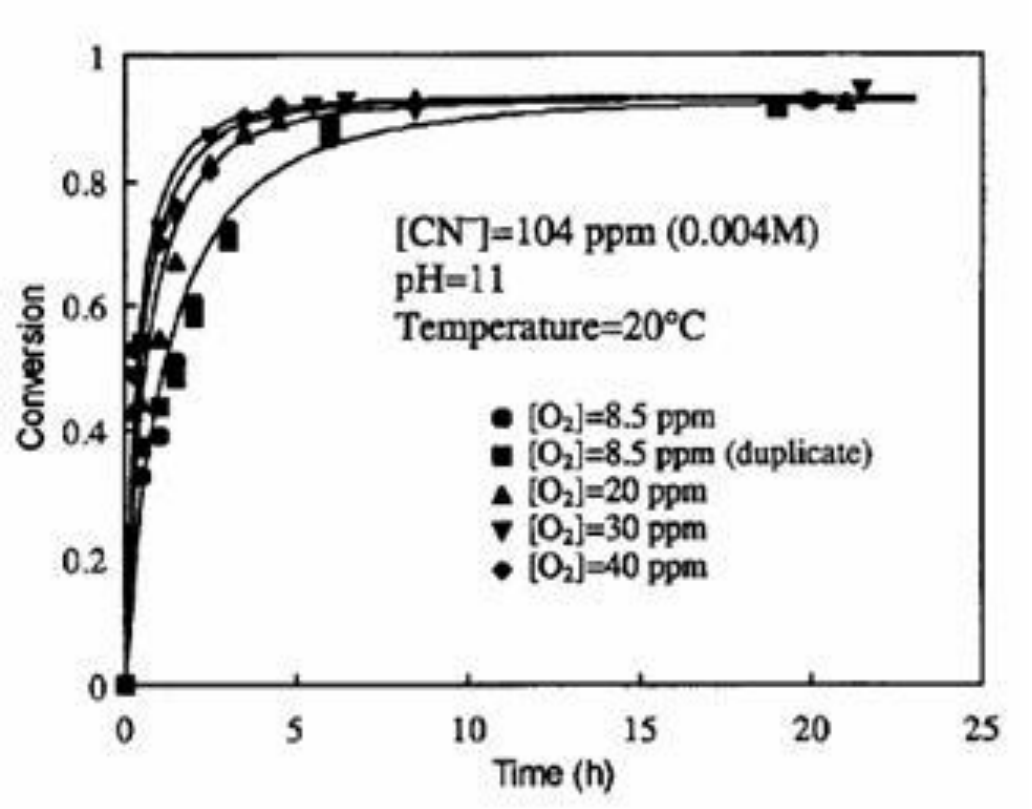

Figure 3.8: Effect of dissolved oxygen concentration on gold conversion (Ling et al., 1996).

Figure 3.9 plots the results Deschênes et al. (2003) reported on the effect of dissolved oxygen on gold extraction. It shows that an increase in the amount of dissolved oxygen increases leaching efficiency. These researchers noted that the concentration of dissolved oxygen had no significant effect on cyanide consumption, and that faster leaching kinetics was achieved when they used higher concentrations of dissolved oxygen.

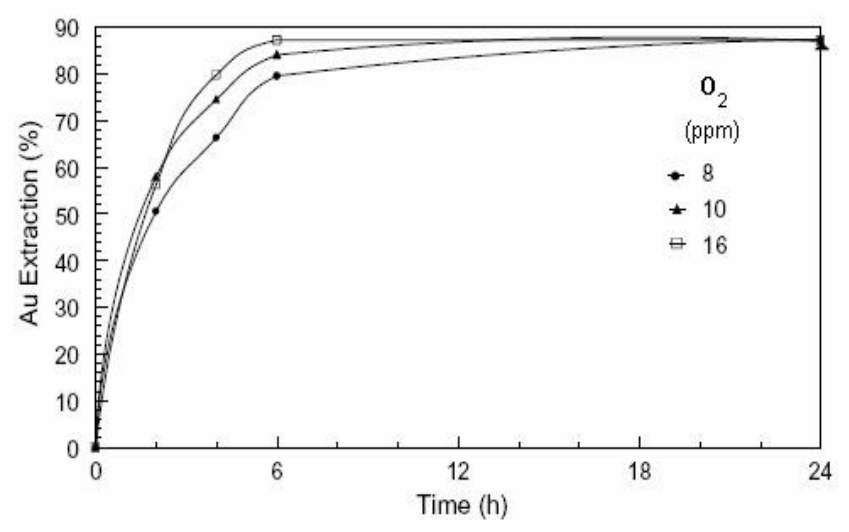

Figure 3.9: Effect of oxygen addition on cyanidation: pH 11.2, 500 ppm NaCN, 24 hours (Deschênes et al., 2003).

Figure 3.10, taken from Ling et al. (1996), shows the effect of cyanide concentration on gold conversion.

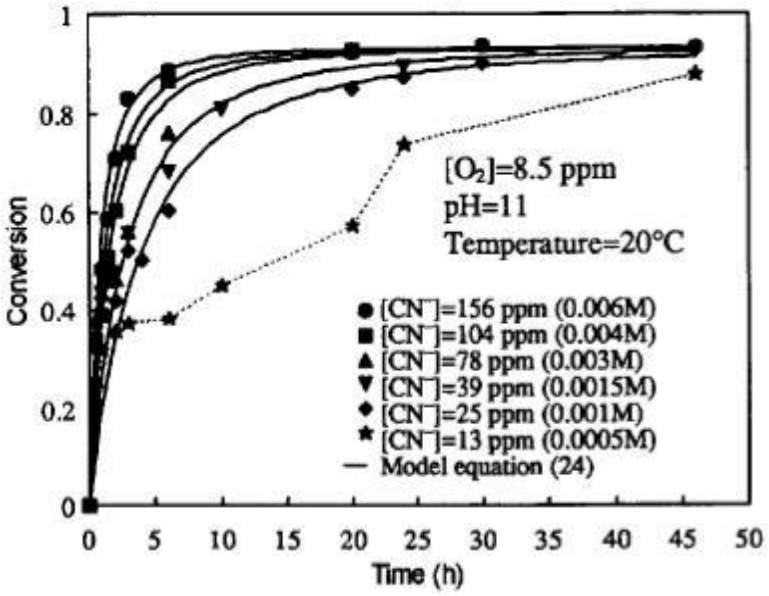

Figure 3.10: Effect of cyanide concentration on gold conversion (Ling et al., 1996).

These researchers found that the gold dissolution rate was not very sensitive to changes in cyanide concentration at high cyanide levels.

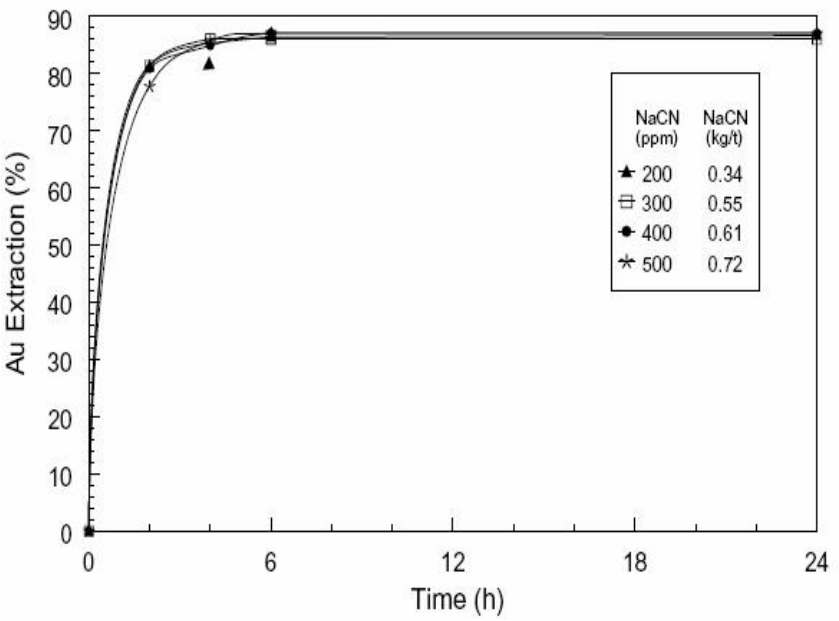

Figure 3.11: Effect of cyanide concentration on leaching. Pre-leaching: pH 11.2, 8 ppm O2, 100 g/t Pb (NO3)2, 12 h; cyanide: pH 11.2, 10 ppm O2 (Deschênes et al., 2003).

This result was confirmed by Deschênes et al. (2003), who reported that they had obtained similar overall gold extraction totals using 400–500 ppm NaCN (Figure 3.11).

3.3 Milling and Leaching Process Costs

African countries are facing a general increase in demand for electrical power. In South Africa, the demand is now surpassing the supply from ESKOM. This has resulted in load shedding strategies being implemented in many local communities in an attempt by the country's energy provider to cope with the high demand. Perhaps, a better approach is to propose use of energy efficient technologies in the country's largest power consuming industry; the mineral processing sector.

In mineral processing, milling is the highest consumer of energy. The objective of carrying out milling is not merely to reduce the particle size of the feed material, but also to liberate the constituent minerals that make up an ore. This is done so that valuable minerals can be separated from the gangue, in downstream processes, such as leaching. However, the milling process is generally performed relatively poorly, and at a considerable expense in terms of electrical power utilization. Tomanec and Milovanovic (1994) estimated that milling accounts for more than 50 % of the total power used in the concentration process, but this can rise to as high as 70 % for hard or finely dispersed and inter-grown ores. Apart from being relatively wasteful of energy, the milling process is also inefficient with regard to mineral liberation because of the indiscriminate nature of the grinding force.

The total milling costs are made up of grinding media, liner and energy costs. In ball milling, the effect of the grinding media plays a significant role in the determination of the milling costs. One can reduce these costs considerably by merely improving the efficiency of the ball impacts inside the mill. The impacts are influenced by the design of

liners as well as the type of discharge mechanism. Improving the efficiency of the grinding media impacts translates into reduced liner and grinding media wear rates as the balls get more involved in impacts that result in size reduction of the feed material, as opposed to ball-ball or ball-liner impacts. Dahner and Van den Bosch (2010) as shown Figure 3.12 studied the contribution made by the different liner designs on the total milling cost and found out that non-optimized liners contributed 10% of the total milling cost.

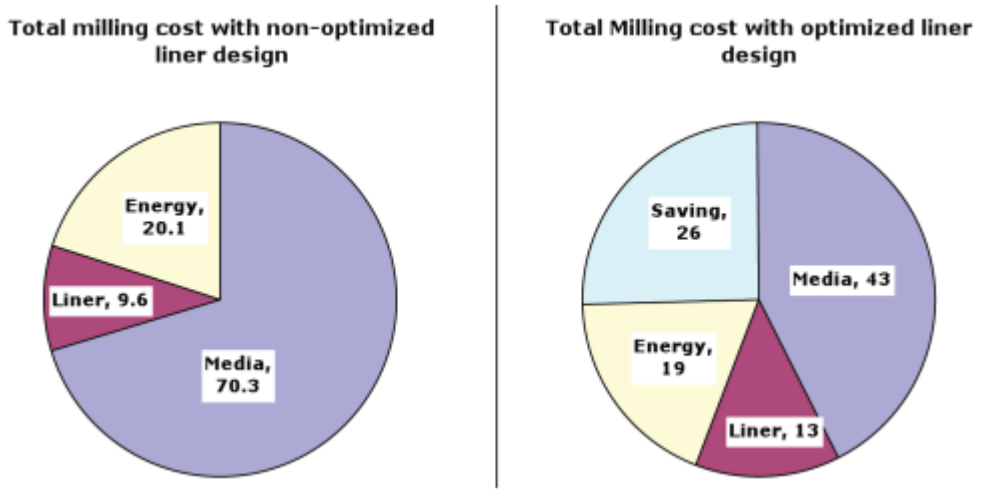

Figure 3.12: Total milling cost difference with optimized and non-optimized liner design (hypothetical case) Dahner and Van Den Bosch (2010).

Liners also play an important role in ball milling due to their strong influence on load motion and load behaviour Makokha and Moys (2006). The efficiency of the milling process also depends on the behaviour of the load inside the mill which governs the

nature of the ore which is being presented to the breakage action Makokha and Moys (2006).

In order to reduce the energy consumption associated with ball mills, autogenous grinding has been proposed Koivistoinen [1989] and there has been a 50 % reduction in energy, as well as milling costs due to elimination of costs associated with the use of steel grinding media. In the last 20 years a number of researchers have been coming up with strategies (Bwalya et al., 2014; Chimwani et al., 2013; Khumalo et al., 2007; and Metzger et al, 2009) and designs (B Dahna et al, 2015; Siraj et al, 2011) meant to reduce energy consumption and hence costs.

The type of discharge is of paramount importance as it has a high impact on the wear of the grinding media. For the same alloy, tests have proved that there is 30% less grinding media wear in overflow configuration vs. grate discharge. A higher percentage could be obtained if breakage occurs inside the mill. For an overflow configuration, the grinding media which has no impact or rather misses the feed material falls into the pool giving rise to less impact on the liner. The pulp cushioning effect causes softening of the impact between media and liner and due to this, breakage wear is much lower in overflow than in grate discharge.

Most of the gold produced in the world is extracted by the cyanide leaching of gold ores. The ore is first ground to expose the gold carriers and the milled material is then reacted with an oxygenated cyanide solution that dissolves the gold, leaving solid gangue minerals that are disposed of. The effect of particle size reduction and liberation on gold

recovery therefore plays a major role in gold leaching process. Most reported studies indicate that gold recovery increases with increase in fineness of the ground product (de Andrea Lima and Houidon, 2005). While it is acceptable that a finer size distribution is favorable to increase gold recovery by leaching, the benefits of the increased recovery could be offset by higher grinding costs and cyanide consumption (Breuer, 2008).

Studies by Stange (1999) on capital (CAPEX) and operation (OPEX) costs (Tables 3.1 and 3.2) associated with leaching, showed that labour, ball milling, reagents and chemicals contribute a high percentage to the overall cost for the process. Therefore when one is to consider optimizing both the milling and leaching processes, a trade-off must be struck in terms of degree of liberation or optimum particle size and recovery, so that both CAPEX and OPEX are kept minimal.

Table 3.1: Typical capital cost break down (Stange, W., 1999)

Item	**% of capital**
General site facilities	7.4
Service facilities	7.5
General piping utilities	6.5
General electrical	4.8
Process control	1.1
Waste reclamation and delivery	0.9
Ore delivery	2.7
Primary crushing	2.7
Ores storage	2.7
Milling	21.1
Thickening	5.1
Leaching	7.5
Adsorption	5.2
Elution	3.5
Gold refining	4.2
Reagent make up and dosing	1.4
Residue disposal	1.0
Tailings dam	5.5
Indirects	9.2

Table 3.2: Typical operating cost breakdown (Stange, W., 1999)

Item	**% of operating**
Reagents and chemicals	12.2
Consumables	16.3
Utilities	26.7
Maintenance	3.38
Labour	37.9
Tailings dam	0.8
Assays	2.8

After size reduction (milling) the pulp obtained is normally dilute and thickening (6-12% solids by mass) is performed to increase the pulp density to about 50% solids by mass. This in turn will reduce the size of the leaching plant that would be required and also the amount of leaching reagents required.

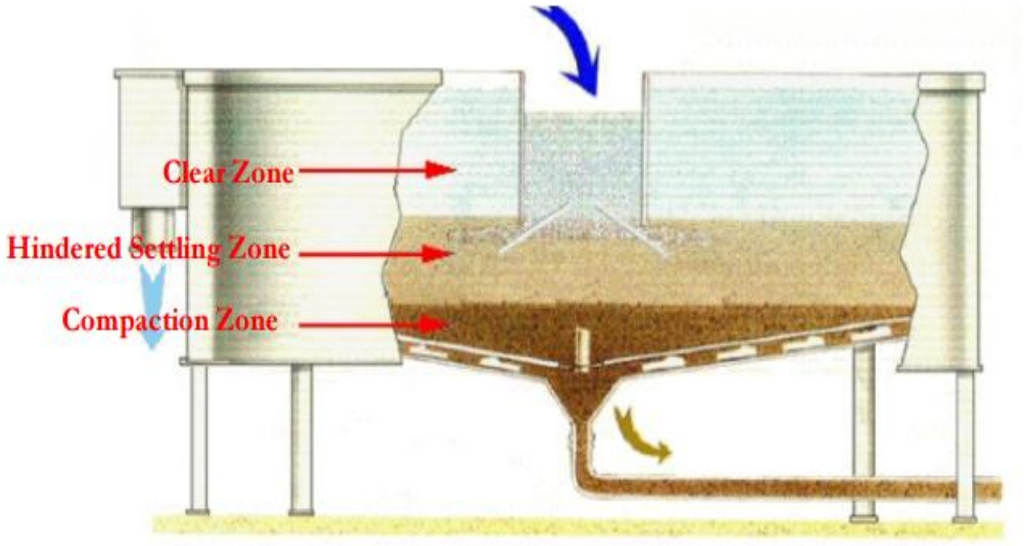

Figure 3.13: Operation of a continuous thickener

During thickening (also called sedimentation), the solids suspended form a thick pulp as they settle under the influence of gravity. The clear liquid, at the top and pulp at the bottom of the tank, can be removed continuously or occasionally. If fine grinding has been done the dewatering of pulps involves both thickening and filtration which has increased overall costs.

The thickening of a fine grained pulp is often supported by the use of flocculating agents. These are chemicals aimed at increasing particle settling rates in a thickener. They allow small individual particles to join together forming agglomerates which tend to settle much faster. The right amount of flocculant and correct flocculation are the most important factors to consider for a thickener. Coarse and hard ores will require less flocculant because particles are heavier and settle faster. Fine or soft clayey ores with fine size distribution require larger amount of flocculant and bigger thickeners because

individual fine particles settle very slowly. More flocculant means more costs for the process.

In leaching, an ore is brought into contact with a liquid phase, so that the values in the ore are removed by dissolving them from the solid into the liquid phase. Over the years, the use of reagents for extraction of minerals from ores has been the major treatment method and has proved to be very effective in the extraction of different ores. The right amount of the reagent under the right conditions should be applied to the process especially if the lixiviant is unstable or harmful. Excessive use will increase the overall cost and reduce the efficiency of the leaching process.

CHAPTER 4

4 EXPERIMENTAL SET-UP AND PROCEDURE

This chapter presents a detailed description of the experimental methods used to achieve the objectives of this study. The laboratory mill used for batch tests is described followed by the discussion of the testing conditions, the experimental programme, the materials used and the procedures used to fulfil the project objectives. The experimental procedure carried out in the laboratory comprises feed preparation; ball size selection; and batch tests, which involve both milling and leaching, and particle size analysis.

4.1 MILLING

4.1.1 Description of the laboratory grinding mill

The first part of the investigation involved the study of the milling kinetics of the gold ore in order to establish the breakage and selection function parameters. All the necessary batch grinding tests on the ore were done using the laboratory mineral processing mill, which is shown the in Figure 4.1, at the University of the Witwatersrand (Wits).

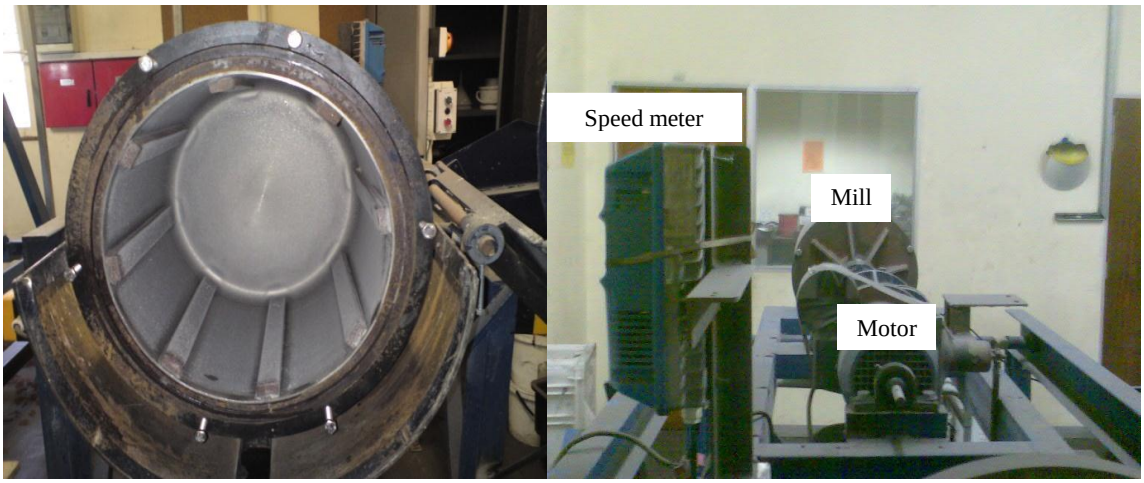

Figure 4.1: The front and rear view of the Mill equipment set up.

The mill has a capacity of ~ 20.2 litres, and is driven by a 2.5 kW speed motor that displays the speed in terms of RPM on a remote computer screen. It is installed on a steel structure that carries various control and measurement functions. The mill speed is controlled through an electronic speed meter that enables one to set and adjust the motor speed. The power of the mill can be measured through an instrument comprising a load beam, which converts the force exerted onto it into corresponding voltage. One of the ends of the load beam is attached to a rod, which is made to turn by the rotation of the mill. The mill is fitted with eight equally spaced lifters, and is driven by a variable-speed motor.

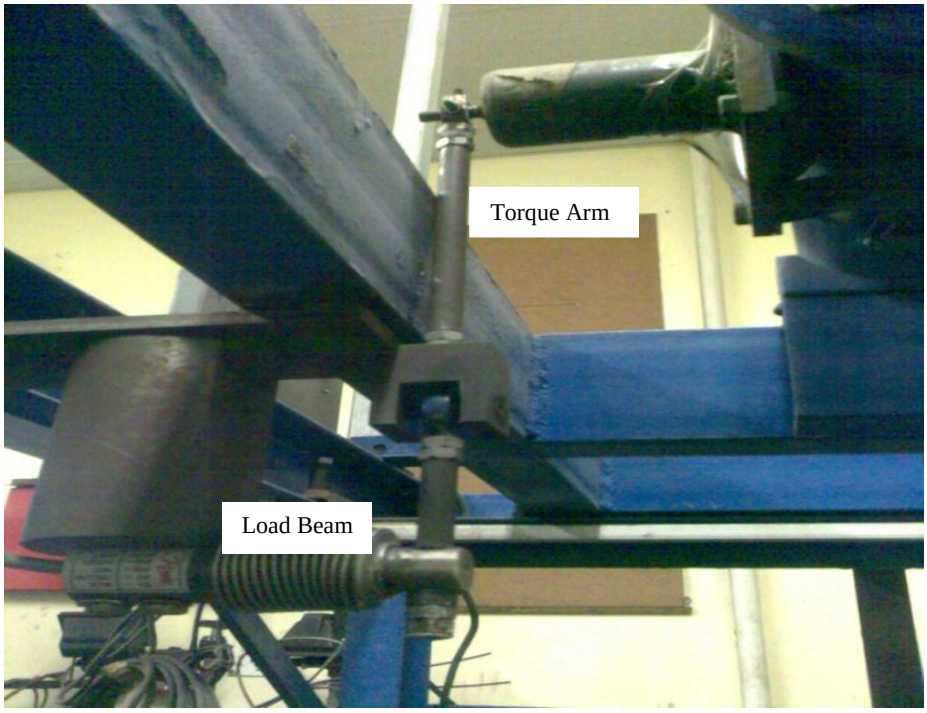

Figure 4.2: The calibration section of the mill equipment (Katubilwa, 2012).

4.1.2 Mill calibration

4.1.2.1 Speed calibration

The mill speed is calibrated by using a Macros scripted program on Excel developed by Moys (1993). The Macros script calculates the time it takes the mill to make one revolution and computes that speed. Then the mill is allowed to rotate for one minute at any given setting, and the program computes the average speed, which is then entered into the mill rig settings.

4.1.2.2 Torque Calibration

A series of known weights were suspended vertically from the end of the load beam when the mill was empty. The mill was then run at a selected speed for 60 seconds, and the average voltage supply was recorded using the wave-view program. Each suspended weight corresponded to a voltage. The load beam was mounted on the frame of the mill rig and connected to the mill axle. The torque was then calculated using Equation 4.1:

$$T(N.m) = mgx \qquad (4.1)$$

where: m is mass of the suspended masses in kg, g is gravitational force (9.81 m^2/s^2); and x is the distance from the center of the mill to the end of the lever arm.

In order to generate torque, the weight was suspended and the output voltage (from the load beam) related to the suspended weight (torque) was recorded. The values are displayed in Table 4.1.

Table 4.1: Relationship between the torque and voltage for cumulative masses.

	Cumulative Mass (kg)	Measured voltage (V)	Calculated Torque (N.m)
Bucket	0.200	-0.05	0.39
Mass 1	4.231	-1.34	8.30
Mass 2	8.341	-2.53	16.37
Mass 3	12.336	-3.70	24.20
Mass 4	16.312	-4.83	32.00
Mass 5	20.250	-5.98	39.73
Mass 6	24.246	-7.16302	47.57
Mass 7	28.258	-8.35635	55.44

A relationship between the two variables (voltage and torque) is obtained by plotting the results in Table 4.1 in excel and this gives a linear plot shown in Figure 4.3:

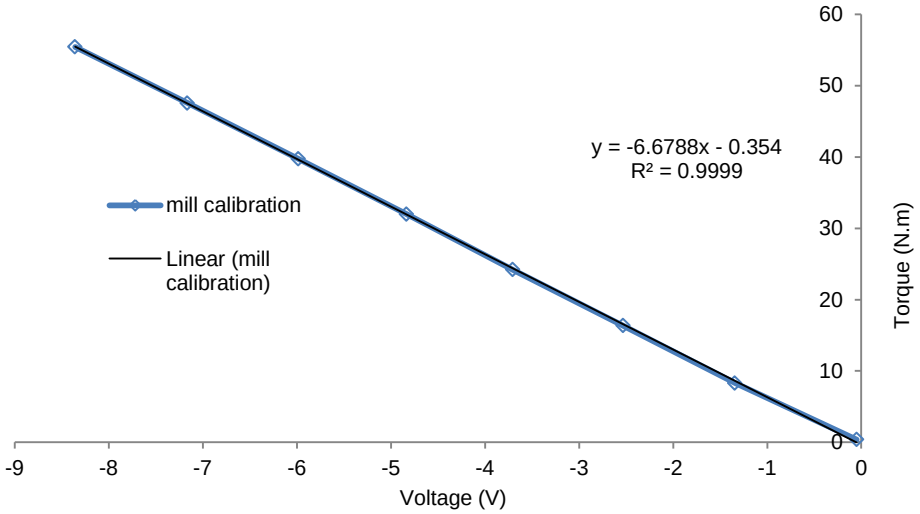

Figure 4.3: Relationship between voltage and torque for different masses suspended off the mill lever arm.

A model equation is then obtained from the graph which is given as:

$$T(N.m) = -6.6788V - 0.354 \quad (4.2)$$

where: T is the torque (Nm) and V is the voltage (V)

The torque obtained from Equation 4.2 can then be applied to obtain the power of the mill for any load using the equation below:

$$P(W) = \frac{1000[Speed\,(RPM) * Torque(N.m)]}{9549} \quad (4.3)$$

4.1.3 Milling conditions

The specifications of the mill are summarized in the table below:

Table 4.2: Mill conditions.

Mill dimensions	Diameter	0.302 m
	Length	0.282 m
	Volume	19.493 litres
	Speed	75% of critical speed
Liner configuration	Number	8
	Dimensions	0.013 m height
		0.025 m width

The operation of the mill follows the conditions described below:

$$\mathrm{Nc} = 42.3/\sqrt{\mathrm{D}-\mathrm{d}}\ (\mathrm{D},\mathrm{d}\ \text{in metres}). \quad (4.4)$$

$$\mathrm{J} = ((\text{mass of balls}/\text{ball density})/(\text{mill volume}))(1.0/0.6). \quad (4.5)$$

$$\mathrm{U} = \mathrm{fc}/0.4\mathrm{J}. \quad (4.6)$$

$$\mathrm{fc} = (\text{mass of powder}/\text{formal bulk density})/(\text{mill volume}). \quad (4.7)$$

The critical speed of the mill N_c is the rotational speed at which the balls just begin to centrifuge on the mill case rather than tumble. D represents the internal mill diameter and d the maximum ball diameter in metres. In general ball mills operate at speeds between 70-80% of the critical speed. The rotational speed of the mill is normally specified by ϕc, the fraction of critical speed. For the experiments, a fixed speed of 75% of critical was used because that is the value used by the plant that supplied the sample.

J gives the fractional ball filling, and is conventionally expressed as the fraction of the mill filled by the ball bed at rest. It is common practice to define the constant formal bed porosity as 0.4 for all calculations.

U is the fraction of the spaces between the balls at rest, which is filled with feed, and expresses the relationship between the powder loading and the ball loading. The formal bulk volume of powder is compared to the formal porosity of the ball bed. A value of U between 0.6 and 1 is normally used. The latter is normally a good feed ball loading ratio to ensure efficient ball loading in the mill.

f_c gives the mill filling by feed expressed as the fraction of mill volume.

Table 4.3: Feed material characteristics and preparation.

Material	Gold ore
Density (kg/m^3)	2650
Particle size	-1700+850 µm
Fraction of voids filled with powder (U)	0.75
Fractional mill filling by powder (fc)	varied
Volume % solids	75%

Ore from the Kloof gold mine, which is located 60 km west of Johannesburg, near Westonaria in Gauteng, a province of South Africa, was obtained for the batch milling and leaching tests. Kloof mine lies in the “West Wits” gold field, part of the Archaenage Witwatersrand Basin, between the north-trending Wit-poortjie Fault to the east and the Bank Fault to the west. The ore containing gold amongst other minerals is found to be quartz pebble conglomerate reefs. The gold generally occurs in association with pyrite and carbon.

The ore used in the experiments was first crushed using Kloof plant crushers to a size of -35 mm and was further processed using a cone crusher (to under 5 mm) and finally a batch ball mill, as shown in Figure 4.4.

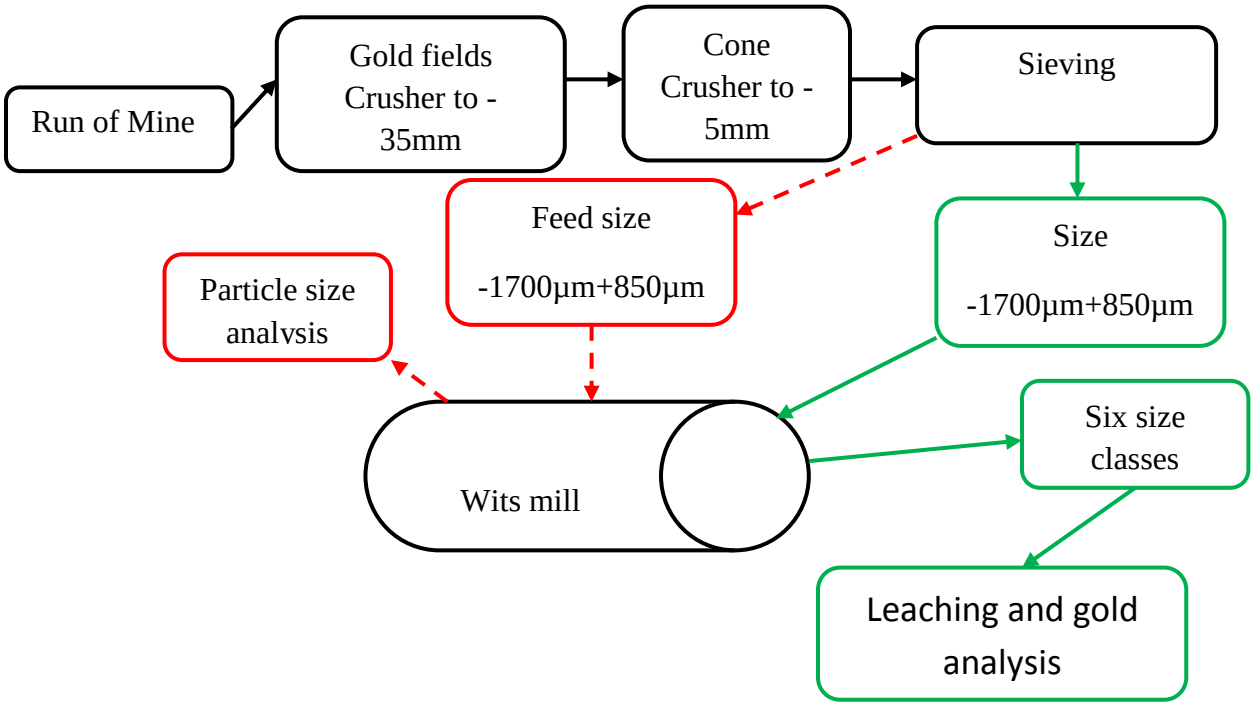

Figure 4.4: Overview of the breakage, leaching and particle analysis stages.

The material leaving the cone crusher (under 5mm) was sieved, and then a size class (-1700 µm + 850 µm) was prepared, separated and then used for milling experiments.

For the leaching tests, we first milled the -1700+850 µm size material, used sieves to classify the product into six size classes and then leached these separately. The size classes selected for the leaching tests (Table 4.4).

Table 4.4: Size classes used

Size class	Upper (microns)	Lower (microns)
M1	-1700	+850
M2	-850	+300
M3	-300	+150
M4	-150	+75
M5	-75	+25
M6	-25	0

4.1.3.1 Grinding Media

Figure 4.5: The 20 mm steel grinding media used in experiments

The *J* value (fractional ball filling) is the percentage of the mill occupied by the grinding media. Values of 5, 10, and 30% were selected to span the range from a low to a high

value. From the different sizes of spherical balls the researcher selected 30 mm for one set of experiments, and 20 mm and 10 mm for the other two sets.

Table 4.5: Media conditions used.

Material	Stainless steel balls
Diameter (m)	10, 20 and 30mm
Density (kg/m^3)	7600

4.1.4 Feed preparation for laboratory tests

The percentage of voids filled by powder (gold ore) gave a U value of 0.75.This was selected to limit the amount of ore to load into the mill in the large J cases. The solids percentage c was kept at 75% and is selected as an average for the whole milling process. The mill rotation rate Φ_c is relative to the critical rotation rate of the mill and a value of 75% of critical speed was used.

The size less than 1700 microns is divided into 6 classes and these were chosen to provide a span within the region on which leaching could be performed in order to test the leaching behavior of the different size particles,

4.1.4.1 The batch grinding test

Experiments were carried out using the laboratory mill shown in Figure 4.1 according to the conditions specified in Table 4.1 using the ball size, media and charge filling shown in Table 4.2. A measured feed (-1700+850 μm), grinding media and calculated amount of water were loaded into the mill and ground for three minutes, after which the mill was stopped and contents emptied in a bucket. Another four more grinding times of 5, 15, 30 and 60 minutes were carried out for each set of conditions. The slurry obtained after each grinding time was sun-dried and mixed using both a riffle splitter and cone and quartering method. The samples collected afterwards were then dry screened using standard laboratory screens and taken for particle analysis.

The experiments were conducted under the conditions specified in Table 4.6; using the ball size distribution, media and charge filling shown.

Table 4.6: Conditions for milling kinetics experiments on varying J (ball filling) on milled material.

Run Number	J (%)	d_m (mm)	Mass of powder (kg)	Mass of media (kg)	Volume of water (ml)
1	5	10	0.491	4.697	163.67
2	5	20	0.491	4.697	163.67
3	15	10	1.474	14.091	491.01
4	15	20	1.474	14.091	491.01
5	30	30	2.946	28.182	982.02

After adding media, feed material, a calculated amount of water was added which causes slurry to form with slurry density given as;

$$c = (w_s/\rho_s) \times 1/\{(w_s/\rho_s) + [(1 - w_s)/\rho_l]\} \quad (4.9)$$

The Equation is explained in detail in section 2.1.4.4

Table 4.7: Conditions for milling kinetics experiments with varying U (Interstitial filling).

Mill speed	Operational	75% of critical			
Balls	Diameter	20mm			
	Assumed bed porosity	40%			
	Ball filling volume, J%	20%			
Material	Feed size µm	1700-850			
	Interstitial filling, U%	50	75	100	175
	Powder filling volume, f_c	0.01	0.015	0.02	0.035

4.2 PARTICLE SIZE ANALYSIS

A stack of sieves with a descending order of fineness was used to make a complete size analysis of ore product collected from the mill. A screening test was initially done in order to establish the optimum screening time required to allow the material to be screened without residual contamination from fines or over-sieving, which leads to pre-breakage of material before milling. Batch sieving over an extended period removes all the near-size material, because the continually abrasion of these particles reduces them to a size that will pass through the screen. This is why a sieving time duration needs to

be chosen long enough to permit small size materials to fall through the sieve, yet short enough to prevent much abrasion had to be determined.

In order to establish an optimum sieving time, a sieving rate study was carried out following a standard procedure set out by Austin *et al*. (1984). A 200g sample of material was sieved for 5, 10, 15, 20, 25 minutes. Material passing through the smallest screen size was monitored for all sieving times, until there were no more significant changes in mass on each sieve. The test was conducted and an optimal sieving time of 20 minutes was established.

The sun-dried material was then screened for 20 minutes, using 850, 300,150, 75, and 25µm mesh sieves and the pan at the bottom of the sieve stack. After dry screening, each sieve was weighed in order to determine the mass of material it retained. The sieves were then re-stacked again in their previous order, without the pan at the bottom, and wet washed until all the finest particles had been removed. The washed samples were then dried in the oven at 50 ˚C, after which the dried material remaining on each sieve was then weighed.

The process was repeated for all samples that were removed from the mill after each grinding time. The same screens were used throughout the experiments, in order to maintain consistency. The mass of the material on each sieve in the stack was added and the total mass was subtracted from the initial mass of the sample before wet sieving. The difference in the mass gave the mass of the washed fine material.

4.3 LEACHING

4.3.1 Material and methods

A 300 ml wide-necked glass container was used as a reaction vessel for this experiment. The central neck holds a plastic seal and shaft of the glass stirrer, which is a plastic two-blade propeller mixer. The vessel was placed in a constant temperature water bath, fastened and clamped to a retort stand. Figure 4.6 illustrates the experimental setup.

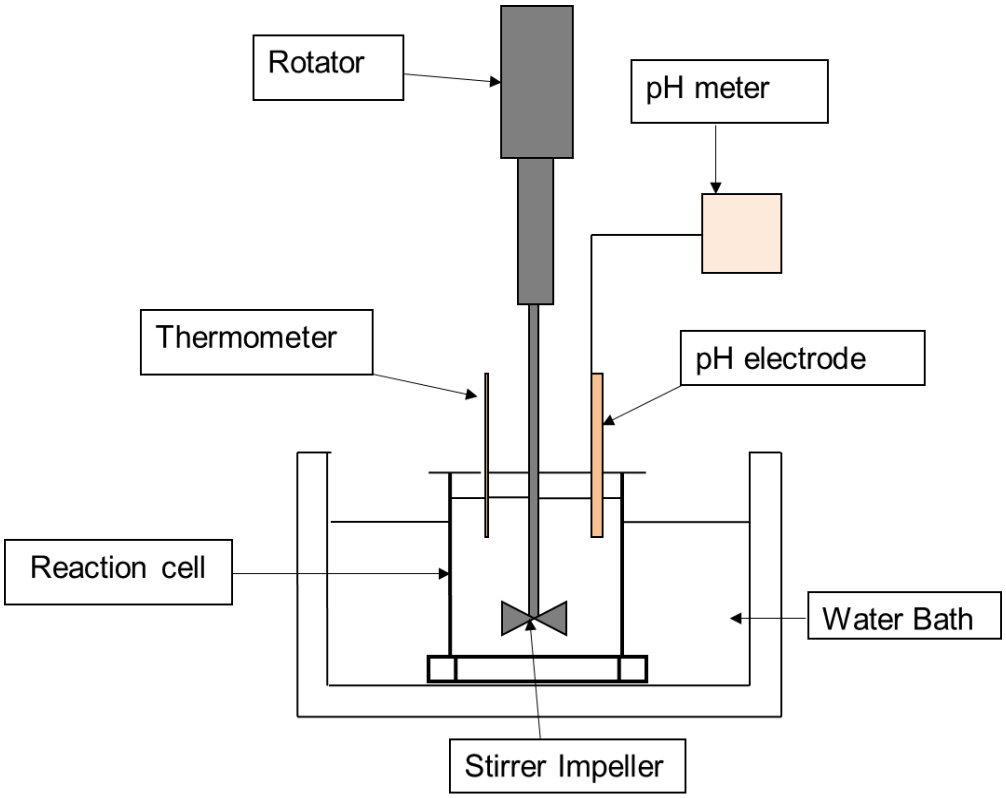

Figure 4.6: Schematic diagram of equipment set-up for the gold leaching process.

The leaching experiments were done covering a range of parameters. The variables tested were particle size, temperature, leachant concentration and agitation speed. Table 4.8 and 4.9 gives the specific conditions applied .

Table 4.8: Leaching test parameters for a base case.

Parameter	Value	Unit
Liquid to solids ratio	1:1	by mass
Dissolution period	24	hrs
Lime addition	1	kg/t CaO
pH	12	
Cyanide addition	0.3	kg/t NaCN

Table 4.9: Leaching conditions.

Parameter	**Concentration of NaCN solution (ppm)**	**Temperature (^{0}C)**	**Agitation speed (Rpm)**	**Particle size (microns)**
Value	30, 75, 210, 400 and 500	25, 40, 60, 80, 100 and 120	180, 360, 720, 900 and 990	Shown in Table 4.4

4.3.2 Feed preparation for leaching tests

An ore sample weighing 200g was poured into the reaction vessel (fitted with a mechanical stirrer as illustrated in Figure 4.6), and 200ml of water was added to make slurry. The pH of the sample was then adjusted by adding lime (CaO), maintaining a pH value of ~12. The lime was added to maintain the pH of the pulp above 11 in order to avert the danger of producing poisonous HCN. The leachant (sodium cyanide) was then added according to the set parameters to begin the leaching process.

4.3.2.1 Sodium cyanide calculation

$$Concentration = Mass/Volume$$

For instance in order to make a solution of 210ppm concentration of cyanide the mass of cyanide to be added to the reaction vessel is given by

$$Mass = C\,V\,/1000 = 210 * 200/1000 = 42\,mg = 0.042g\ of\ NaCN$$

Therefore 0.042g of NaCN is added into the reaction vessel.

4.3.3 Leaching test

The reactor containing the ore sample, distilled water and lime was conditioned for one hour before adding the calculated amounts of sodium cyanide. This was done at the start of each leach test and tests are carried out for one, two, three, five and 24 hours,

on material from each of the chosen size classes. After the completion of each leaching run, the samples were filtered through a Buchner funnel to remove the leach liquor. The leach liquor was re-filtered on a Millipore filter before being taken for gold analysis, using an Atomic Adsorption Spectrometer. The same procedure was then repeated for all the samples that were being investigated. After analysing the filtrate for gold, the slurry was washed two to three times with distilled water. Thereafter the solid was dried and sent for gold analysis.

4.4 DATA COLLECTION AND PROCESSING

4.4.1 Milling

Raw data collected from the experiments was used to determine the breakage function parameters (β, γ, $\boldsymbol{\Phi}$) and selection function parameter (α) using the progeny fragment distributions from the breakage of the mono size classes.

4.4.2 Leaching

The collected data were then analysed using the shrinking core-model first developed by Yagi and Kuni (1955). The rate of the reaction is given for the models, based on control by either chemical reaction at the surface, or diffusion by film or ash.

When diffusion through the product layer controls the kinetics, the equation is given as follows (Levenspiel, 1972):

$$1 + 2(1 - x) - 3(1 - x)^{\frac{2}{3}} = \frac{6aMDC}{\rho r_0^2} t = k_d t \quad (4.10)$$

If controlled by the surface reaction the following equation applies:

$$1 - (1 - x)^{\frac{1}{3}} = \frac{k_c MC}{\rho a r_o} t = k_r t \quad (4.11)$$

where k_r and k_d are chemical rate constants (cm/ min), X is the fraction of gold dissolved in time t, D is the diffusion coefficient of ions in porous media ($m^2/\min$), k_c is kinetic constant, M the molecular mass of the solid, C is concentration of lixiviant (cyanide), a is the stoichiometric coefficient of the reagent in the leaching reaction, ρ is the density of the solid and r_0 the initial radius of the solid

4.4.3 Experimental repeatability

Some replicates were run so as to study the repeatability of the tests. This is of paramount importance as it provides great awareness into experimental variability and it also helps distinguish real effect of operational variables from ordinary differences, which are within experimental error.

Figure 4.7 and 4.8 illustrates results of selected batch tests to show repeatability and variability of the experimental data. Each curve and its respective duplicate show good agreement, indicating the existence of very small errors during the experimental procedure and thus the degree of variability of each experiment.

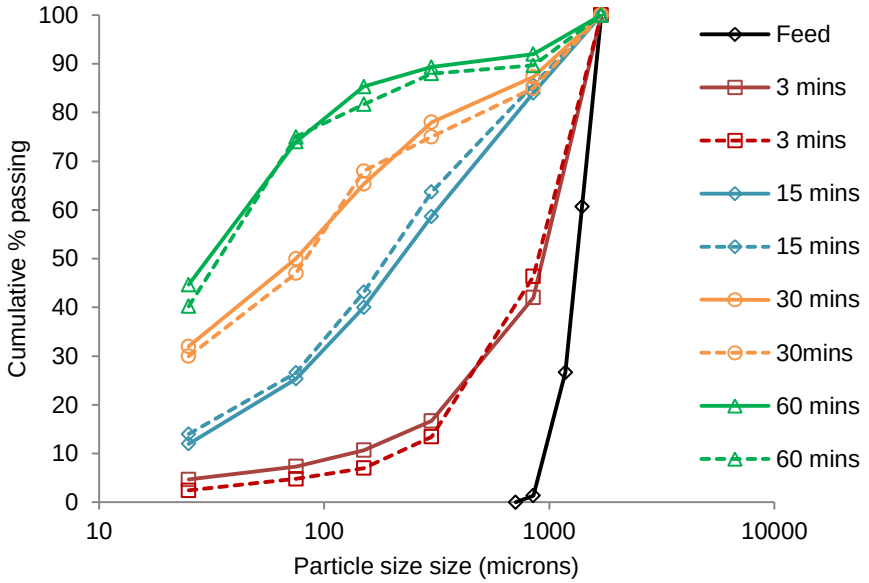

Figure 4.7: Replicates for class size distributions with J= 5%. Cumulative % passing profile vs. particle size comparisons for 10 mm ball sizes.

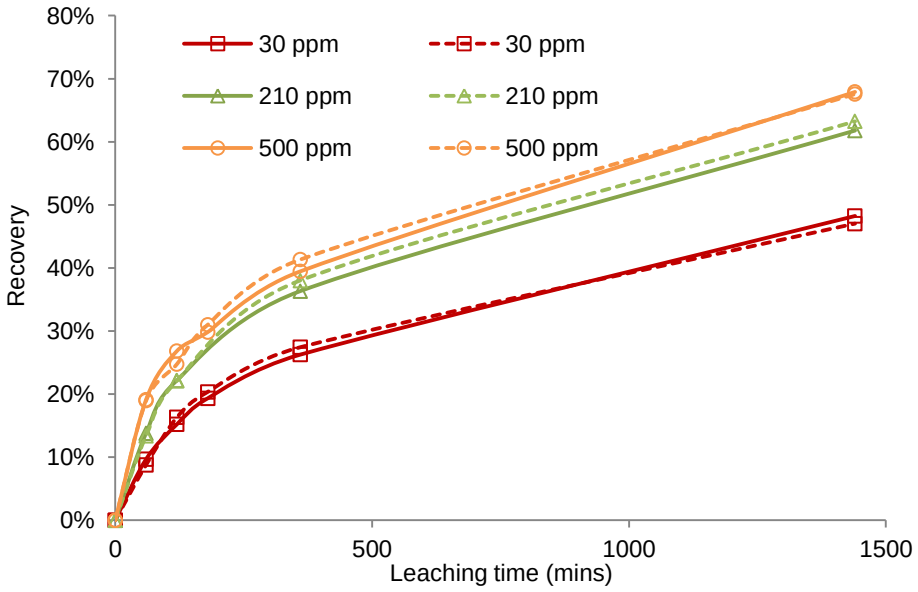

Figure 4.8: Replicates on effect of sodium cyanide concentration on gold dissolution (experimental conditions: particle size, -150 + 75 µm; temperature, 25^{o} C).

SUMMARY

Experimental tests were successfully completed using the equipment and conditions described in this section. The data that relates to the internal dynamics of the mill are dependent on design and operational factors such as the mill filling, mill rotational speed, grinding media filling and media size. The results were generated and analysed.

CHAPTER 5

5 A LABORATORY INVESTIGATION OF AN INTEGRATED COMMINUTION AND LEACHING PROCESS.

The content of this chapter has already been submitted to a journal as an article for publication. The article has a number of authors. The specific contribution made by the writer of this thesis consisted of designing and conducting experiments, making an analysis, discussing the results with his supervisors (who are named as co-authors of the article) and drafting the manuscript. Some of the data were presented at a "Comminution 2012" Cape Town international conference. Many of the details given in this article repeat matter already covered in previous chapters of the thesis.

Abstract

Comminution and leaching unit processes play a major role in extracting valuable minerals from ore. Most of research reported in the literature has focused on optimising individual unit operations rather than on integrating the whole process. The development of an integrated approach to mineral processing systems and flow sheets was intended to create a methodology for process synthesis that can be applied throughout the extractive metallurgical industry. This would lead to improved efficiency in the overall process by obtaining optimum recovery and, most important, a reduction in energy and material costs.

In this chapter laboratory scale grinding and leaching profiles for a gold feed sample (1700–850 µm) in a laboratory mill are presented. Various combinations of grinding media filling level and ball size were investigated, and the results showed that breakage is most pronounced with ball size of 20 mm. Using a higher filling (J = 30%) and a ball size of 30 mm, more energy was consumed with less liberation occurring, so that low amounts of gold were extracted during a 24-hour leaching period. Surprisingly, when adopting a smaller J of 15% and 20 mm media, more gold was liberated and less energy was required. In terms of overall profit, 15% and 5% J with the 20 mm media provided a maximum profit of US$489 per ton of feed processed. In attempting to explain this result, a number of experiments were carried out that involved an investigation into the relationship between comminution and leaching in terms of energy usage and particle size, the former to establish the most efficient application of energy, and the latter to identify the degree of fineness that would ensure optimal recovery.

5.1 INTRODUCTION

In processing gold ore, comminution is carried out on slurries. The material is gradually reduced in size to produce material of the desired size class. This is done to expose, or to free, the valuable mineral (in this case gold) from the gangue material before the crushed slurry is leached.

The comminution process is extremely energy-intensive, and currently consumes between 3–4% of the electricity generated worldwide, and accounts for up to 70% of all

the energy required in a typical cement plant (Fuerstenau et al., 1999). Therefore a small improvement in comminution efficiency can significantly reduce the amount of energy used, and consequently have a large impact on the operating costs of a plant while conserving resources.

Many researchers have studied various aspects that characterise the comminution process. Milling kinetics (Austin et al., 1984), load behaviour (Liddell and Moys, 1988; Dong and Moys, 2003) and mill power (Yildirim et al., 1998; Morrell, 1993) have been investigated in terms of media size; feed particle size distribution, fraction of mill filled with balls and powder, mill diameter, mill speed and other variables that affect this kinetics. However, very little research has been done on applying an integrated approach to the comminution process that takes into consideration the requirements of the downstream recovery processes such as leaching.

5.1.1 Milling and power usage

The amount of power drawn is of paramount importance in comminution. The relationship between comminution energy and product size has been extensively studied. Theoretical and empirical energy size reduction equations have been proposed by Kick (1885) and Bond (1952). Mill power is a function of the mill's size, length and diameter, loading *J* and operating conditions such as mill speed *N*, slurry/void ratio and slurry density (Rose et al., 1958). Power prediction for a tumbling mill (Taggart, 1945) involves determining its internal dynamics and the net power required for a particular

purpose (for example, the hardness of the ore and the particle size required). Therefore a clear understanding of the motion mechanics of mill charge is crucial.

5.1.2 Leaching

Leaching is fundamentally a separation process, which involves the dissolution of a metal or mineral in a liquid. Crundwell (1997) describes leaching, a downstream process that is used in the recovery of valuable metals, as central to the hydro-metallurgical treatment of ores.

Maclaurin introduced cyanidation (leaching using cyanide) in the late 19th century (1893). Ever since, this process, which is widely used, has been the subject of intensive investigation (Habashi, 1967). It is an electrochemical process that relies on the fact that gold dissolves in alkaline cyanide solutions and forms a gold cyanide complex [$Au(CN)_2^-$], which is then processed further. Chapter 3 section 3.2 contains a detailed description of this operation.

5.1.3 The integrated milling and leaching process

During the recovery process, ore is ground to expose the gold carriers, and the ground material is reacted in an oxygenated cyanide solution that dissolves the gold, which is removed, leaving solid gangue minerals that are then disposed of. The degree of gold particle liberation is the major focus of the leaching operation, and recent research by De Andrea Lima and Houidon (2005) confirms the consensus among other scientists in

the field that gold recovery increases with the fineness of the milled product. The reason is that, as the particle size becomes finer, the leach reagent has better access to the gold in the material. However, while a finer size distribution favours greater gold recovery, this is offset by the higher costs consequent on the increases in grinding time and cyanide consumption required (Breuer, 2008).

As a result of this it is proposed that a new process that integrates the grinding and cyanide leaching operations may provide a tool that helps to identify more precisely the optimum size distribution in processing a gold ore and to study various flowsheet configurations, such as the separate leaching of coarse and fine particles.

In leaching, particle size or degree of liberation are major factors that affect the dissolution rate of an ore. Larger particle sizes require a prolonged residence time in a sequence of leaching vessels. Finer particles leach faster, as the valuable material has been liberated to a larger extent beforehand, and therefore require a shorter residence time and fewer leaching reactors. This has a direct effect on the capital expenses involved in carrying out the leaching process. Therefore, when optimising a joint leach and comminution process, the engineer needs to strike a trade-off between the milling costs relating to particle size and the costs of the amount of reagent used for liberation.

The main objective in this chapter was to investigate the effect of milling conditions on the amount of gold recovered through leaching.

5.1.4 Numerical Approach

5.1.4.1 Discrete Element Method (DEM)

The soft-sphere Discrete Element Method (DEM) model is a numerical simulation method that calculates the motion and collision contacts of each particle within a granular system. Originally DEM was developed for use in calculating molecular dynamics, but due to the pioneering work carried out by Cundall (1971), Cundall and Strack (1979) and Mishra and Rajamani (1990), this technique has been extended to milling. The DEM involves the application of Newton's laws to describe the motion of particles and the implementation of a surface response procedure when a collision occurs.

The soft contact approach proposed by Cundall allows an overlap to occur between two approaching entities. Small overlaps in the normal and tangential directions, which result in a repulsive force created by contact between the particles, are calculated according to the force-displacement model of Tsuji *et al.* (1992). This repulsive force is entered into Newton’s equations of motion to determine the resultant accelerations, which are then used to determine the velocities and positions of all elements at the next time step. This process is repeated, with the DEM calculating new overlaps, forces, accelerations, velocities and positions to develop flow profiles and simulate the bulk behaviour of the granular assembly. Remy et al. (2009) gives more detail on the simulation method and (Cleary, 2009) reviews some practical applications of DEM. The properties of the grinding media and mill shell are selected to be close to that of steel and properties of the material are chosen to be close to that of quartz. The potential of

applying this technique to the minerals industry in general is vast, as particles are encountered in many unit operations.

5.2 EXPERIMENTAL TECHNIQUE

The experimental programme was carried out on the laboratory mill as discussed in Section 4.1 with the specifications and test conditions described in Tables 4.2 and 4.6. The tests were conducted using mono-sized balls on different feed sizes. All the experiments were done with wet milling, as this is the norm for all industrial comminution of gold ore.

5.2.1 Experimental Energy usage

It is generally accepted that the amount of power required to grind material in a ball mill to the desired product size is an indication of the mill's capacity, and that the energy needed depends on the varying behaviour of the load. In that respect, any change in the operational variables of the milling that have a direct impact on load behaviour will cause a change in the mill power and subsequently the mill capacity.

In this research study, an estimation of the amount of mill power required as a product of the mill's rotational speed and torque (Section 4.1.2.2) was done.

5.2.2 Feed material preparation and milling experimental method

Ore from a Witwatersrand gold mine was crushed in a jaw and cone crusher and classified by sieving through a stack of sieves. The ground material was sieved for 20 minutes into the 1700–850 µm size class range as preparation for the feed to the laboratory ball mill.

The overall preparation of the ore for laboratory tests is described briefly in Section 4.1.3.

The procedure for milling and leaching tests is illustrated in Figure 4.4. The feed sample was ground for a short time, and the ground material was then split into the six different size classes shown in Table 4.4. A sample of each size class was taken for head grade assaying, to determine the amount of gold in the sample. Thereafter, 200g samples of the gold ore were leached from each of these size classes for the five different time periods. After leaching, these samples were assayed to recover the amount of gold that remained. The data obtained were used to characterize the gold distribution within the different size intervals of the samples.

5.2.3 Leaching experimental method

Dissolution experiments were carried out on 200 g samples from each size class in a glass reactor with a mechanical stirrer. The leaching procedure and conditions are all described in Section 4.3.

5.3 RESULTS AND DISCUSSION

One of the major goals of this investigation was to determine the extent of the trade-off between the additional gold recovery that is a function of reduced particle size, versus the cost of the energy consumed to achieve that reduced particle size. To that end, the power draw of the experimental mill was investigated following two approaches: 1) the measurement of the power draw in the laboratory via the torque-arm approach described in section 4.1.2; and 2) a computational estimate obtained from the Discrete Element Method (DEM) approach, which is used extensively to study the general flow behavior within a tumbling ball mill environment, and in particular, the power draw (Djordjevic, 2003).

The DEM can simulate the dynamic interaction of particles in any environment, and it can predict the dynamics of charge motion for individual particles, and provides a means of measuring the forces or stresses between particles. This information can be combined with particle strength distribution data and load holdup estimations to predict the breakage rates of the size fractions in the charge.

Table 5.1: Results for calculated and measured power values.

Test Condition	Power (Watts)	
	DEM	MEASURED
J=5% dm=10mm	13.79	11.63
J=5% dm= 20mm	9.98	9.539
J=15% dm=10mm	48.61	44.94
J= 15% dm=20mm	37.42	35.52
J= 30% dm=30mm	80.99	75.081

The power measured and that obtained through DEM are shown in Table 5.1 above. The results show at a mill filling of 5% and 15% the 10mm balls consume as much as 30% more power than the 20 mm. Also the power draw increases > 3.5 times as J is trebled from 5% to 15%.

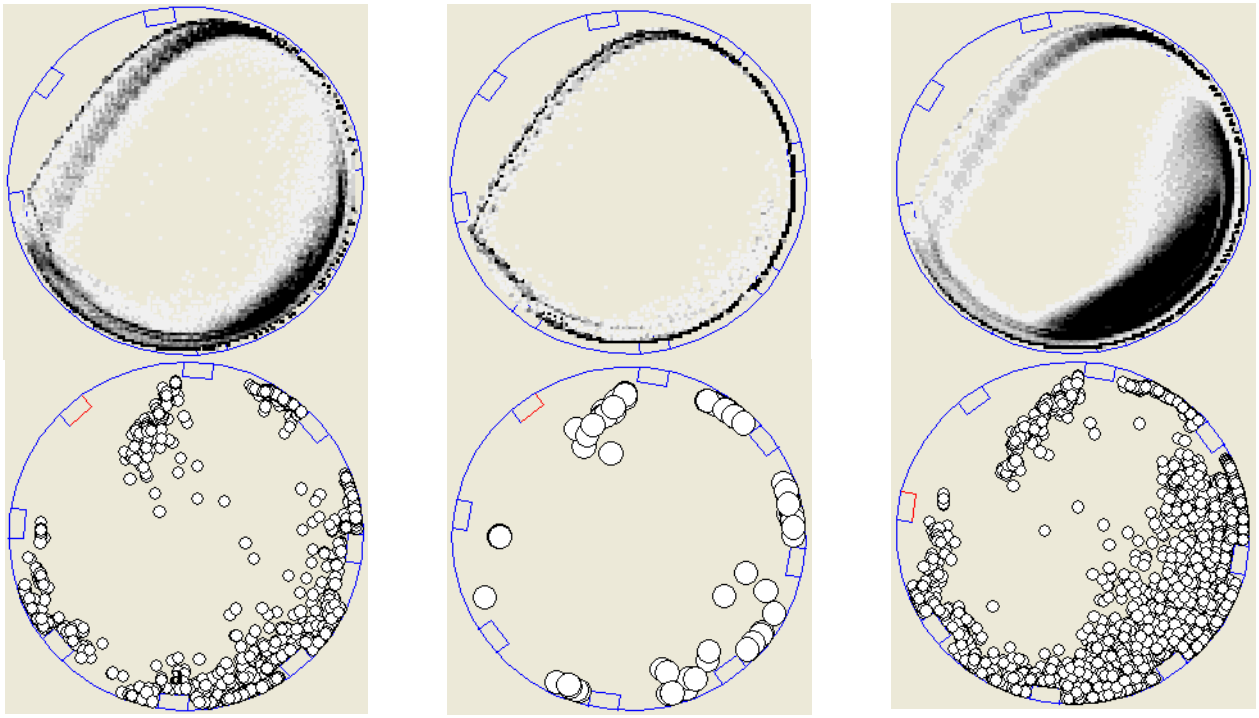

(a) J=5% (4.5kg) 10mm balls (b) J=5% (4.51kg) 20 mm balls (c) J=15% (13.49kg) 10mm balls

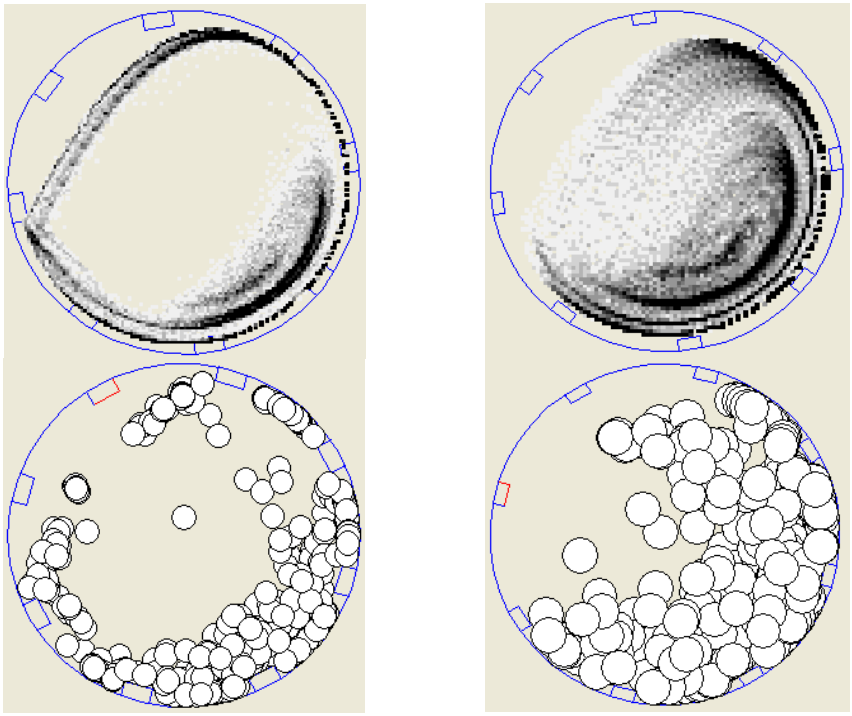

(d) J=15% (13.49kg) 20 mm balls (e) J=30% (28.1kg) 30mm

Figure 5.1: Simulated charge motion of 19.49 litre mill.

Figure 5.1 (a) and (c) shows that the smaller 10mm balls are raised higher by the lifters before rolling off the liners, and therefore the mill has to draw more power to raise them. Diagrams (b) and (d) explain why 20 mm balls draw less power. It is also possible that that the 20 mm balls give back more kinetic energy to the mill, as they fall on the toe side. Instead of the mill lifting the balls, the balls are trying to turn the mill as they fall on the toe side of the mill. In a ball mill, the power consumption varies according to the shifting of the centre of gravity in the internal volume of the mill. When the mill is empty, the fraction of volume occupied by the grinding media is greater; but when the mill is filled with feed, as the centre of gravity of the grinding media shifts upwards, the fraction of volume occupied by the grinding media decreases and therefore the power consumption diminishes.

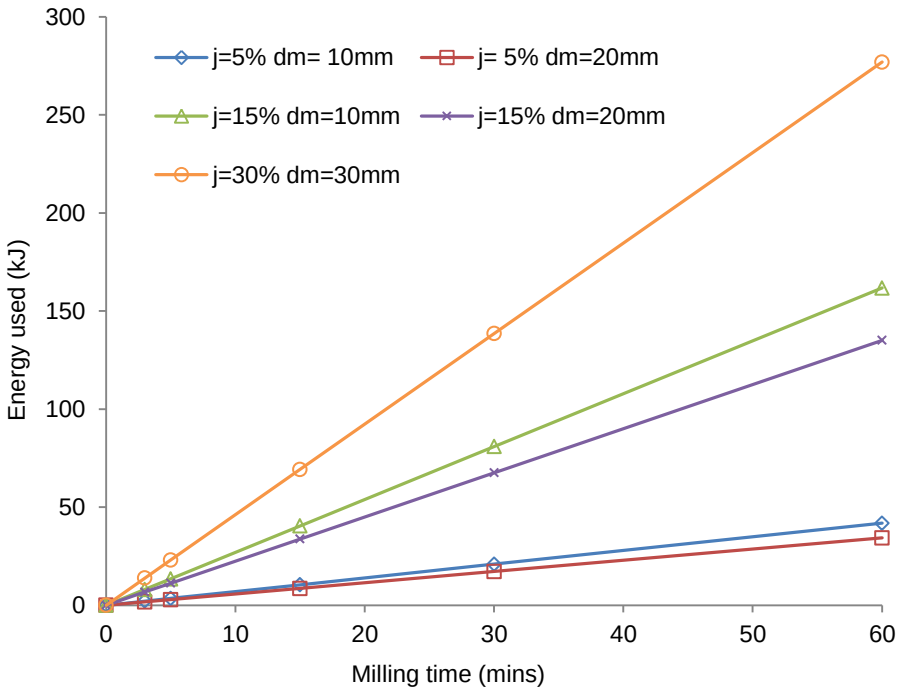

Figure 5.2: Variations in the energy used with milling time.

Figure 5.2 shows how the energy varies with grinding time and ball fill (J). From the results presented, total energy consumption increases with the ball fill and milling time. Interestingly, it can be seen that for both low ball filling values ($J = 5\% \; and \; 15\%$), the bigger balls draw less power than the smaller balls.

5.3.1 Milling particle size distributions

Figure 5.3 gives the grinding and the cumulative passing profiles for the low J value of 5% using 10 mm media. It can be seen that, as the mill rotates, material of size class one breaks and therefore decreases as it passes into a smaller size class. In the intermediate classes (M_2–M_5), the mass initially rises then finally reduces as milling proceeds. The mass fraction of size class six is ever-increasing, until all the material breaks into that size class.

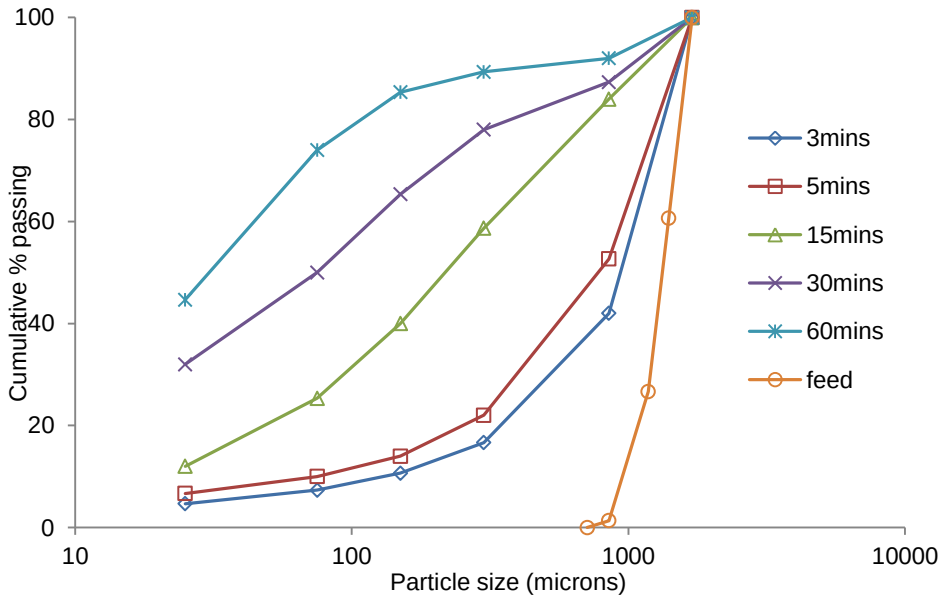

(a)

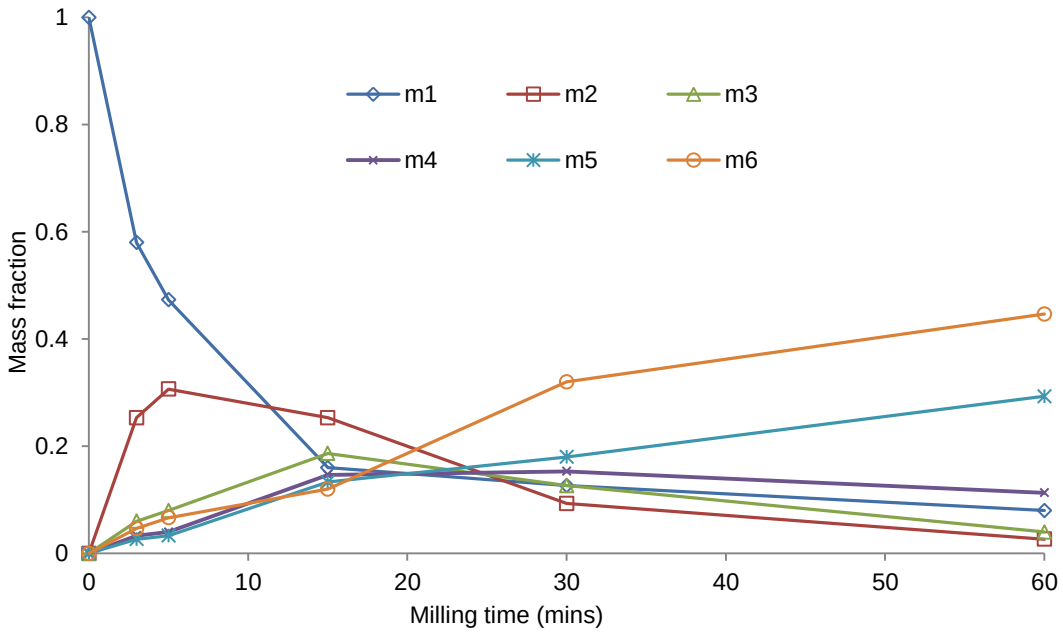

(b)

Figure 5.3: Class size distribution at (J = 5% d_m = 10mm). (a) Cumulative % passing vs. particle size (b) Grinding profiles of all six class sizes vs. time.

Figure 5.4 shows the particle size distributions for the J = 5% case with the different ball sizes of 10mm and 20 mm. As shown, the 20 mm balls are more effective in breaking material to a finer size than the 10 mm media. The breakage can be attributed to the 20 mm balls having sufficient energy to smash the particles into fine and medium-sized classes while 10 mm balls lack the energy and can only chip and abrade the larger particles, which explains why the 20 mm balls contribute more to the M_2 size classes.

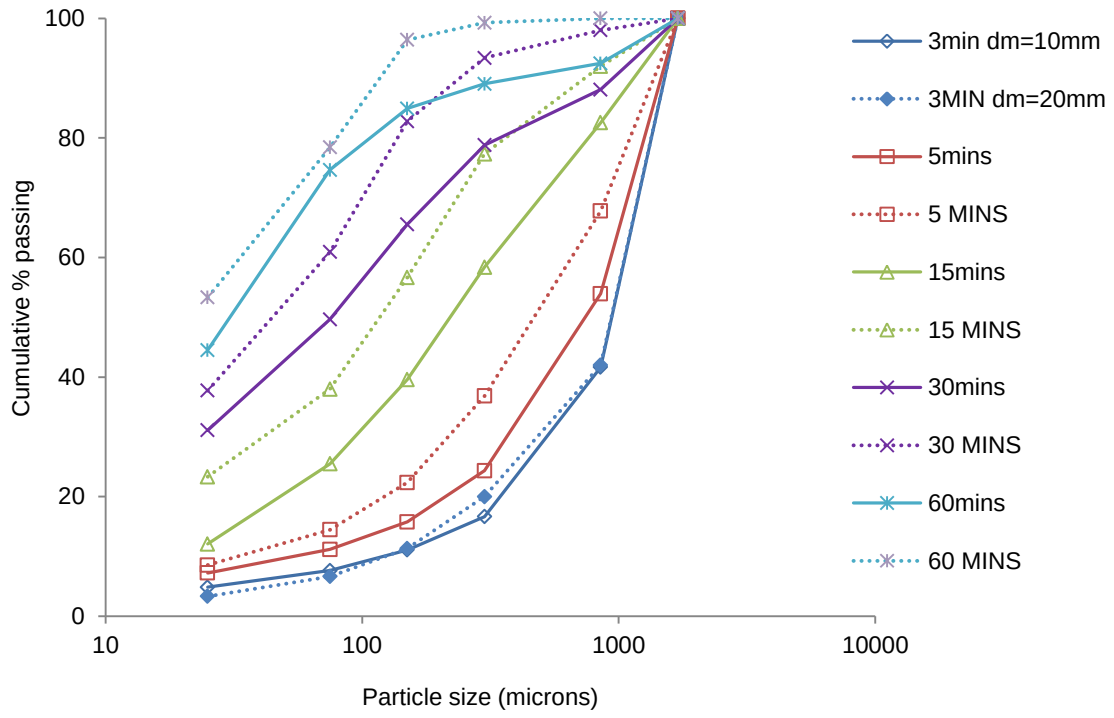

Figure 5.4: Class size distribution comparisons. J= 5%. Cumulative % passing profile vs. particle size comparisons for 10 and 20 mm ball sizes.

The same trend is observed for the *J* =15% (Figure 5.5). The 20 mm is more effective in breaking the M_1 size class into the smaller size classes, and during the initial stages of the milling process, more of M_2 and M_6 are formed.

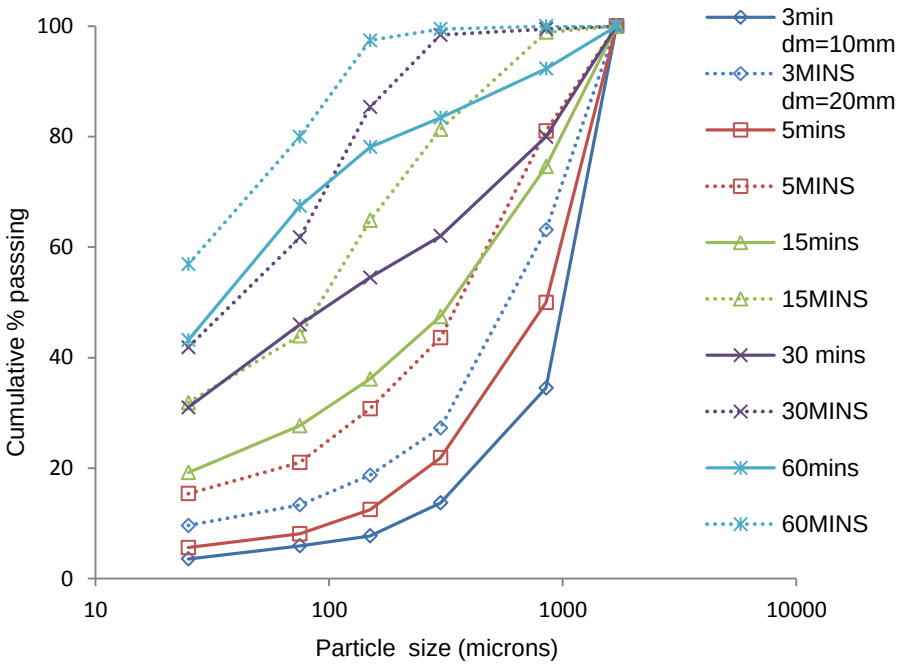

Figure 5.5: Class size distribution comparisons. J= 15%.Cumulative % passing profile vs. particle size comparisons for 10 and 20mm ball sizes.

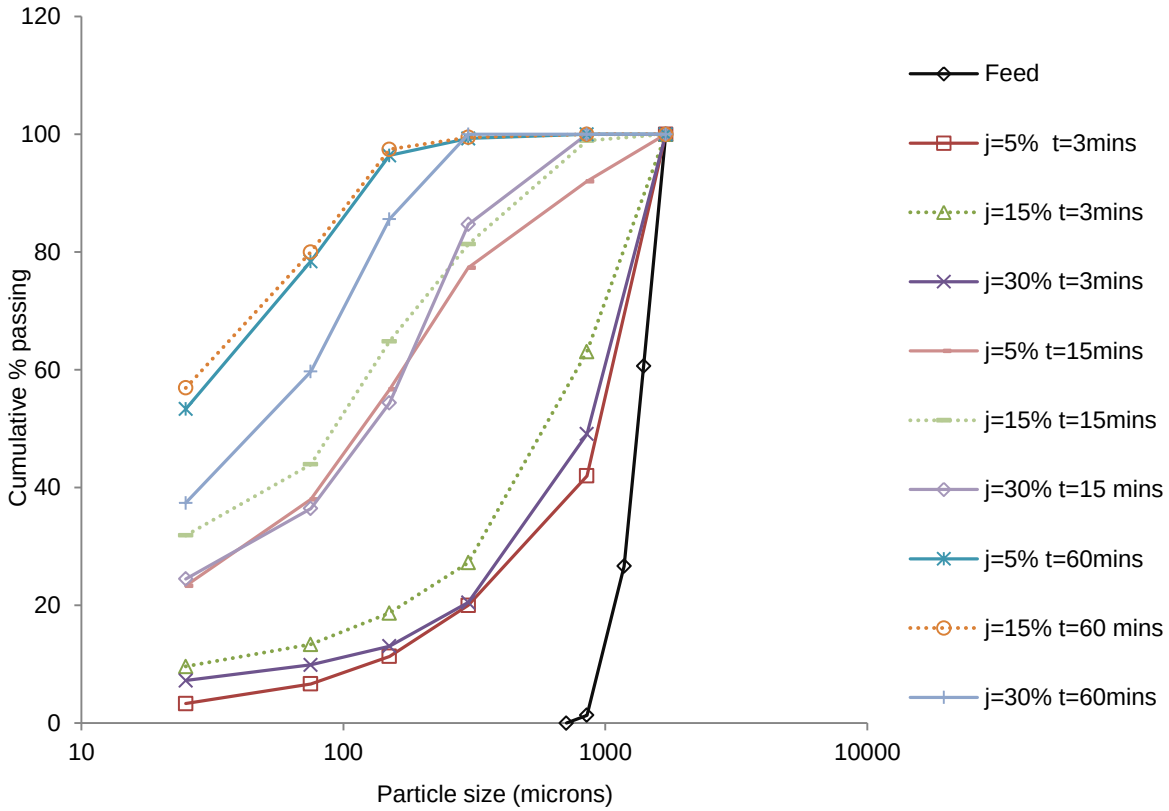

Figure 5.6: Class size distribution comparisons. J =5%, 15% and 30%. Cumulative % passing profile vs. particle size comparisons for 30 and 20 mm ball sizes.

Figure 5.6 shows the particle size distribution for J = 5% and 15%, using the 20 mm balls, and also high ball filling 30% with 30 mm media. It can be seen that using 30 mm balls with high ball filling is not as effective as the smaller ball fillings and smaller media. This is because there is less breakage or formation of finer material after a total milling time of 60 minutes.

5.3.2 Leaching results

The leach curves arising from the test are depicted in the Figure 5.7. The recoveries are based on the individual size class head assays and the gold content of the leach liquor at the end of each bottle rolling test.

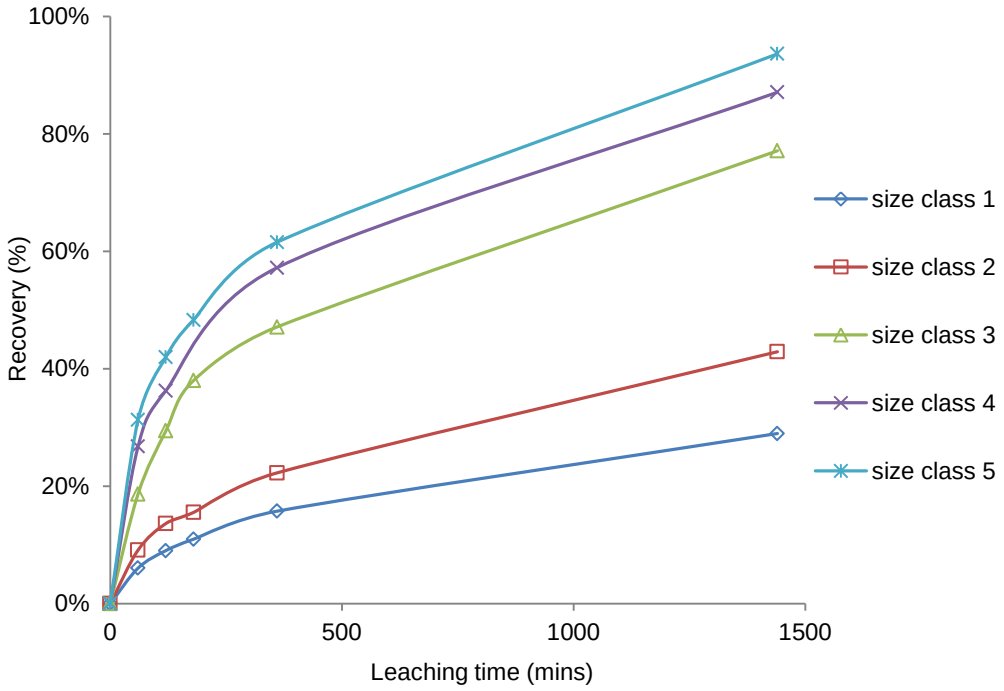

Figure 5.7: Leach profiles for milled size classes of a typical Witwatersrand Far West Rand Gold ore.

For comparative purposes, tests were carried out for maximum of 24 hours, although in practice residence times in a typical leach cascade are around 44 hours. In general it was found that recovery increases with the leaching time. This means that the leaching reagent has better access to gold in the finer material (M_5), hence the highest gold recovery of ~94%. Size class 1 has the lowest recovery rate of ~29 %, which is attributable to the fact that at this stage the valuable material is still locked in the mineral matrix.

The total amount of gold available after a particular milling time was calculated from the % recovery, the average head grade and the mass fraction of each size class for that particular milling time. Figure 5.8 illustrates the results obtained.

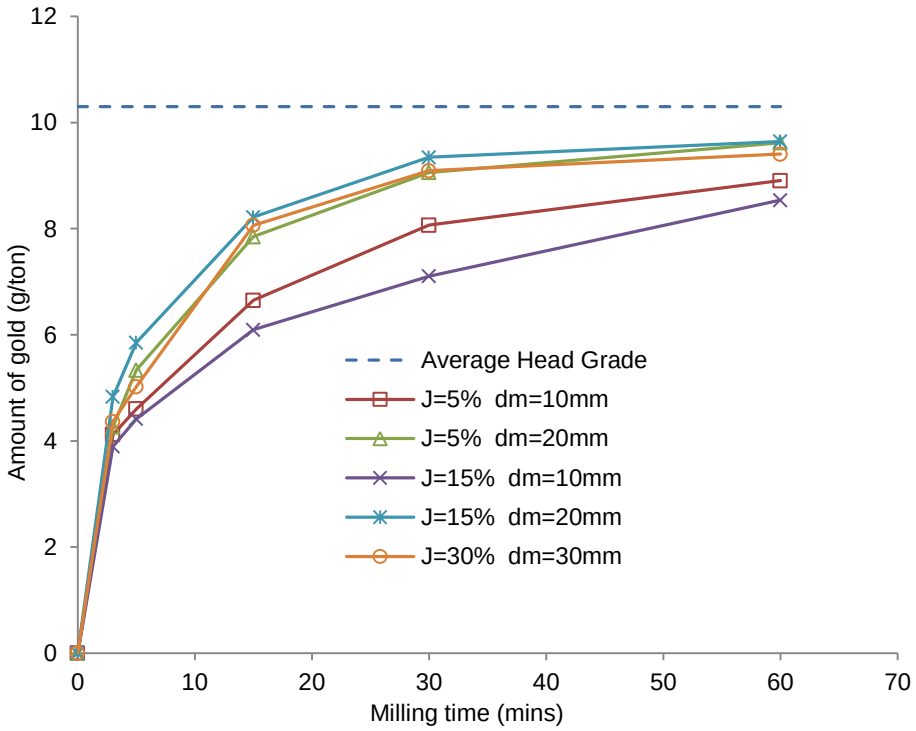

Figure 5.8: Variation in the amounts of gold recovered and milling time, for a 24-hour leach.

The average head grade from six measurements was found to be 10.3 g/ton ± 0.67 g/ton. It determines the concentration of gold in the ore but a significant amount of gold that is not exposed to the leaching solution causes the rate of leaching to be very slow and finite for an extended period of time (Crundwell and Godorr, 1995). The increase of the gold dissolution as particle size gets finer (M_5) is due to the better access of the reagents to the gold. The graph shows that when J=15% with 10 mm media, the amount

of gold after each particular grinding time is lower than any of the others, because less gold has been liberated. The figure also shows that at J = 5% and 20 mm leaching is at a slower rate than J = 15% and 20 mm. As the goal is to maximize the recovery of gold in the shortest amount of time, thus of the conditions explored it is recommended that the best operational settings are J = 15% and 20 mm.

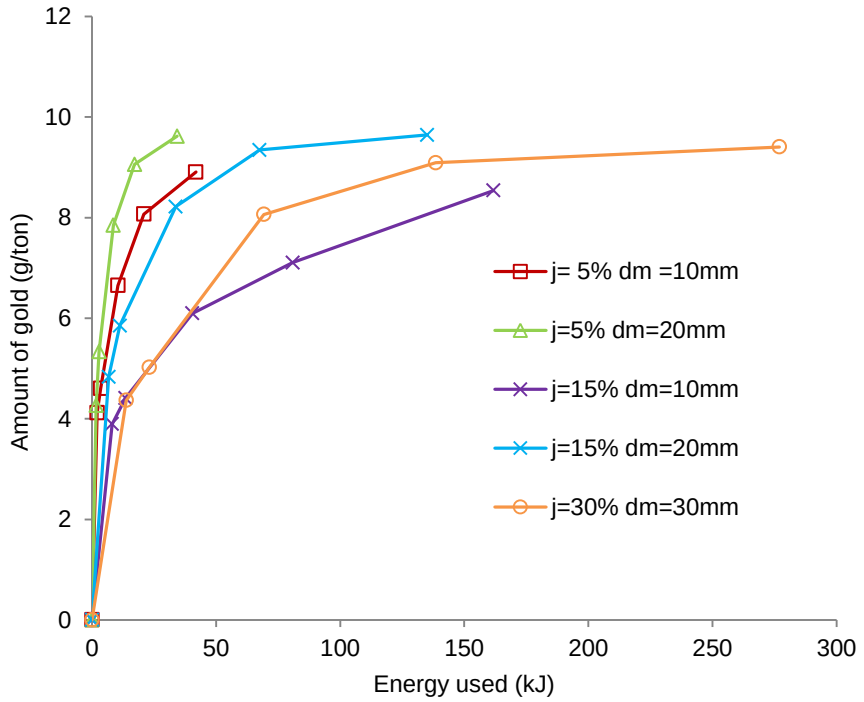

Figure 5.9: Variation in the amount of gold and energy used for different J and d_m values.

A graph showing the amounts of gold obtained and energy used during the 24-hour leach period for different ball sizes and J values is given in Figure 5.9. The low J values use a small amount of energy and achieve a high gold recovery in longer amount of time. The J = 15% with 20 mm balls gave the highest amount of gold recovery but with realatively high energy usage. The J = 15% with 10 mm balls consumed a high amount

of energy to obtain about ~8.5 g/ton of gold. Using a ball filling of 30% and 30 mm balls also achieves a high recovery, accompanied by highest energy consumption.

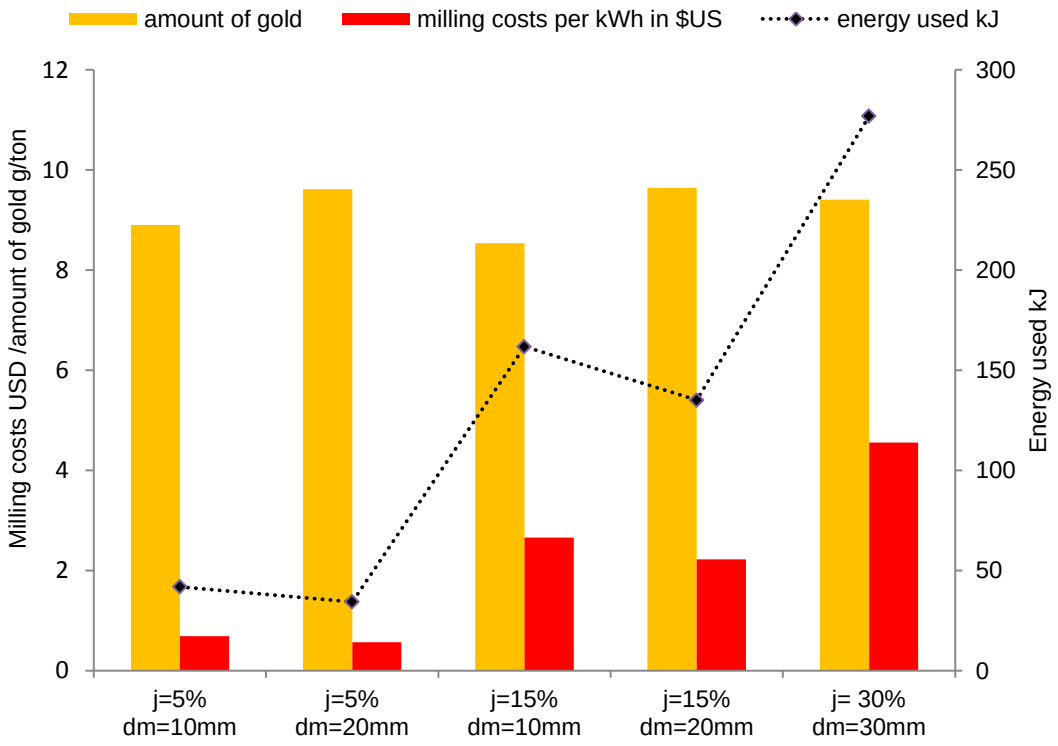

Figure 5.10: Graph of milling costs USD/ amount of gold g/ton and Energy used vs. milling conditions.

The best case of recovery from the milling time yielded ~9.64 g/ton of gold using ~135.09 kJ energy, which would cost ~ USD 2.2 (assuming the South African equivalent would be R50.3c per kWh or USD 0.0592 in 2012). The next best case was *J*=5% with a media size of 20 mm, which recovered 9.62 g/ton and consumed 34.34 kJ of energy.

Assuming a gold price of USD 1584.26 per ounce equivalent to (USD 51.1 /g 20 July 2012), the selling prices and the profits for the different mill conditions calculated are plotted in Figure 5.11.

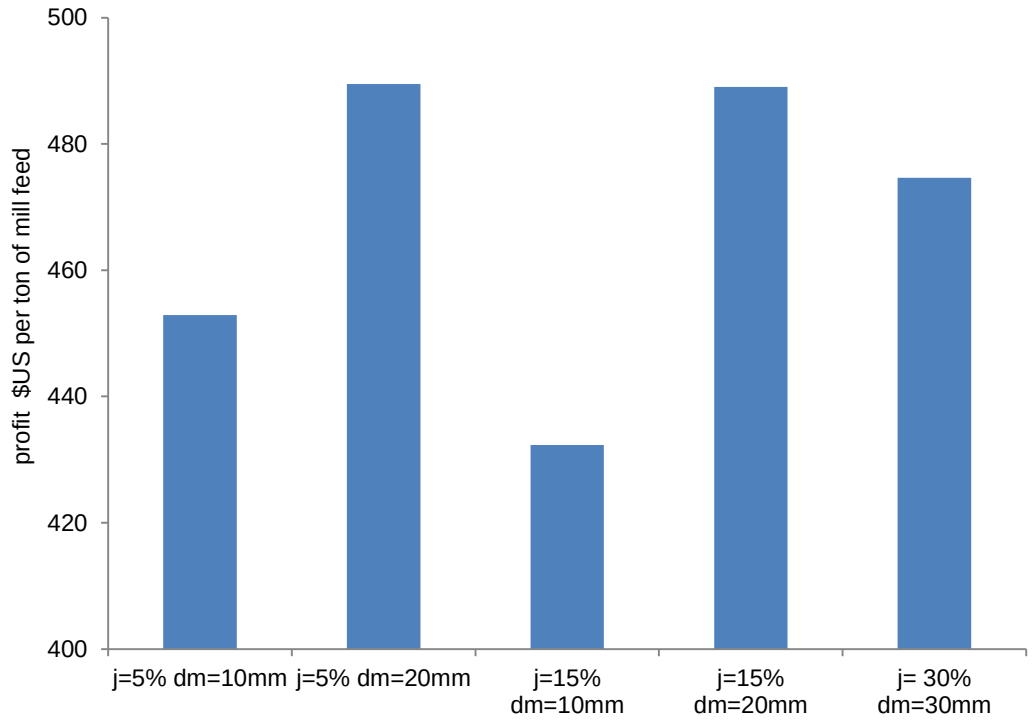

Figure 5.11: Graph of profit USD per ton of mill feed vs. milling conditions.

In terms of overall profit, a *J* = 15% and 5% with the 20mm media size seems to be the most economically viable for the experimental conditions investigated. These two conditions provide a profit of ~ USD 489 per ton of feed processed. This indicates that using a lower amount of energy accompanied by a high recovery would be ideal for an integrated leach and milling circuit. It was also shown that the 20 mm ball size is effective for both 5% and 15% filling, as they provide high liberation and more recovery, coupled with lower energy consumption.

5.4 CONCLUSION

The investigation described in this chapter showed that the 20 mm media were effective in milling for both J = 5% and 15% values under the experimental conditions used. The increase in gold dissolution as the particle size becomes finer was attributed to the better access of the leaching reagents, because the M_5 size class (-75 µm) yielded the highest recovery of ~94% during the 24-hour leach. The d_m = 10 mm cases produced a lower amount of gold after each particular grinding time owing to poorer liberation. It was also observed that the J= 5% and 20 mm curves required a little longer than the J = 15% and 20 mm curves to attain maximum gold recovery. Another finding taken from the leaching curves was that the size class M_4 (-150 +75 µm) produced recoveries comparable to the smaller size M_5 (-75 +25 µm), which suggests that a milling cut-off size closer to -150 µm could be adopted, since it would mean a saving in capital and operational expenses. In terms of energy, using lower and high ball filling with 20 mm media gave a higher recovery of gold with less energy used after 60 minutes of milling and 24 hours of leaching. In terms of overall profit, the J = 5% and 15% with the 20 mm media size provided a maximum profit of ~ USD 489 per ton of feed. This proved that using less energy to obtain a high recovery would provide a template for an integrated leach and milling circuit.

The overall main costs in the mineral processing industry are functions of time, energy and capital. A balance between these three must be struck. Further work in this field should look at modelling, integrated systems, and experimenting with changing some of

the factors, like mill speed and percentage of solids, to see how they affect gold recovery.

CHAPTER 6

6 DISSOLUTION KINETICS OF WITWATERSRAND FAR WEST RAND GOLD ORE IN SODIUM CYANIDE LEACHING

The content of this chapter has already been submitted to a journal as an article for publication. The article has a number of authors. The contribution made by the writer of this thesis consisted of design, conducting experiments including gold analysis and analytical discussion of the results with my supervisors and the drafting of the manuscript. The data was presented at conferences, namely SAIChE 2014 and AIChE 2014, national and international respectively.

Abstract

This chapter describes an investigation into the dissolution kinetics of gold ore in a solution of NaCN. These were found to depend on the stirring rate, reaction temperature, particle diameter and the concentration of the leachant. The rate increased with the stirring speed, reaction temperature and leachant concentration, but decreased when the particle size was greater. The activation energy for the dissolution was estimated at about 3 kcal/mol. Furthermore, the linear relationship between the rate constant and its reciprocal of square of particle size is a strong indication that the gold dissolution process is diffusion-controlled. The experimental results are fitted to a shrinking core model that offers greater understanding of the leaching reaction.

6.1 INTRODUCTION

Gold is classified as a noble metal because of its value. Another virtue of this metal is that it is inert to most chemical reactions in complexing media. It occurs primarily in the elementary state, not only in nugget form but also finely disseminated in rock-forming minerals such as carbonates, silicates, sulphides, tellurides and oxides (Gasparrini, 1983).

Because of the depletion in gold resources which is causing the price of this metal to rise, there is a strong incentive to commercially recover as much gold as possible and by the most efficient methods. Leaching is one of the ways that is mostly used. However, the process was introduced in the 19th century (Maclaurin, 1893) but it is a process that is not fully understood (Habashi, 1967), even though it is very widely used.

There has been considerable debate among engineers concerning the mechanism of dissolution. Some of them claim that the chemical reaction involved in cyanide leaching is too slow (Habashi, 1967). Others, such as Mills (1951), have shown that the presence of heavy metals like lead and mercury has a significant effect on the extent of reaction, causing passivation. The published work on dissolution provides few results for research into gold dissolution, and offers a very small number of rate expressions to describe leaching.

The investigation reported in this thesis was intended to remedy the gap in understanding the process. The research was devoted to identifying the type of dissolution that occurs during the leaching of ore from the far west Witwatersrand. The

enquiry also involved finding the model that best describes the kind of leaching mechanism that the process entails.

6.2 EXPERIMENTAL PROCEDURE

The experimental programme was carried out on size classes shown in Table 6.1 as it is discussed in Section 4.3 with the specifications and test conditions in Tables 4.8 and 4.9.

The resultant gold-bearing ore is then sieved through a dry screen to separate the particles into size classes, as shown in Table 6.1 below. The size range normally used for leaching is ≤75 microns, but finer and coarser size classes were also tested in order to develop a broader context within which to understand the process.

Table 6.1: Particle size classes used during the leaching experiments.

Size class	Upper (microns)	Lower (microns)
M1	-1700	+850
M2	-850	+300
M3	-300	+150
M4	-150	+75
M5	-75	pan

6.3 RESULTS AND DISCUSSION

6.3.1 Dissolution of gold

6.3.1.1 Effect of particle size

The effect of particle size on the leaching of the gold can be seen in Figure 6.1. At the beginning of the tests, the cyanide concentration was 210 ppm and the experiment was carried out at ambient temperature. The recovery calculations were based on the individual size class head assays and the gold content of the leach liquor at the end of each leach interval.

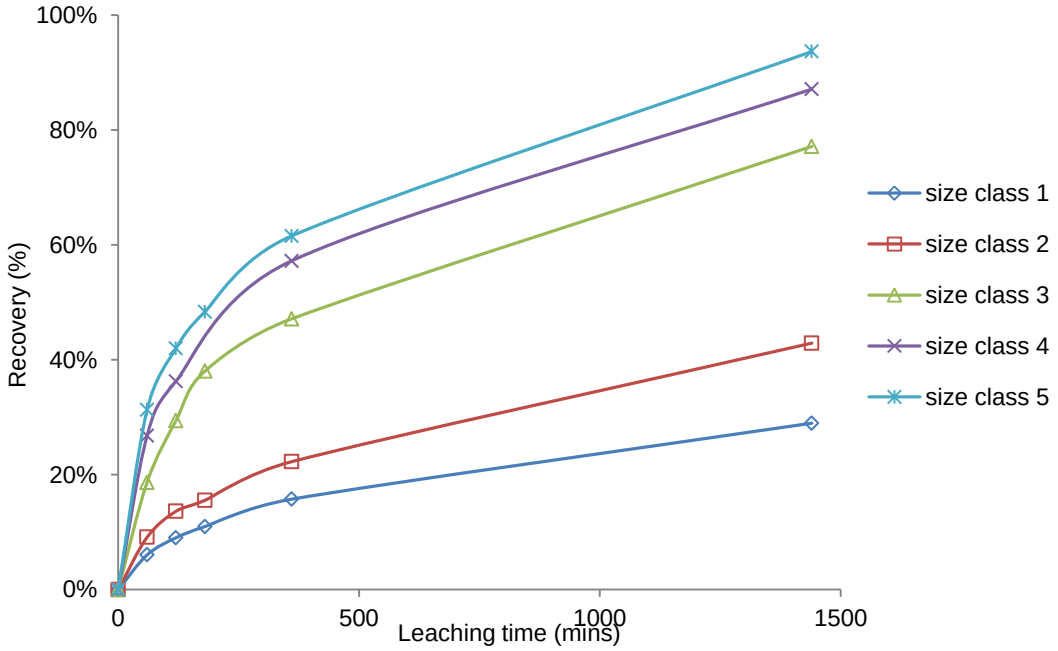

Figure 6.1: Effect of particle diameter on gold dissolution (experimental conditions: sodium cyanide concentration 210 ppm; temperature 25^{o} C).

The leach duration was set at 24 hours for the experiments, although the actual residence times in a typical leach cascade are around 44 hours. The test results show that particle size has a marked effect on the dissolution rate of the gold. The smaller the particle size, the higher the fraction of gold present in the liquor. The smaller particles provide a larger contact surface area between solid and liquid. They also reduce the penetration distance required by the cyanide to reach the soluble gold within the particle. de Andrade Lima and Hodouin (2005) showed that the residual gold concentration increased with the particle size. However, increasing the fineness of grinding will also increase cyanide consumption and does not improve gold extraction (Kondos et al., 1995).

6.3.1.2 Effect of mixing

The effect of the stirring rate on gold dissolution in a 210 ppm cyanide solution is shown in Figure 6.2.

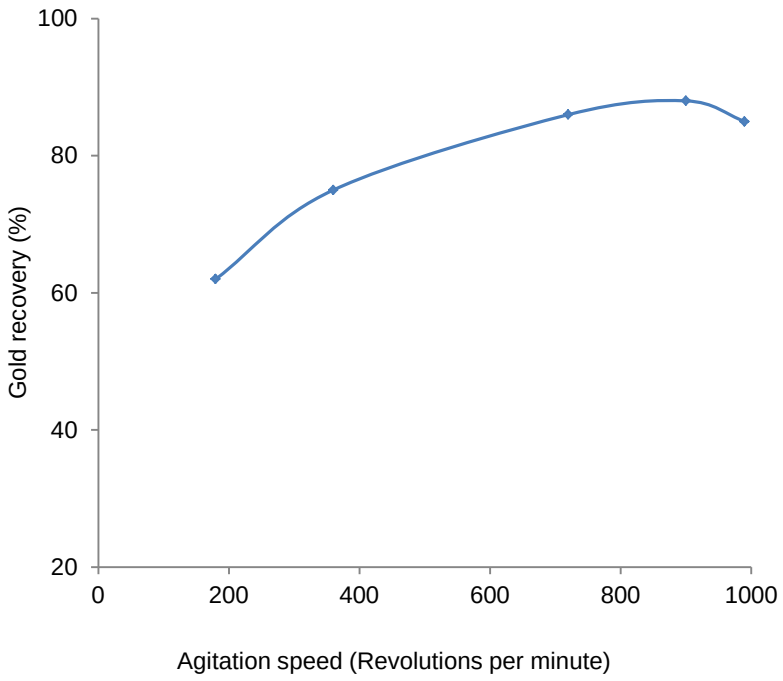

6.2: Effect of agitation speed on gold dissolution (experimental conditions: sodium cyanide concentration 210 ppm; temperature 25^{o} C).

The results show that agitation is a significant factor in gold leaching; however, the rate reached a plateau as you approach higher stirring speed. For the purpose of these experiments, the stirring rate of 360 rpm was deemed sufficient. The agitation allows the particles in the slurry to be sufficiently suspended and be in good contact with bulk solution. As observed from Figure 6.2, increasing the agitation speed enhances the dissolution rate until external mixing is no longer a rate limiting step. We can thus speculate that intense mixing reduces an external diffusion layer thickness and thus increasing the mass transfer rates from leach sites and diffusion of oxygen to the sites. This also allows the possible saturation of the slurry with oxygen to achieve high dissolved oxygen levels.

6.3.1.3 Effect of sodium cyanide concentration

In order to determine the effect of cyanide concentration on gold dissolution, experiments were carried out in which the initial NaCN concentration was varied. These were carried out at room temperature, and used size fraction (-150 + 75 µm). The results are shown in Figure 6.3.

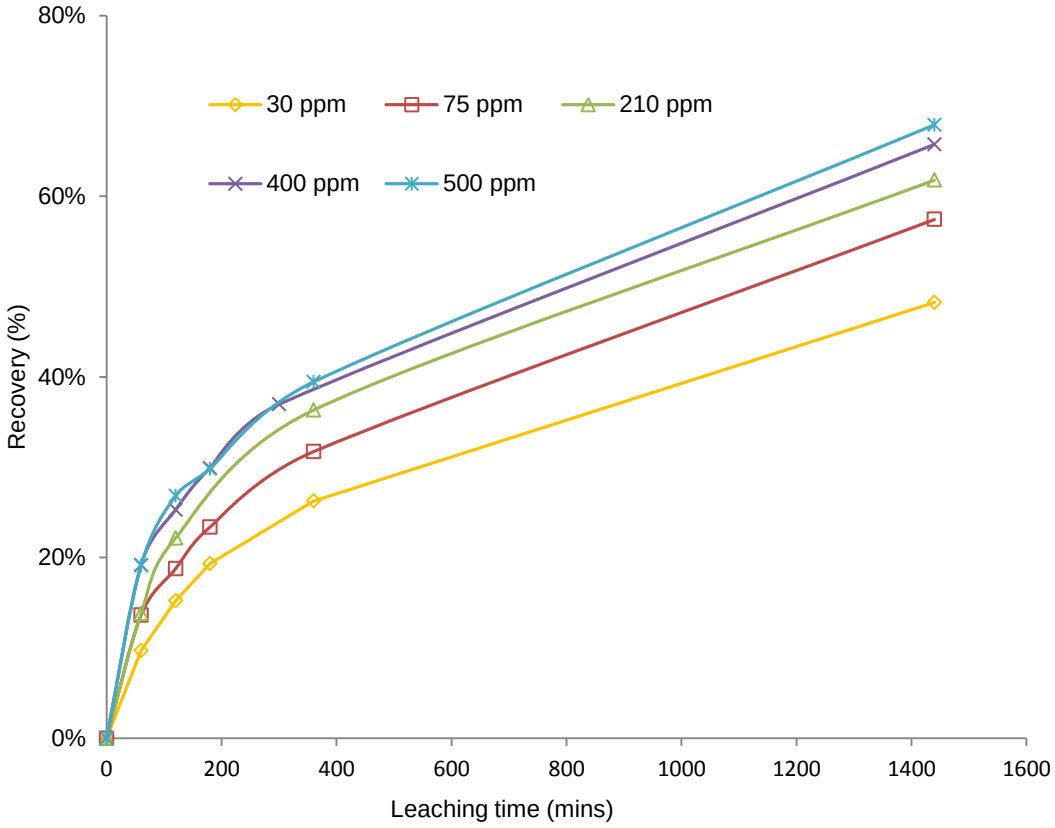

Figure 6.3: Effect of sodium cyanide concentration on gold dissolution (experimental conditions: particle size, -150 + 75 µm; temperature, 25^{o} C).

The results graphically represented in Figure 6.3 clearly indicate that raising the cyanide concentration caused a corresponding climb in recovery, especially between 30 and 210 ppm while increasing the concentration further to 400 and 500 ppm did not improve the recovery much. Using an excess of cyanide is therefore unnecessary, as this would raise operational costs. Another disadvantage of excess cyanide is that it leads to the formation of cyan complexes with the impurities.

6.3.1.4 Effect of temperature on gold dissolution

The next set of experiments conducted involved investigating the effect of a range of temperatures (room temperature to 110°C) on dissolution, with cyanide concentration of 210 ppm. The results are shown in Figure 6.4. It is seen that the fraction of gold dissolved increases with the temperature reaches a peak at about 80 ^{o}C.

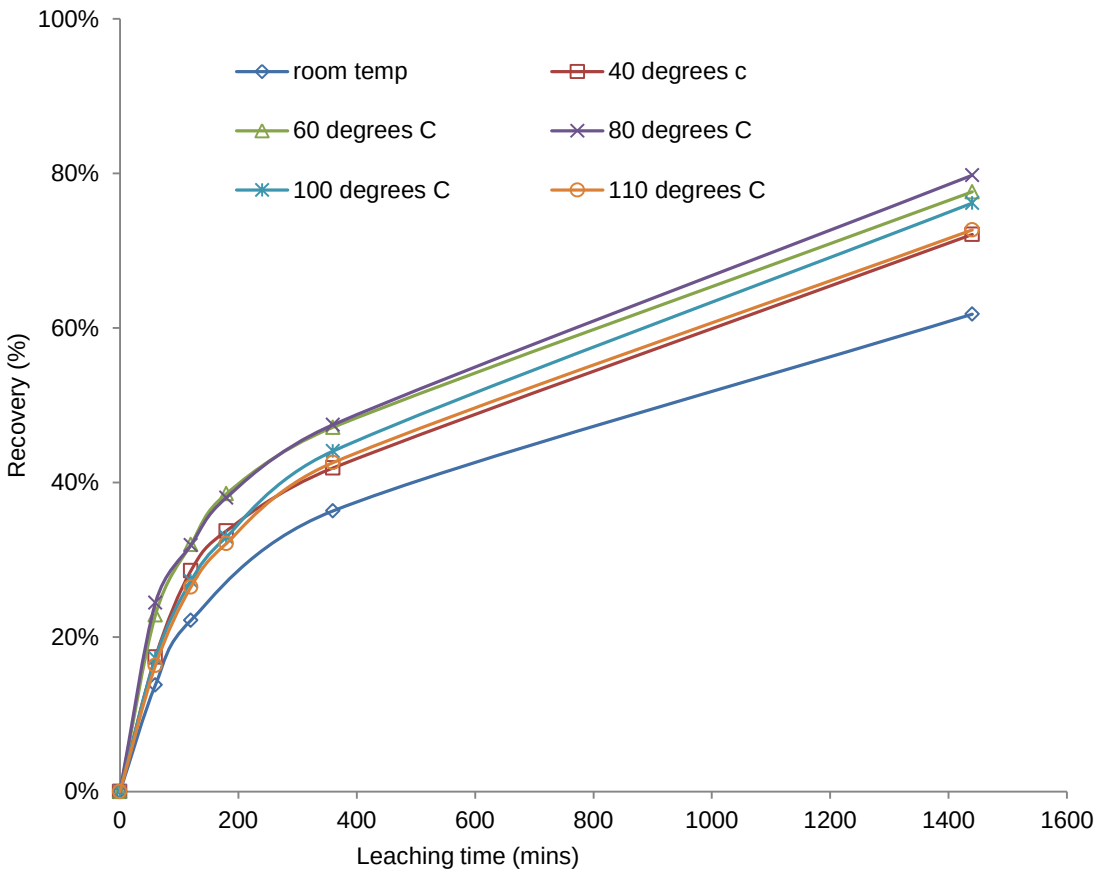

Figure 6.4: Effect of temperature on gold dissolution (experimental conditions: particle size -150 + 75µm; cyanide concentration 210ppm).

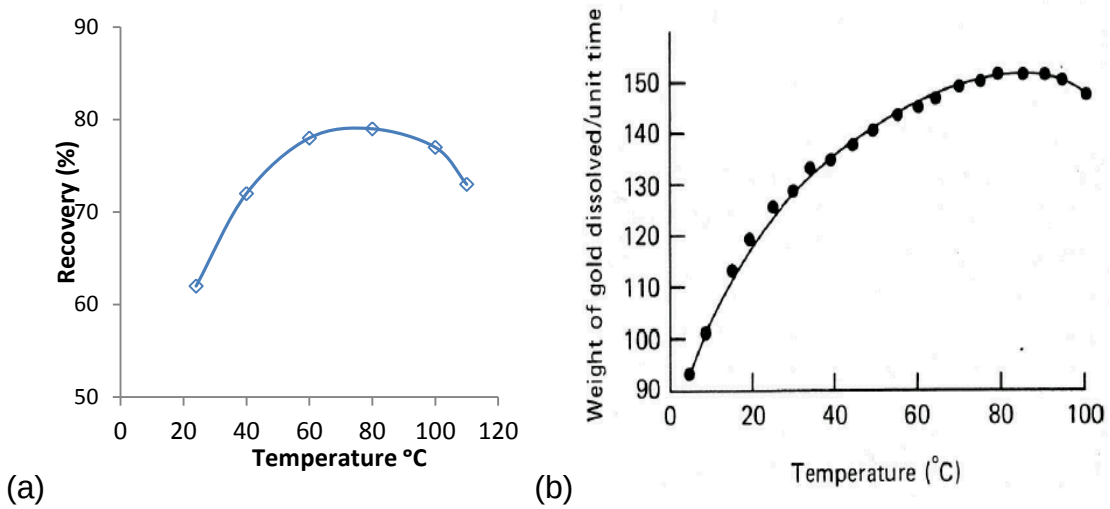

Figure 6.5: Comparison of the researcher's experimental recoveries (a) and those obtained by Marsden and House (b) in 1992.

The graphs demonstrate clearly that the gold dissolution rate increases with temperature. This is due to the reduction in the viscosity of the liquid material, which increases the diffusivity. Accordingly, one expects dissolution to increase as the temperature rises. Figure 6.5 shows that the dissolution rate of gold in cyanide solution reaches its maximum at around 80–85^{o}C. It is noteworthy that when the temperature rises above 80^{o}C, the recovery starts to decline. This can be attributed to the solubility of gas (oxygen), which tends to decrease with an increase in temperature.

6.3.2 Kinetics of dissolution

The leaching of gold from an ore can be described by the following reaction:

$$4Au + 8CN^- + O_2 + 2H_2O \rightarrow 4Au(CN)_2^- + 4OH^- \qquad 6.1$$

The shrinking core model is widely used to predict the kinetics of mineral dissolution so that researches can make comparative analyses of the dissolution kinetics of gold when cyanide is used. The general equation is represented as

$$A_{(fluid)} + bB_{(solid)} \rightarrow Fluid\ product + Solid\ product \qquad 6.2$$

where A represents the solvent, B represents soluble component undergoing leaching, and b the stoichiometric coefficients of B.

The rate of the reaction is given for models based on its control by either chemical reaction on the surface, film, ash diffusion, or a combination of these. When diffusion through the product layer controls the kinetics, the equation is given as follows (Levenspiel, 1972):

$$1 + 2(1 - x) - 3(1 - x)^{\frac{2}{3}} = \frac{6aMDC}{\rho r_0^2} t = k_d t \qquad 6.3$$

If controlled by the surface reaction, the equation below applies:

$$1 - (1 - x)^{\frac{1}{3}} = \frac{k_c MC}{\rho a r_o} t = k_r t \qquad 6.4$$

where: k_r and k_d are chemical rate constants (cm/ min), x is the fraction of gold dissolved in time t, D is the diffusion coefficient of ions in porous media ($m^2/\min$), k_c is the kinetic constant, M is the molecular mass of the solid, C is the concentration of lixiviant (cyanide), a is the stoichiometric coefficient of the reagent in the leaching reaction, ρ is the density of the solid, r_o is the initial radius of the solid and k is a rate constant.

The left sides of Equations 6.3 and 6.4 were plotted against leaching time in Figure 6.6.

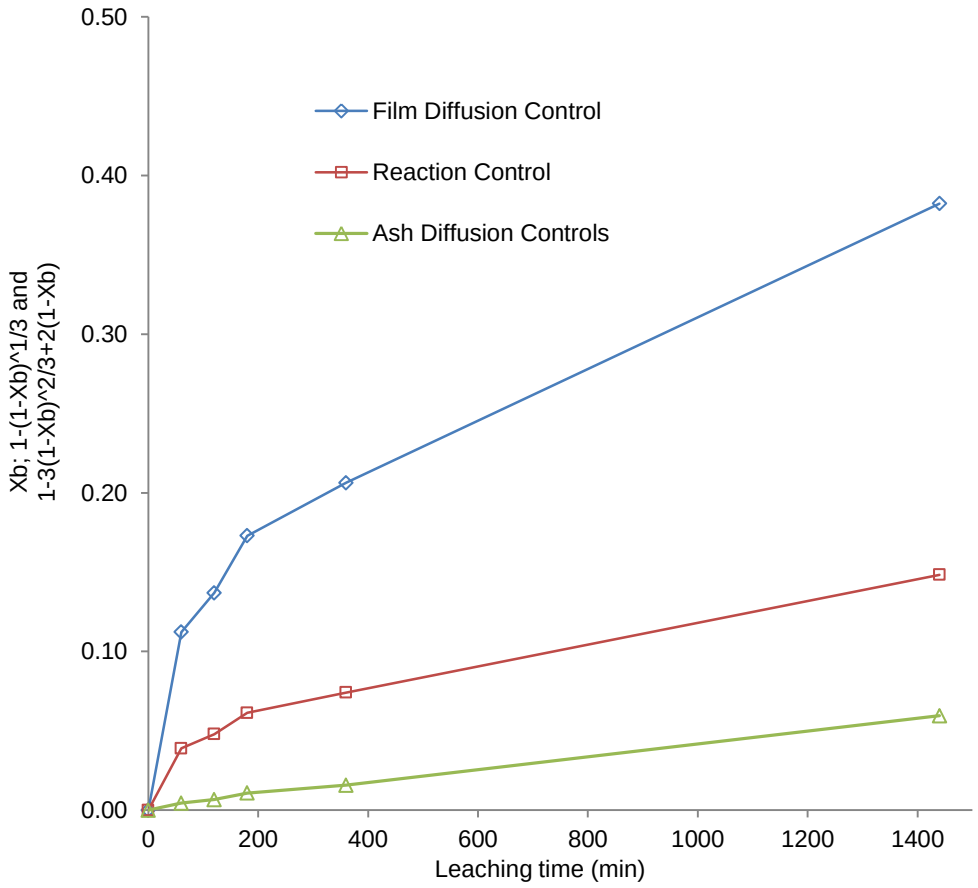

Figure 6.6: Variation of different shrinking core model equations with a leaching time of particles of -300 +150µm diameter.

Figure 6.6 shows that the ash diffusion control model gives a straight line, which suggests that it is the slowest part of the dissolution reaction, namely the rate limiting step.

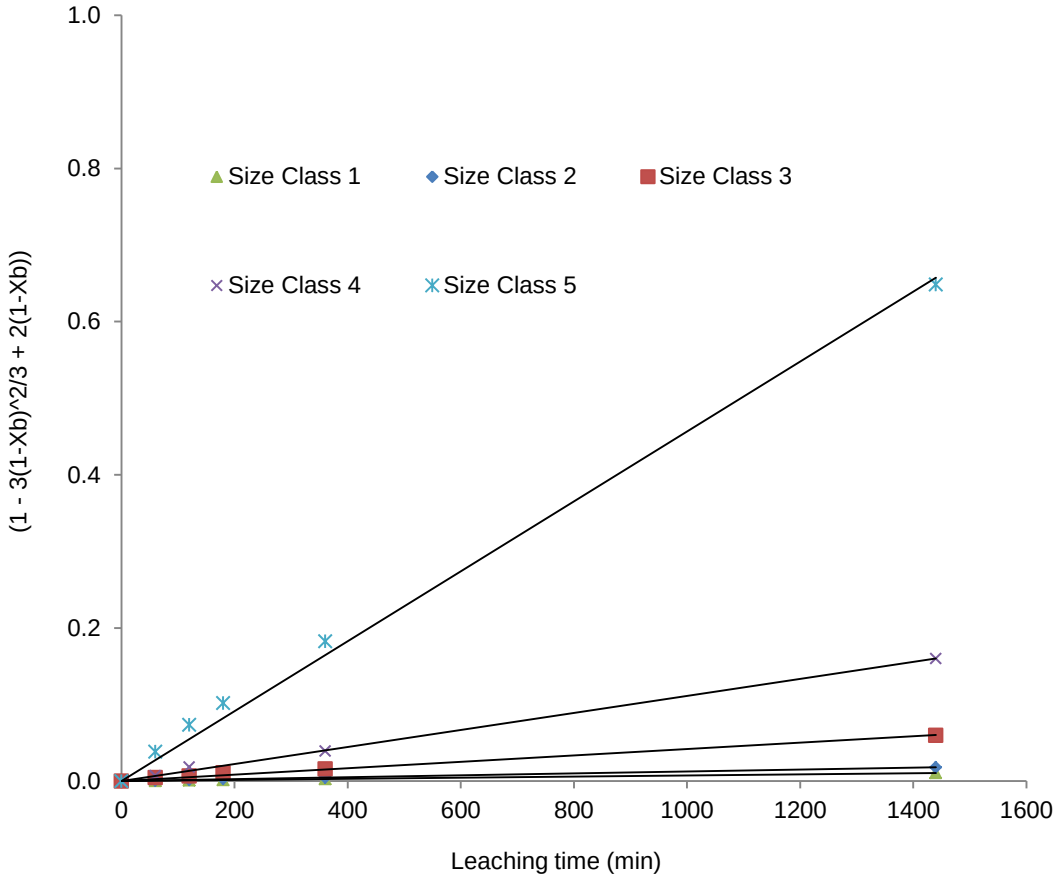

Figure 6.7: Plot of the ash diffusion control model equation applied to different particle sizes as against the leaching time required for gold dissolution (experimental conditions: sodium cyanide concentration 210 ppm; temperature 25^{o} C).

Figure 6.7 plots the variations between all the size classes used during the experiments against time when the ash diffusion model is applied. This also produces straight lines, which suggest that ash diffusion is the rate controlling step.

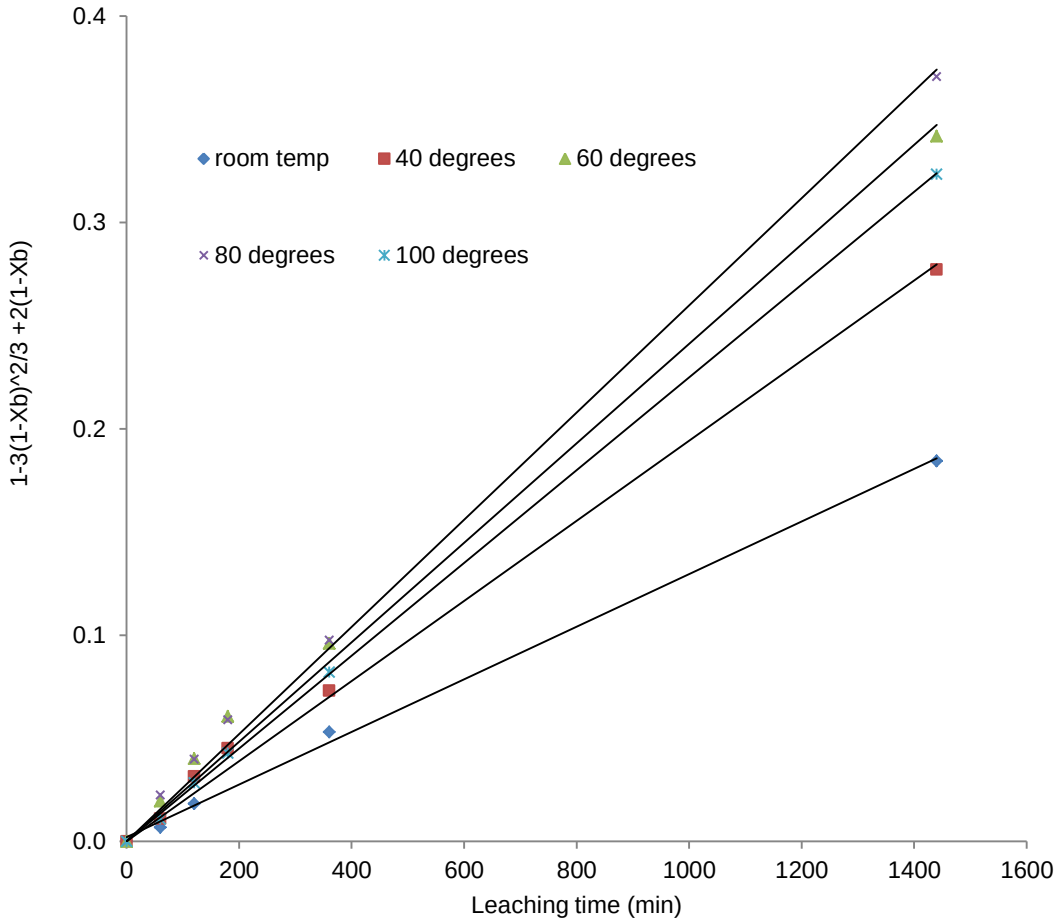

Figure 6.8: Plot of ash diffusion control model equation with the leaching time at different temperatures for gold dissolution (experimental conditions: sodium cyanide concentration 210 ppm; particle size -150+75µm).

The rate constants, for the shrinking core model examined at different temperatures were calculated from the slopes of the straight lines obtained from Figure 6.8. These values and their corresponding correlation coefficient rate are summarized in Table 6.2.

Table 6.2: The rate constant k for the ash diffusion control model with the correlated coefficients for gold ore dissolution in a 210 ppm NaCN concentration at different temperatures.

Temperature ^{O}C	Rate constant (*10^-1) (min^-1)	Correlation coeffient
25	1.09	0.9977
40	1.94	0.9965
60	2.41	0.9998
80	2.54	0.9930
100	2.25	0.9969
120	1.98	0.9989

The apparent rate constant, k derived from the slopes of the lines in Figure 6.8 were used to obtain the Arrhenius relation in Figure 6.9 (c), from which the energy of activation, E_a, was calculated for the dissolution process.

6.3.3 Activation Energy

The temperature dependence of the reaction rate constant can be calculated by the Arrhenius equation:

$$k = A \exp[\frac{-Ea}{RT}] \qquad 6.5$$

where A is the frequency factor, E_a the activation of the reaction, R the universal gas constant and T is the absolute temperature.

Due to the unusual trend of the temperature effect on the gold dissolution process, the activation energy is calculated from a temperature of the highest four temperatures used before it starts to drop (see Figure 6.5). The apparent rate constant derived from the slopes of the line in Figure 6.8 was used to obtain the Arrhenius relations given in Figures 6.9, a, b and c.

It can be seen from Figure 6.9 that the values of the so-called activation energies are not very satisfactory but the slopes shown do give a very rough idea of the affect of temperature on the rate prior to reaching the maximum rate.

The slope for the reaction in the Arrhenius plot ($ln\ k\ vs.\ 1/T$), shown in Figure 6.9 (c) gives an activation energy of 3,09 kcal/ mol or 12,9 kJ/mol. According to Habashi (1969), the activation enegy of a diffusion-controlled process is typically between 1 and 3 kcal/mol, while for a chemically-controlled process it is usually greater than 10 kcal/mol.

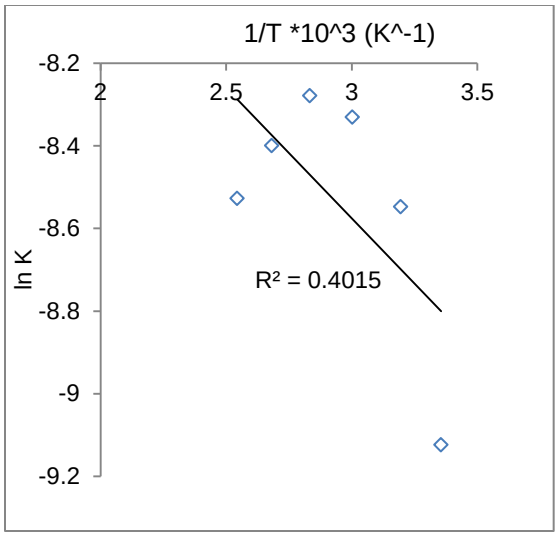

(a)

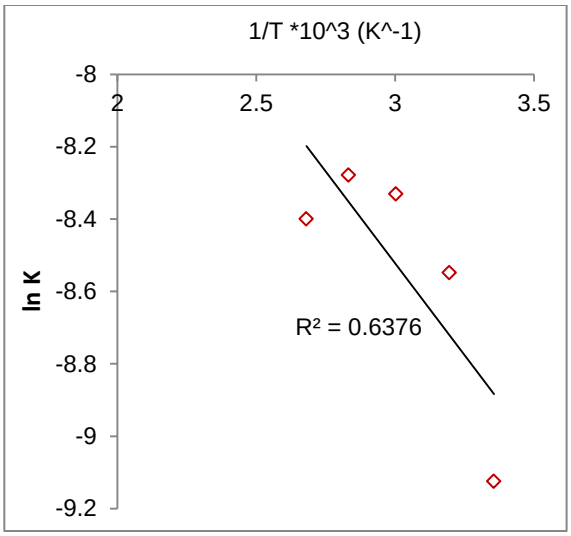

(b)

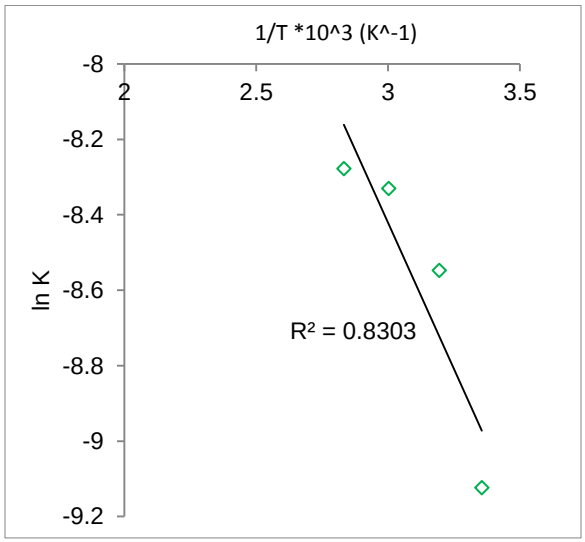

(c)

Figure 6.9: Arrhenius plots for gold dissolution in 210 ppm NaCN.

The linearization of the kinetic curves in Figure 6.1 versus time was carried out by applying Equation 6.3. The values of the rate constants were plotted versus the reciprocal of the square of the particle radii ($\frac{1}{r_0^2}$), yielding a linear relationship with a correlation coefficient of 0.9901. This is shown in Figure 6.10.

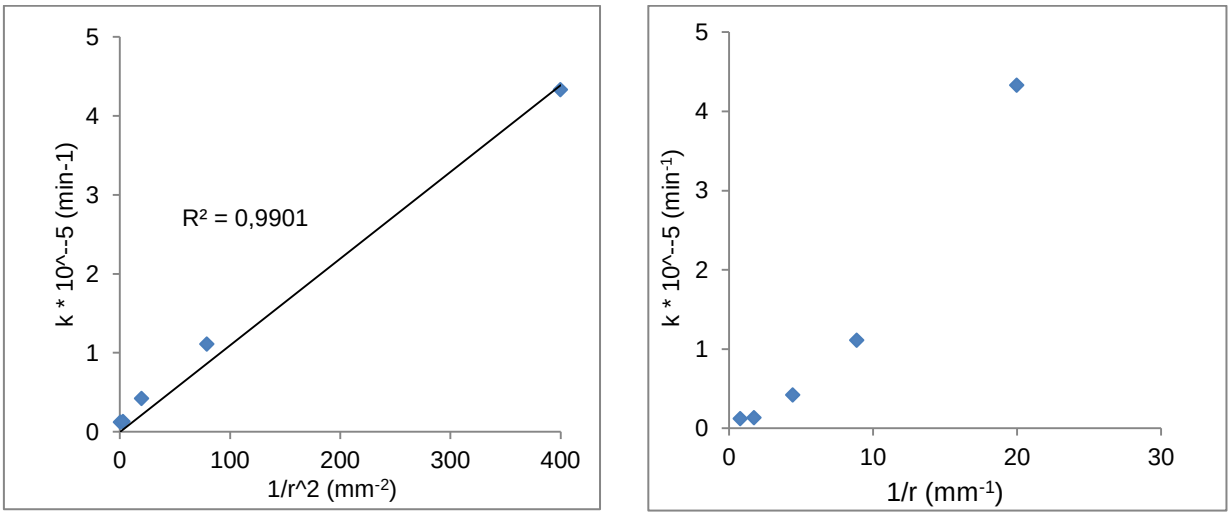

Figure 6.10: Dependence of the rate constant on (1/r) and 1/(r^2) for the leaching system

A plot of rate constant k versus the reciprocal of the particle does not give a straight a linear relationship. The linear dependence of the rate constant k on the reciprocal of the square of the particle radii passing through the origin supports the hypothesis that ash diffusion is the rate-controlling step during the gold dissolution process.

6.4 CONCLUSION

A range of experiments were conducted on the rate of dissolution of gold using a cyanide solution in the presence of lime. It was observed that both the temperature (up

to a point) and the cyanide concentration accelerate the rate of dissolution. A higher stirring rate proved to raise the reaction rate while reducing the diameter of the particles. These results were also successfully fitted to the shrinking core model, with ash diffusion as the rate-controlling step. The linear relationship between k and $1/r^2$ confirmed the feasibility of the ash diffusion model. The calculated activation energy was about 12.9 kJ/mol, which is consistent with some of the values of activation energies reported by other researchers for diffusion-controlled reactions.

CHAPTER 7

7 USE OF ATTAINABLE REGION (AR) ANALYSIS TO OPTIMISE JOINT LEACHING AND MILLING PROCESS.

Abstract

Particle size reduction is a process carried out either on dry materials or on slurries where a material is gradually reduced in size to produce material of the desired size class. It is an energy intensive process concerned with the relationship between energy input and the particle size made from the given feed size. It is of paramount importance to mill to the right size while minimising the energy costs. In this study, the specific rate of breakage and primary breakage distribution functions for a gold ore sample taken from Carletonville plant, Johannesburg, were determined in a laboratory size ball mill. Grinding at about U= 1 for instance, gave the maximum amount of a particular size class for leaching (-150+75 µm), and is a good powder-ball loading ratio (U) to give efficient breakage in a ball mill for the gold sample. The AR analysis is then used to show how to choose the leaching and milling time to optimize the value of the leached material.

7.1 INTRODUCTION

Ball milling is an important unit operation for size reduction used in the mining industry. It is the most encountered mineral processing operation of size reduction and is an

energy inefficient process, and focus has mainly been on ways of reducing the energy consumption incurred by the operation. During milling a lot of energy is used to break up particles. Over-grinding must be avoided as this only wastes energy and to some extent can negatively impact downstream processes. Several researchers have therefore come up with ways of improving energy utilisation based on plant experience and empirical modelling. This however on its own does not address the major problem which is what size should we mill to in order to make the most profit for the plant as a whole.

One of the primary reasons for milling materials down to smaller particle sizes is to liberate valuable components dispersed in the host matrix. Once the material has been reduced to a size small enough to give sufficient liberation, the valuable components are then recovered from the host matrix by downstream processes such as leaching. It must therefore be understood that mill products should be tailored to satisfy leaching requirements. For this to successfully happen, milling has to be carefully studied to enable the determination of the trade-off between milling itself and leaching.

If one is to optimise the milling stage, requirements of the leaching in terms of particle size or liberation have to be considered first, since grinding finer leads to higher leaching reagent costs and on other hand coarse material gives lower recoveries. This would be followed by understanding the breakage properties of the ore to be used. Austin (1971) and Lucky *et al.* (1972) used selection and breakage functions to study the kinetics of size reduction in tumbling mills. The two functions are then applied in population balance model, which provides the basis for the modelling of the grinding process.

7.2 THEORETICAL BACKGROUND

Many researchers have studied the milling-leaching process. The Attainable Region (AR) analysis has not as yet been applied to this situation. Only some aspects of the subject relating to population balance models are reviewed here. Also, basic principles of the AR method as previously applied to milling have been used.

7.2.1 Kinetic model

The milling kinetics is based on a population balance model that has been briefly discussed in Section 2.1.2. This describes the correlation between the particle size distribution of the starting material and that of the product milled material. The traditional size-discrete form of the population balance equation for batch comminution is linear and assumes first-order breakage kinetics (Austin, 1972).

$$\frac{dw_i(t)}{dt} = -S_i w_i(t) + \sum_{j=1}^{i-1} b_{i,j} S_j w_j(t) \qquad (7.1)$$

Therefore breakage of material in the top size class can be expressed as:

$$\frac{dw_i}{dt} = -S_i . w_i(t)$$

For normal breakage the size reduction process is a first order process, that is, it is assumed that S_1 does not change with time, and the above equation integrates to:

$$\log w_i(t) - \log w_i(0) = -S_i t/2.3 \qquad (7.2)$$

where $w_i(t)$ is the weight fraction of the mill hold-up that is of size i at time t

A plot of $log\ w_i(t)$ versus t should give a straight line if the grinding is first order. Any deviation from first order gives non–first order grinding which can either be slowing down or acceleration of breakage rates. The breakage described above refers to a specific size class.

Across size, Austin et al. (1984) proposed a formula for variation of specific rate of breakage Si with particle size as:

$$S_i = a_T X_i^{\underline{\alpha}} \qquad (7.3)$$

where X_i is the upper limit indexed by i, mm, and a_T and $\underline{\alpha}$ are model parameters that depend on the properties of the material and grinding conditions.

When grinding material even of a single size class in the mill, a wide range of product sizes are produced. The breakage distribution function $b_{i,j}$, that accounts for material breaking into size i from some upper size j is expressed as:

$$b_{i,j} = \frac{mass\ of\ particles\ from\ class\ j\ broken\ to\ size\ i}{mass\ of\ particles\ of\ class\ j\ broken} \qquad \text{where } i < j$$

L.G. Austin, R.R. Klimpel, P.T. Luckie 1984 found the cumulative primary breakage function a convenient term for modelling and it relates to $b_{i,j}$ as follows :

$$B_{ij} = \sum b_{ij} \qquad (7.4)$$

B_{ij} is the sum of the fractions of material less than the upper size of screen interval i obtained from primary breakage of size j material. The following expressions were shown by Austin et. al (1984) which showed that B_{ij}value from sizes can be estimated from size analysis of the product from grinding of the size j material.

$$\mathrm{B_{ij}} = \frac{\log[(1-\mathrm{P_i}(0))/(1-\mathrm{P_i}(\mathrm{t}))]}{\log[(1-P_{\mathrm{j+1}}(0))/(1-\mathrm{P_{j+1}}(\mathrm{t}))]} \qquad i > j \qquad (7.5)$$

where $P_i(t)$ is the cumulative fraction by mass in the mill less than size x_i at time t. B_{ij} can be fitted to an empirical function (Austin et. al , 1984) for non-normalized B_{ij} values. The empirical model relating the cumulative breakage function to the particle size has been proposed (Austin *et al*., 1984). For a normalisable material, the model for the cumulative breakage function is as follows:

$$B_{i,j} = \Phi_j \left(\frac{x_{i-1}}{x_j}\right)^{\gamma} + (1-\Phi_j)\left(\frac{x_{i-1}}{x_j}\right)^{\beta} \qquad \mathrm{n} \geq \mathrm{i} \geq \mathrm{j} \geq 1 \qquad (7.6)$$

where β ,γ ,Φ, and *δ,* are model parameters that depend on the properties of the material.

7.2.2 Attainable Region approach applied to milling

There exist some similarities between comminution and chemical reaction and these have encouraged the use of the attainable region analysis in studying comminution

(Khumalo et al., 2006, 2007, 2008). Khumalo et al. (2006) developed a population balance model that described the comminution process in an equipment independent fashion, relating the extent of breakage directly to the specific energy input to the device. They theoretically demonstrated that the same net energy input did not produce the same product particle size distribution and the AR could be utilized to perform simultaneous process synthesis and optimisation of the desired size class.

This work describes what was done to use an Attainable Region analysis to optimise U (interstitial filling), the leaching and milling time of the integrated process. In particular, Khumalo et al. (2006, 2007 and 2008) focused on achieving a desired product with optimal use of energy during the milling process. In this case, the downstream process, which is leaching, is also included. In some industries (e.g. the gold mining industry) time of operation (milling and leaching time) have a large impact on the overall costs of the process.

7.3 EXPERIMENTAL TECHNIQUE

7.3.1 Material and methods

Gold ore samples taken from Witwatersrand Far West gold local mine in Carletonville were used as the experimental material. The laboratory work was aimed at estimating the selection and breakage functions of the gold ore. Four monosize fractions (-1.7+1.18 mm,-1.18+0.85 mm,-0.85+0.6 mm, -0.6+0.425 mm) were prepared and ground batch-wise in a laboratory-scale ball mill for determination of the selection function. Extra material ground using the conditions in the Table 4.7 were also prepared

and ground batch-wise in the mill for the determination of the breakage functions. Samples were taken out of the mill and dry sieved for product size analysis.

7.4 RESULTS AND DISCUSSION

7.4.1 Determination of S function from six monosize fractions

The first-order plots for various feed sizes of gold ore are illustrated in Figure 7.1.

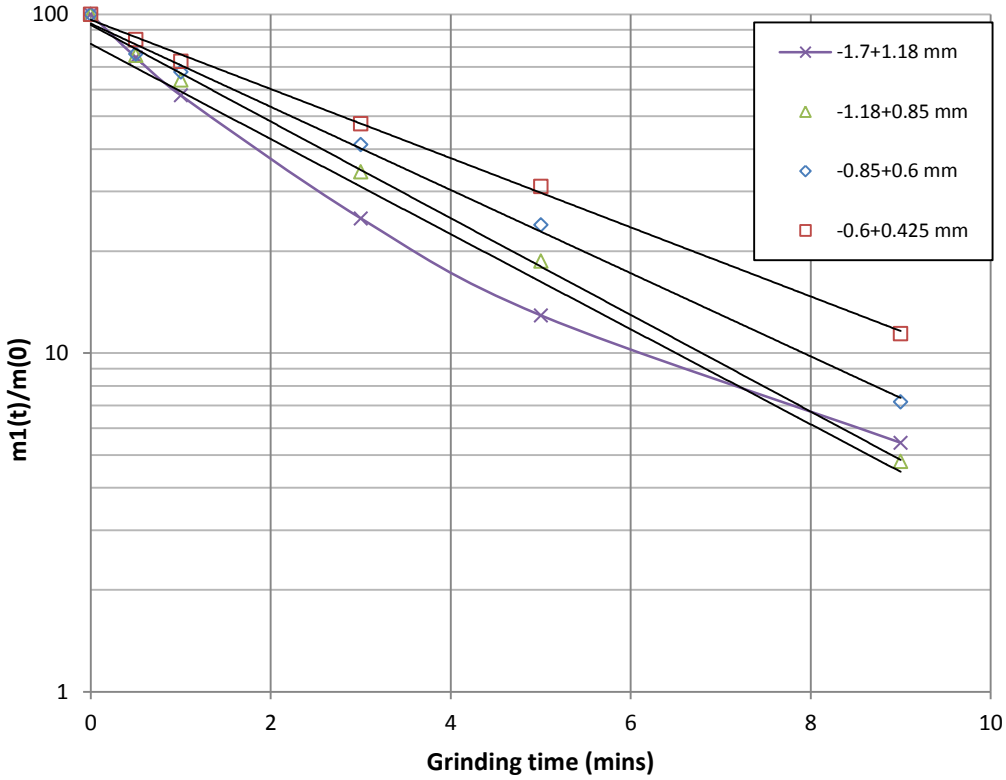

Figure 7.1: First-order plots for various feed sizes of gold ore ground in a laboratory-scale ball mill.

The results indicated that grinding of fine size fractions could be described by a first-order law. However, the coarse size fraction (-1.7+1.18mm) showed deviation from it. It probably occurred in an abnormal breakage region where particles were too large to be properly nipped by the balls.

Table 7.1: Selection function values for different feed size classes.

Mono-sized Gold ore material	Selection function value
-1700+1180 µm (S1)	0.3230
-1180+ 850 µm (S2)	0.3286
-850+600 µm (S3)	0.2827
-600+425 µm (S4)	0.2351

The specific rates of breakage of each monosize fractions that exhibited first-order grinding kinetic behavior were determined from the slope of the straight-line portion of the first-order plots. The selection function values in Table 7.1 were plotted against particle size as shown by Figure 7.2. It is seen that the increase in selection function with increase in particle size is linear for particle sizes less than ~1.2 mm. It is also noted that the maximum value of the selection function for the 20 mm balls was reached and the breakage rate decreases with a further increase in particle size. Using a power function, the parameter alpha (α) was determined from Figure 7.2 and the value obtained for was 0.5.

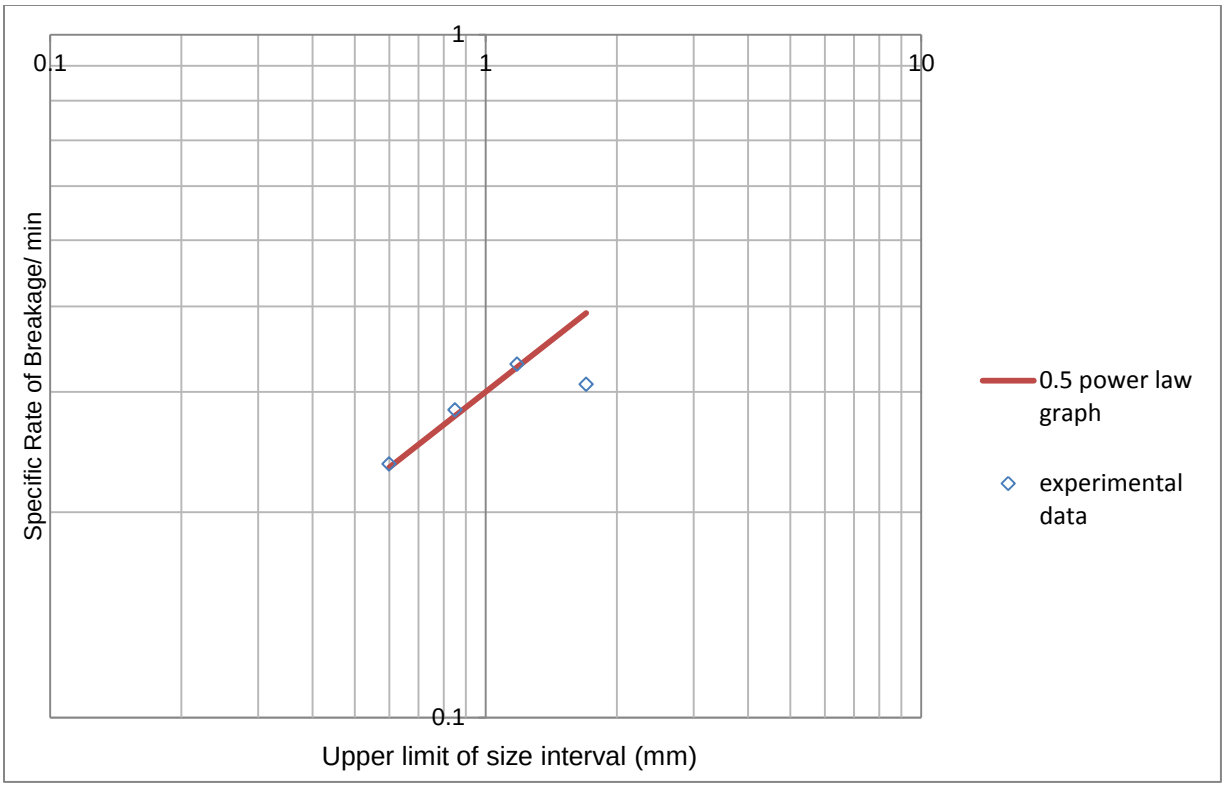

Figure 7.2: First-order plots for various feed sizes of gold ore ground in a laboratory-scale ball mill.

7.4.2 Determination of the breakage function parameters

By definition, these values are to be determined from the size distributions at short grinding times, that result in 20–30% broken materials out of the top size, and these give more accurate estimates of the parameters. Previously Austin and Luckie (1971) showed that even with 65% broken material; the procedure is still accurate enough to be used. The parameters were determined according to the BII method (Austin et al. 1984), and are shown as graphical representations in Figure 7.3. The diagram shows the primary breakage distribution plots of all feed size classes for 10 mm, 20 mm and 30 mm media and different U values.

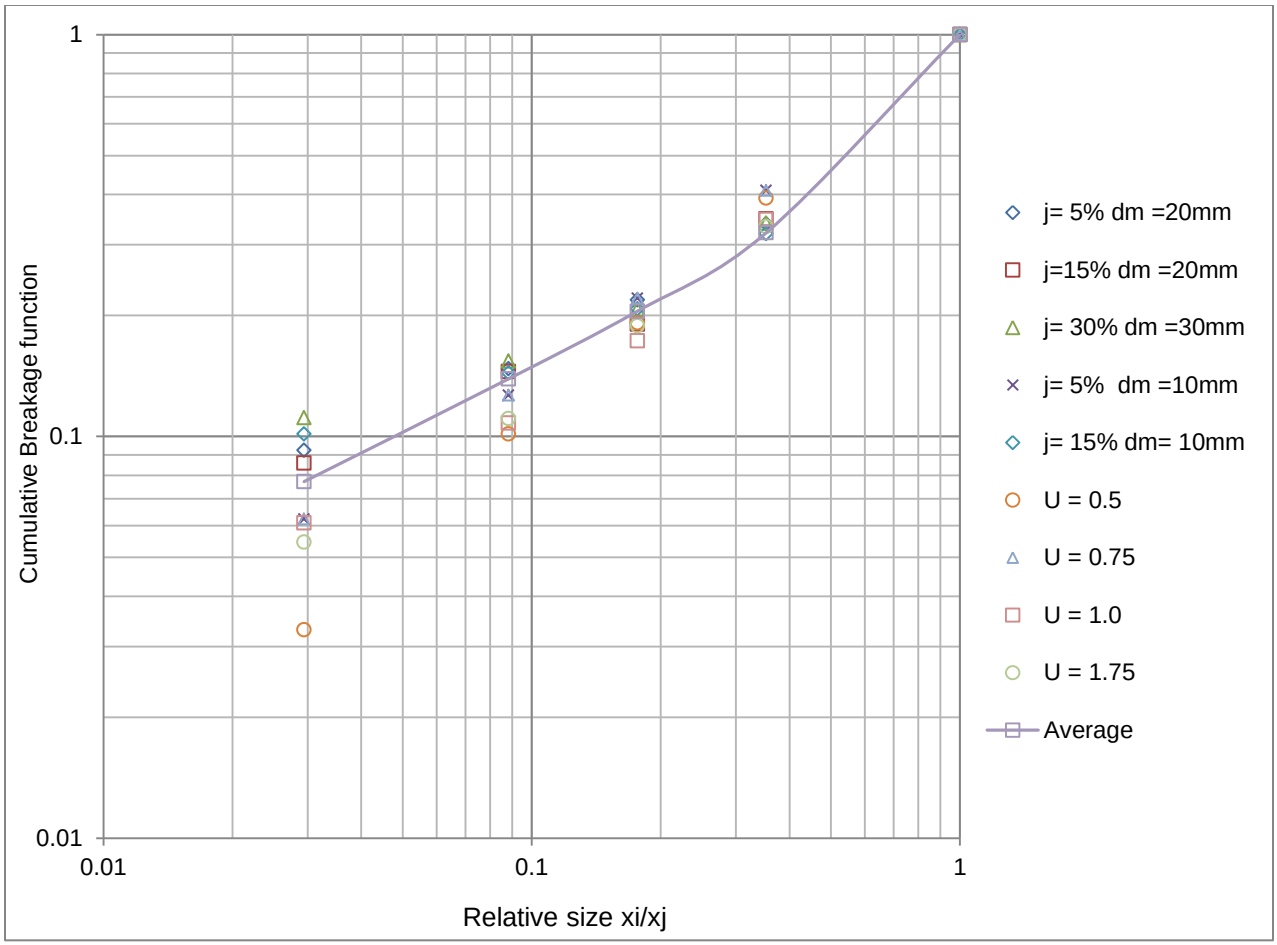

Figure 7.3: Variation of breakage function values with feed size

B_{ij} values obtained were fitted to the empirical model in Equation 7.6 (Austin *et al.*, 1984) and the breakage function parameters for the gold ore were evaluated. The average breakage function parameters determined for all feed size classes and media sizes used were $\beta = 3.6$, $\gamma = 0.5$ and $\Phi = 0.68$. Because these B values are effectively independent of milling conditions such as powder load, media load and mill diameter as verified by many experiments, average values were used (Austin *et al.*, 1984).

7.4.3 Effect of interstitial filling U (Attainable region analysis)

The size classes shown in Table 4.4 were further grouped as explained in Section 2.2.2 (AR plots) into 3 classes so that the simplest form of the AR analysis can be applied (Table 7.2).

Table 7.2: Sizes classes used for AR application.

Size class		**Type**
M1	-1700+150	Feed
M2	-150+75	Intermediate (size class of interest)
M3	-75	Fines

It is observed that as the milling process progresses the larger size class (M1) decreases as shown in Figure 7.4. The intermediate size class (M2) initially increases as larger particles break into this size class. The mass fraction curve will then pass through a maximum and then start declining as more intermediate class continues to breaking into the finer material.

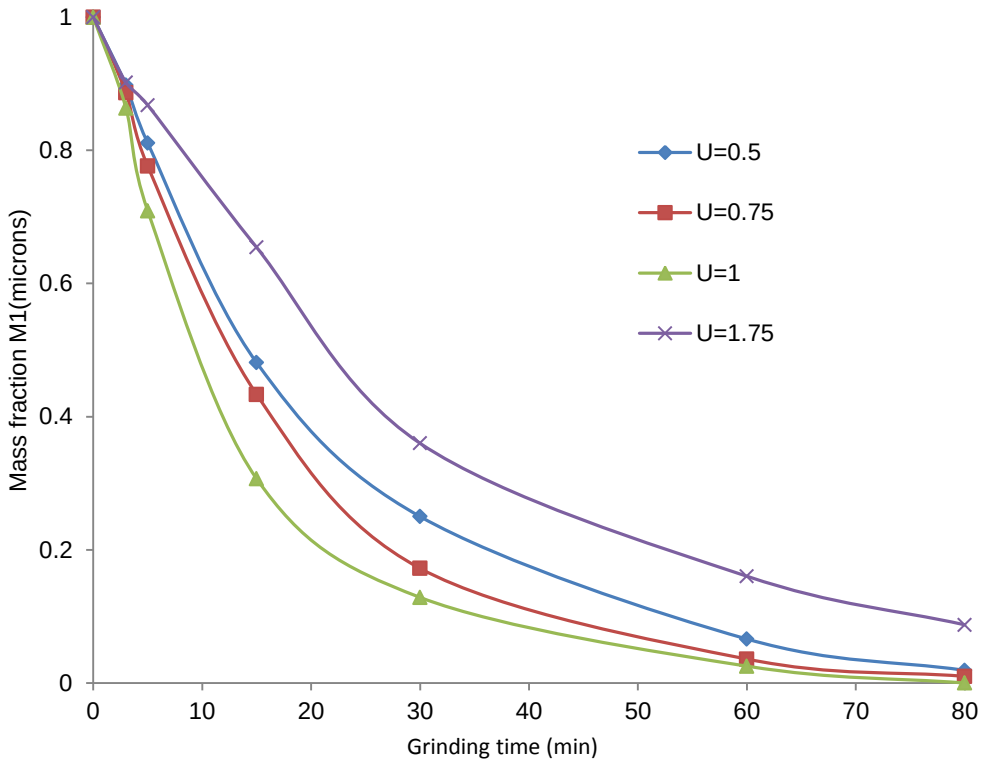

Figure 7.4: Plot of mass fraction of mass fraction of material in size class 1 (+1700-850µm) versus grinding time.

Figure 7.5 illustrates the formation of size class M2 under different interstitial filling conditions. During the initial stages of milling M2 rises sharply until it climaxes at a certain point beyond which it starts to decline. The maximum value of M2 is obtained when the U value is one (M2 = 0.245 and milling time = 18 mins). Further milling beyond this optimal point increases the value of M3 which is the finer size class. In Figure 7.5, the optimal values necessary for U are illustrated for getting the desired size class.

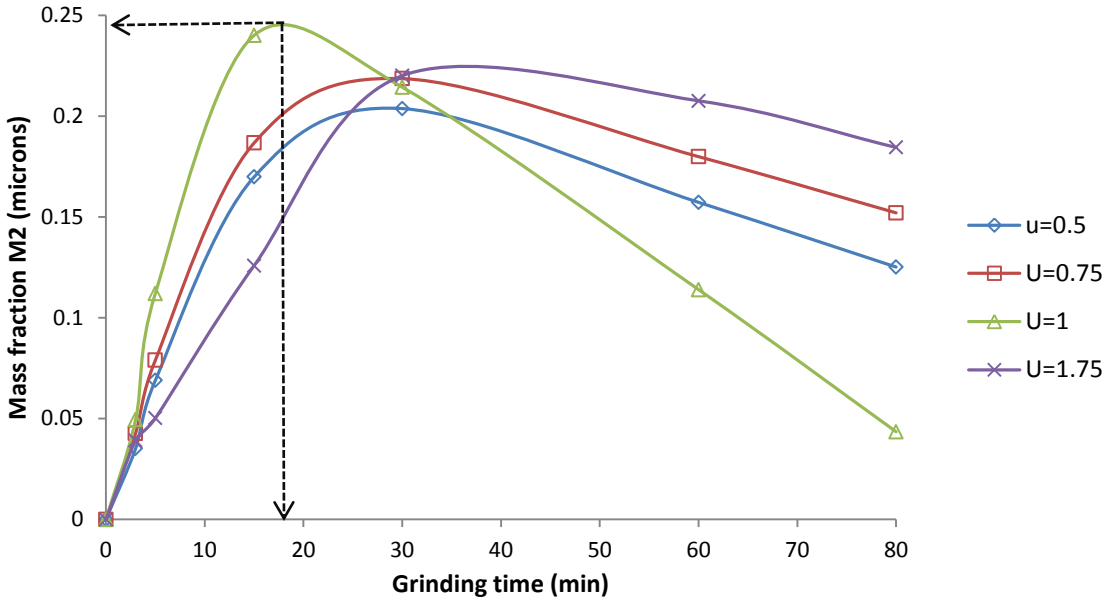

Figure 7.5: Plot of mass fraction of mass fraction of material in size class (+150-75µm) versus grinding time.

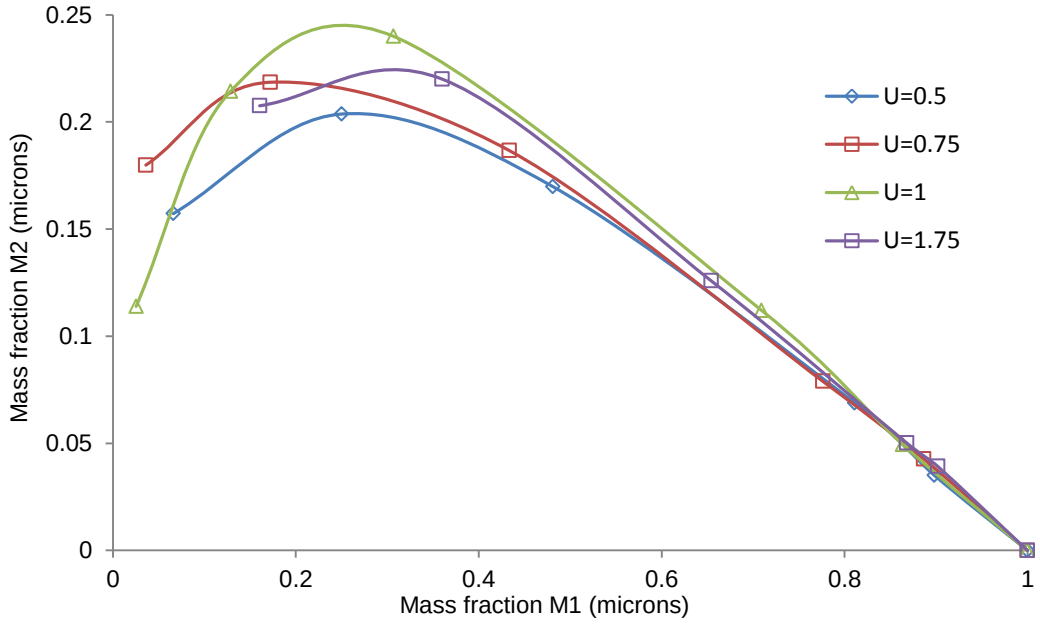

Figure 7.6: Attainable Region plot of mass fraction of material in size class 2 (+150-75µm) versus mass fraction of material in size class 1(+1700-150µm).

Figure 7.6 is an attainable region plot showing mass fraction of feed plotted against the size class of interest. As the U value is increased from 0.5 to 1 collision spaces between the balls are filled and breakage becomes more pronounced. The rate of production reaches a maximum when a value of U=1 is attained. As the amount of powder increased to U = 1.75, the collision zones are saturated hence less breakage rate accompanied by less production of required size class.

7.4.4 Milling and leaching (Attainable region analysis)

The graph (Figure 7.7) shows the experimental conversion versus the leaching time for the different size classes. The trend in recovery has been explained in section 5.3.2. The graph was further used in optimising leaching and milling time in terms of cost.

Using data for U = 1, a milling and leaching time are first selected, (say for example 60 mins milling and 2400 mins leaching). We then proceed to get the amount of mass fractions of each size class after that milling time. For 60 minutes of milling ($\underline{\alpha}_1$= 0; $\underline{\alpha}_2$= 0; $\underline{\alpha}_3$= 0.0253; $\underline{\alpha}_4$= 0.1139 and $\underline{\alpha}_5$= 0.8608).

where $\underline{\alpha}_i$ is the mass fraction of size class i.

The average recovery at a specific milling time and leaching time would be given by the equation below:

$$\text{Average Recovery} = \{\underline{\alpha}_1 C_1 + \underline{\alpha}_2 C_2 + \underline{\alpha}_3 C_3 + \ldots\} \qquad (7.7)$$

where C_i is the recovery of size class i from the leaching curve for a given milling curve (Figure 7.7). For instance, 60 minutes milling and 2400 minutes leaching average recovery is calculated as 99.52%. The data for recovery obtained for all the leaching

and milling times is populated in Table A21 in Appendix A and a surface plot is then obtained that clearly shows how the three variables relate.

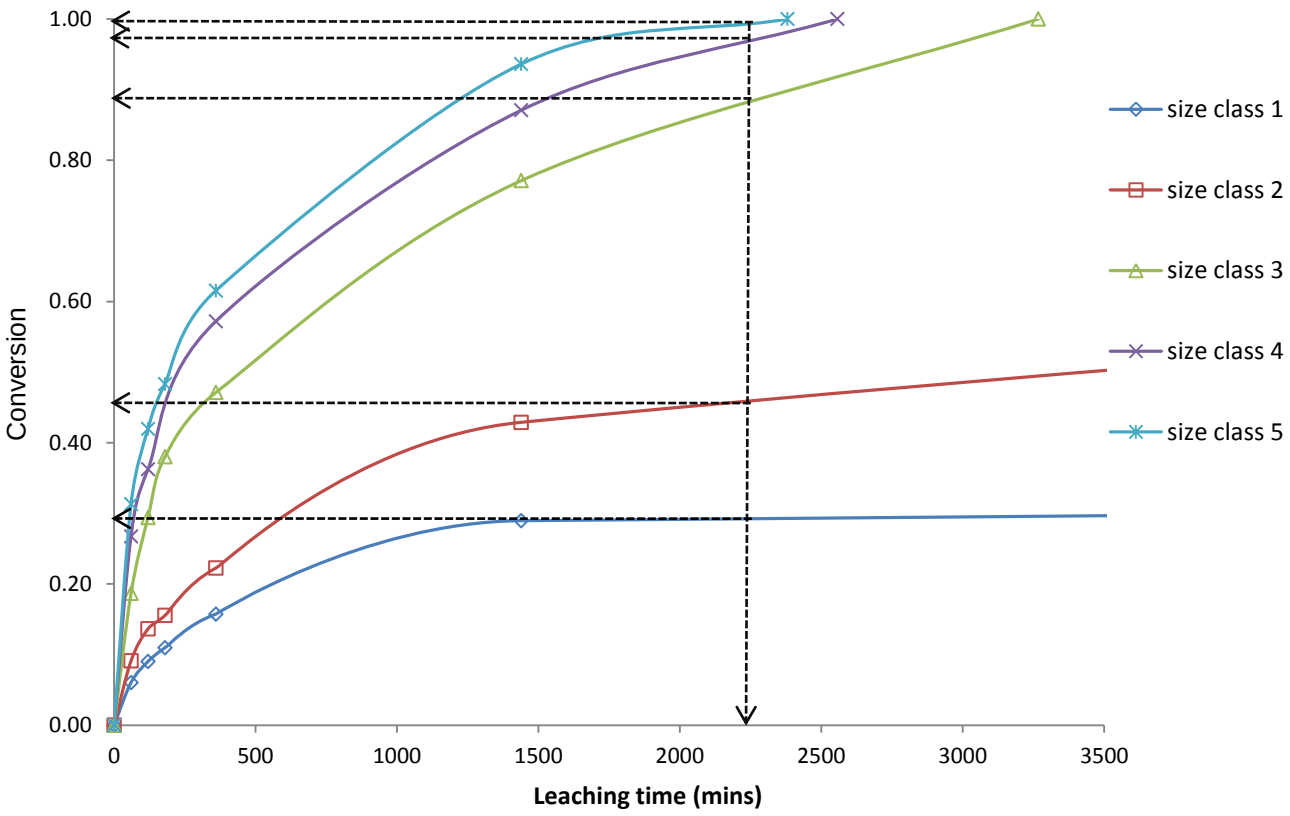

Figure 7.7: Effect of particle size on gold dissolution: (Experimental conditions: pH 11.2; 210 ppm NaCN, 24 hours).

Figure 7.8 is a 3D plot that shows that as milling and leaching times are raised the recovery also is increased to high values. It is also important to note that from the graph it is possible to leach a feed that has not been milled to obtain a certain recovery (that is, milling time = 0) though the recovery is very low.

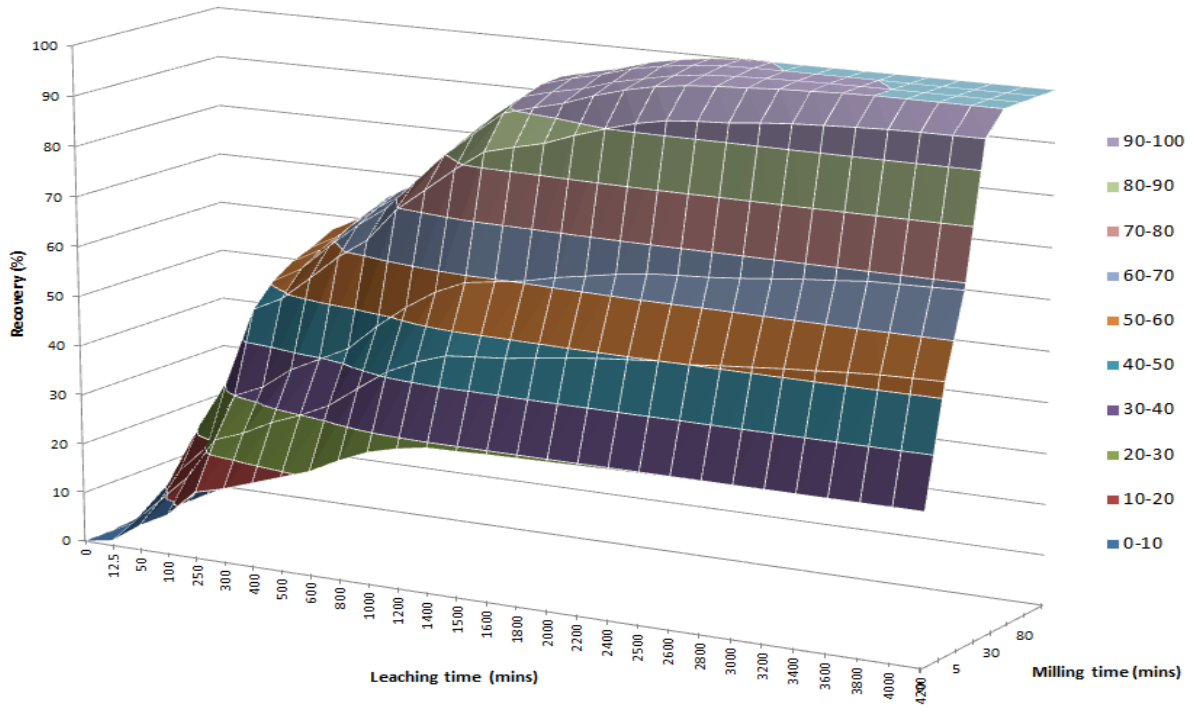

Figure 7.8: A 3D plot of recovery vs. leaching time vs. milling time.

Once the 3D plot is constructed, it can then be used to give all the possible recoveries obtained using different milling and leaching times. It is now possible to determine the optimum for a specified objective function. The optimum can be found by overlaying a contour plot of the objective function on the 3D plot. The objective function we selected was that of optimizing a linear function of the value of the recovered material minus the cost of both milling and leaching. Suppose the profit (value) is given by the equation:

$$Profit\ Value = aR - bt_{mill} - ct_{leach} \qquad (7.8)$$

where R is recovery, t_{mill} is milling time and t_{leach} is the leaching time. aR, bt_{mill} and ct_{leach} are all expressed in terms of \$/tonne of ore in hour.

The coefficient a is a composite term that is calculated by multiplying together the price of gold and the grade of the ore which is then multiplied by the fraction of gold recovered, R. This first term gives the value of gold in mining one tonne of ore in units of \$/tonne. The second term is the cost of the milling operation. The term b corresponds to the cost of running the mill per tonne of ore milled in one hour. The b term is multiplied by the milling time needed to mill one tonne of ore to the liberation size. The term b has both capital and operating expenses in it. It can be given by the sum of operating expense (electricity costs, water, chemical costs, maintenance costs, etc. per hour milling one tonne of ore) and the product of an hourly interest rate(or hourly return on investment if the money borrowed to build the plant has been paid off) times the total capital investment associated with comminution's physical plant. The c term is an analogous term to b term accounting for both operating and capital costs on an hourly basis per tonne of ore processed but for leaching operations.

We then select values of a, b and c depending on the leaching and milling properties of of particular ore. It is noted that some costs maybe be similar or fixed for different ores (e.g. labour and ore storage). Table 7.3 shows some of the costs that may affect the milling and leaching processes.

Table 7.3: Estimated process operating and capital costs that may be used to calculate b and c

Milling Costs \$ (b)	Leaching Costs \$ (c)
Operational and Capital	*Operational and Capital*
Power, Ball mill steel media, Process control, waste reclamation and delivery, ore delivery, primary crushing, ores storage, thickening	Reagents and chemicals, consumables, utilities, maintenance, labour, tailings dam

For instance, if an ore grinds slowly and has its value metal locked up in its hard matrix, it would require more grinding and might need longer leaching times to recover the values. In that case, the factors (b) and (c) would be very high. Table 7.4 summaries the simple various situations investigated to show how profit value changes with variations of factors b and c

Table 7.4: Scenarios for different values of b and c investigated

Coefficient	Value		
b	low	high	high
c	low	low	high
	Figure 7	Figure 8	Figure 9

Figures 7 - 9 illustrate how the profit value varies as b and c are changed. In order to obtain the optimum profit, we make use of contour plots as shown in Figures 7.9 – 7.11. This is done through a process of choosing a milling time and calculating the recovery and these would correspond to points on the surface of Figure 7.8.

Alternatively this data is drawn on a two dimensional plot as contours of recovery for various values of milling and leaching times as can be seen in Figure 7.9. These are the dashed lines on Figure 7.9 labeled for various percentage recoveries. Therefore, knowing a particular value of milling and leaching time, one can read off the recovery and substitute these into equation 7.8 to get a value of profit. When we have done this for many points we can use a contour drawing programme to get the closed contours on Figure 7.9. When we have found the highest point this corresponds to the maximum profit and then we can read off the associated milling and leaching times and read off what the recovery is.

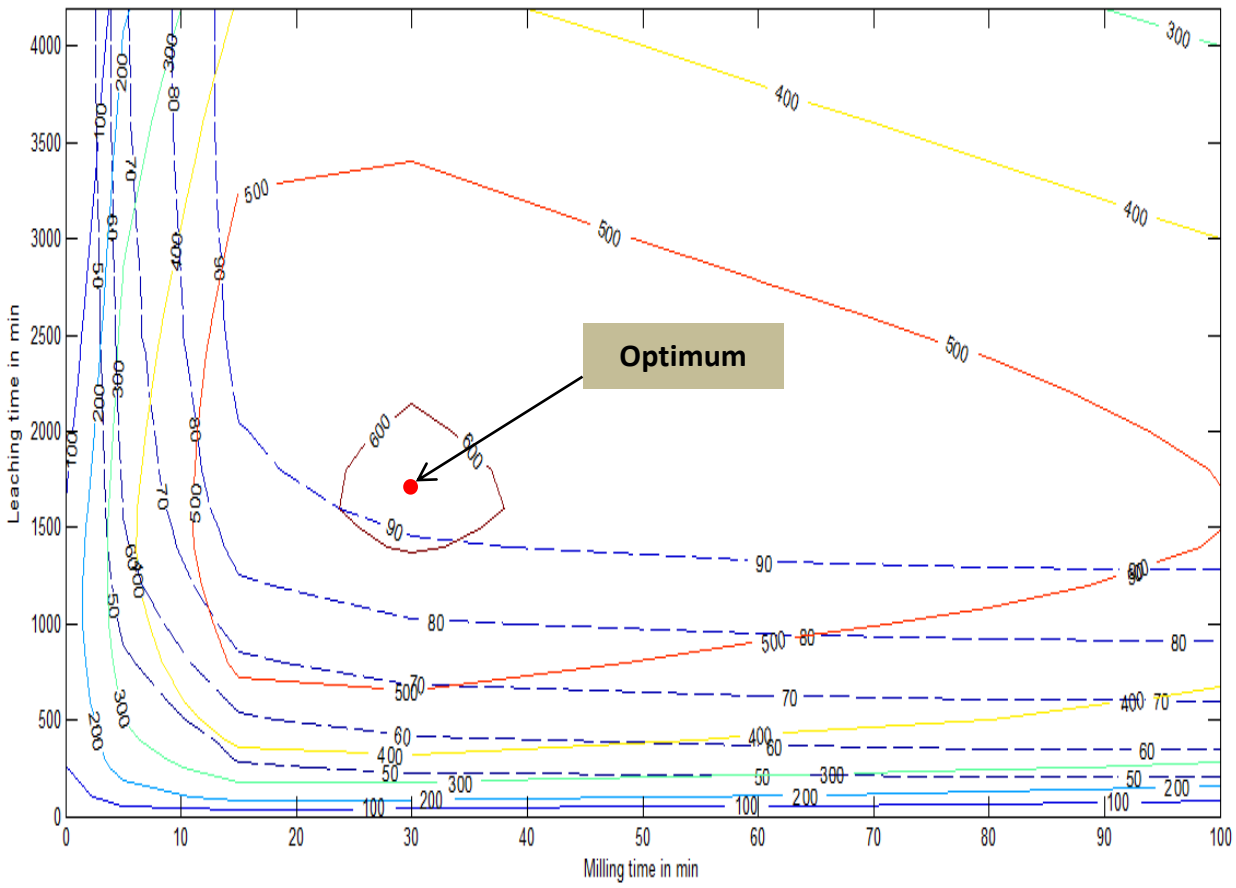

Figure 7.9: Contour plot showing optimisation for a joint milling and leaching circuit: (values: b = low, c = low).

The dashed lines represent the recovery in terms of leaching and milling times whilst the bold lines show the cost value also in terms of leaching and milling times.

From Figure 7.9, it can be seen that from the contour plot the optimum is obtained at 90% recovery (profit value of 600, milling time ~30 minutes and leaching time ~1750 minutes)

More policies are also shown below where the values of b and c are varied.

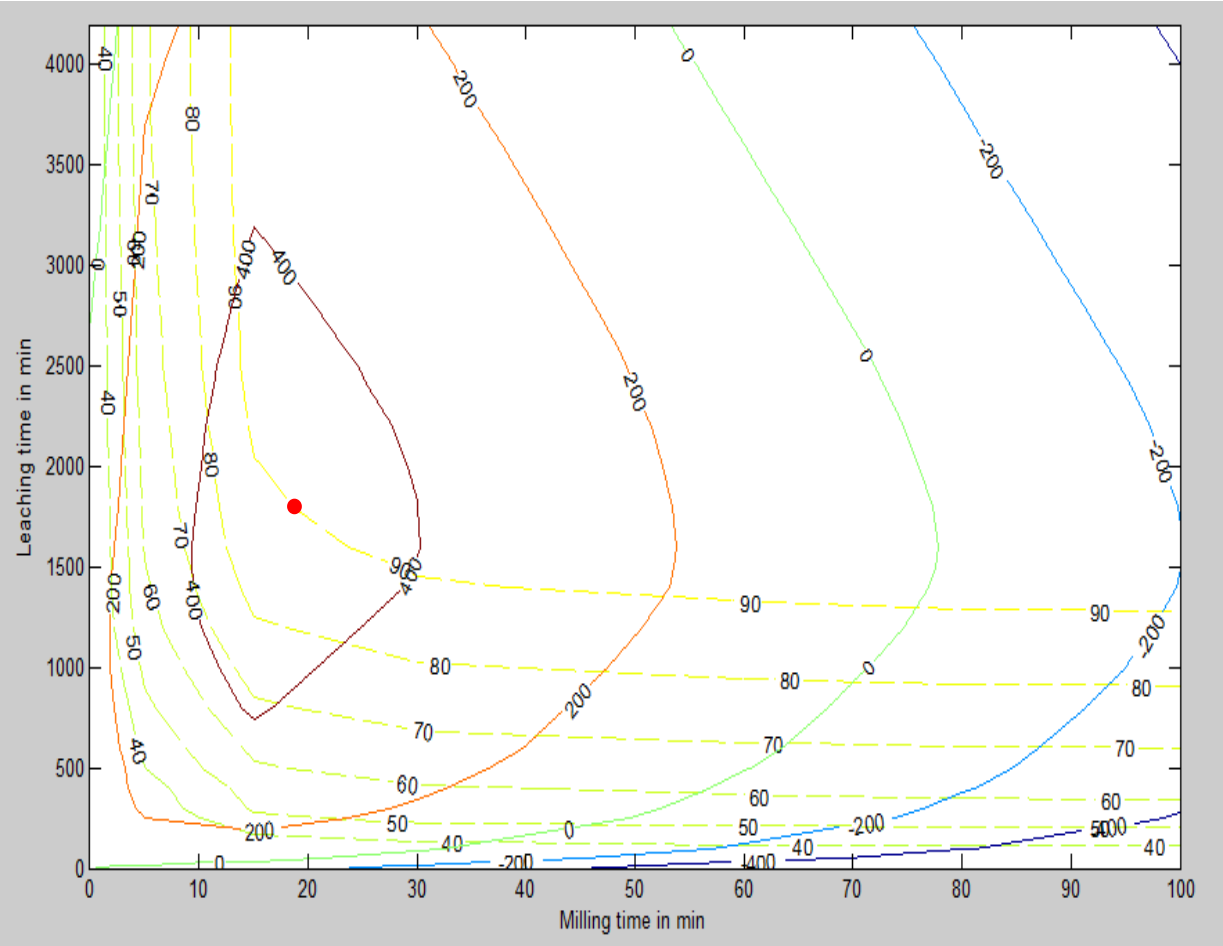

Figure 7.10: Contour plot showing optimisation for a joint milling and leaching circuit: (values: b = high, c = low).

The dashed lines represent the recovery in terms of leaching and milling times whilst the bold lines show the cost value also in terms of leaching and milling times.

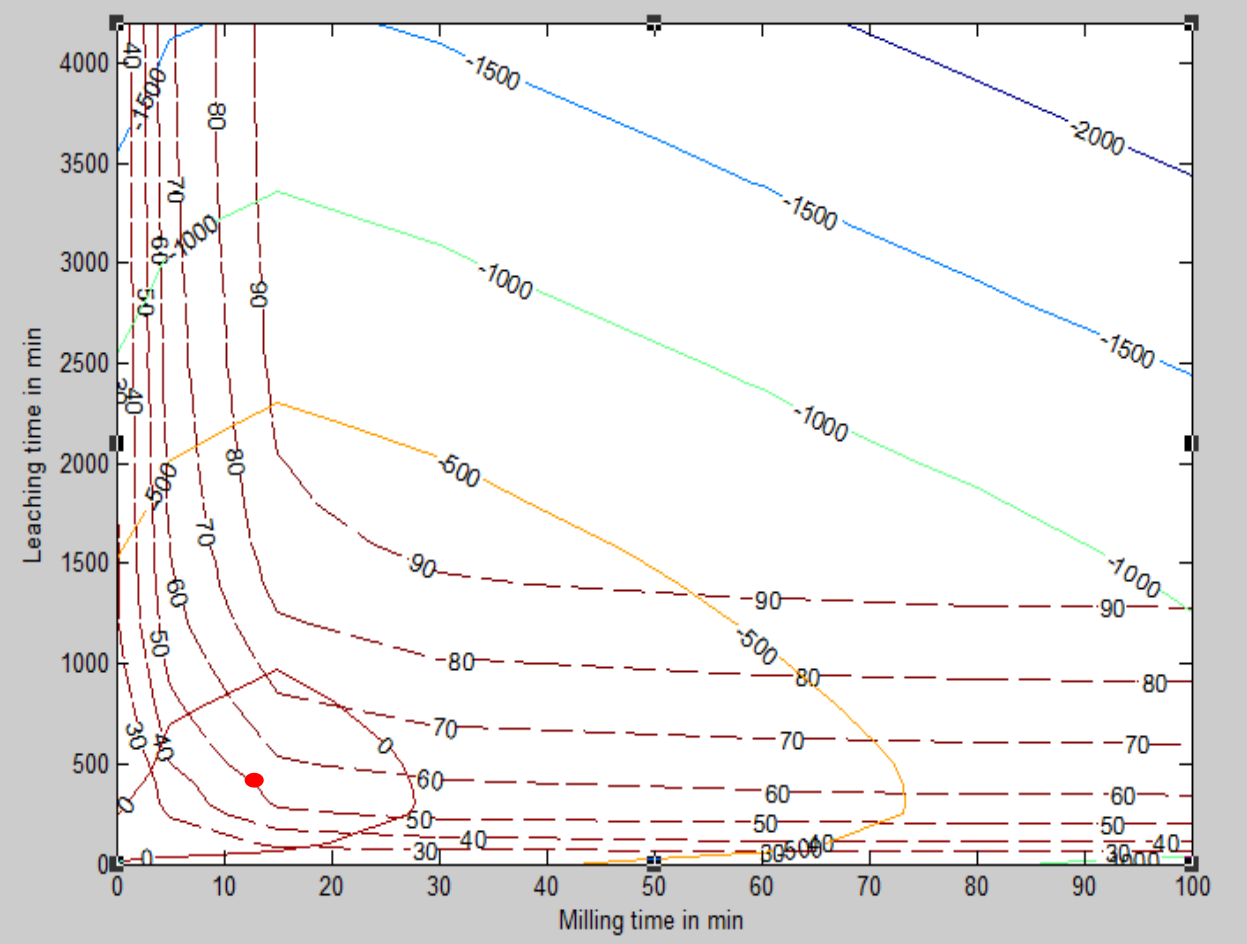

Figure 7.11: Contour plot showing optimisation for a joint milling and leaching circuit: (values: b =high, c= high).

The dashed lines represent the recovery in terms of leaching and milling times whilst the bold lines show the cost value also in terms of leaching and milling times.

Figure 7.10 shows a situation when a, b are raised and c is kept minimal. This is a scenario were milling has a high cost and leaching time then becomes minimal. In this case the profit is lowered.

Increasing both milling and leaching time has the ability to unlock the value material but the profit obtained is very low or one runs at a loss (Figure 7.11). Clearly in this case the profit margin is very low.

In a real situation one will be able to get real data for a, b and c and find the best operating conditions for that plant at that time. As time goes on the values of these coefficients may change (for instance electricity costs increase!) but one is able to use the same graph to calculate the profit. This is because in drawing these graphs and contours we have been able to separate the technological from the economic aspects. This makes the AR method a potentially powerful tool for optimizing complex operations such as found in this example.

7.5 CONCLUSION

A study of the milling and leaching behaviour of the dissolution of Far West gold ore was investigated. The breakage parameters of the gold ore were calculated and also the optimum U (interstitial) filling required to gain the maximum amount of a preferred size class for leaching (-150+75μm) was found. In this research, results show that using a value U = 1 is an effective ratio because it gave a high value of the required intermediate material. Shoji et al. (1982) found the maximum at U = 0.83 for the quartz mineral. Tangsathitkulchai (2003) found that grinding at about U = 1 gave the maximum in net mill power.

This study showed that grinding kinetic parameters could be different for different powder filling methods. Therefore, it appears that in order to lower the energy costs in grinding process each material's grinding kinetics must be evaluated.

Finally the results of the technological model are plotted using an attainable region approach and this is then used to find optimum values of milling and leaching time that

would give a maximum profit for a given objective function. As the technological and the economic aspects using this method are separated it becomes easy to re-evaluate the optimum conditions as the economic climate changes.

CHAPTER 8

8 CONCLUSIONS AND RECOMMENDATIONS

The aim of the thesis was to investigate a joint milling and leaching circuit. In order to achieve this task, an investigation was done to determine how the material feed behaved when it was milled. The milled mono-sized material was then leached in order to find how much liberation occurred during the process. Different media sizes and ball filling values were used and these gave different amounts of energy and recovery values. It was concluded that the overall main costs in the mineral processing industry are functions of time, energy and capital and a balance must be struck between these.

After establishing the model for ball size and ball filling, the next phase of experiments investigated the type of leaching that occurs and also the factors affecting this downstream process. The anticipated benefits were to achieve high recoveries. Results obtained fitted the shrinking core model with ash diffusion as the controlling step with activation energy of approximately 12.9kJ/mol.

After the leaching kinetics of the ore, the milling kinetics of the ore were determined in order to obtain the selection and breakage function parameters for a population balance model.

The Attainable Region analysis was then applied to find the grinding period required so as to maximise the profit associated with a joint milling and leaching circuit.

No work on utilizing the AR to optimise the size reduction and leaching of an industrial ore has been reported previously. The experimental results show that the AR method could be successful in reducing the cost associated with a joint milling and leach process. Different milling and leaching times will offer different recoveries and hence different costs. It is therefore of paramount importance that the profit is evaluated using the particular combination of milling and leaching operational times.

It must be emphasized at this point that in the current analysis we have made the assumption that the objective function (profit function) is only a function of the two variables, namely the milling times and leaching times. While it would make the analysis more complicated as one would be working in a higher dimensional space, there is no reason why other state variables on which the objective function might depend, could not be added to the Attainable Region.

The next step could be to apply the analysis using actually plant operation and capital costs and comparing the amount of profits obtained. We also need to devise ways of validating all the findings on an industrial scale. The proposed route is to resort to a detailed modelling of a processing plant. The data would then be optimally analysed with the AR technique. In doing so, it should be possible to say from an AR perspective whether the operating conditions currently in use in equipment are indeed optimal; these conditions in this example refer to ball milling, and leaching.

Of importance to industry would be the proposition of a more holistic way of analysing, designing, and optimising flow-sheets subject to more stringent requirements ranging from technological and energy constraints to environmental and economic considerations.

The anticipated success of such an undertaking would give an edge to the South African industry and would help reinforce its global position in the area of mineral processing. Furthermore, the penetration of the AR technique as a tool of choice for the analysis, design and optimisation of mineral processing circuits would be seen as a valuable asset. Numerous opportunities that could revolutionise the way the industry is viewed could follow.

In conclusion what has been presented in this thesis is an example of a simple mineral processing system where it has been shown how to go through all the steps required to optimize the profit from an operating plant using the Attainable Region method.

REFERENCES

Austin, L.G., & Brame, K. 1983, 'A comparison of the Bond method for sizing wet tumbling mills with a size-mass balance simulation model'. Powder Technology, 34: pp. 261-274.

Austin, L.G., Luckie, P.T., Klimpel, R.R. 1984, 'Process Engineering of size reduction: ball milling. SME/ AIME, New York.

Austin, L.G., Shoji, K., Luckie, P.T. 1976, 'The effect of ball size on mill performance', Powder Technology, vol. 14, no. 1, pp. 71-79.

Austin, L. G., Shoji, K. & Bell, D. 1982, 'Rate equations for non-linear breakage in mills due to material effects', Powder Technology, vol 31, pp. 127 – 133

Austin L.G., Concha F., Disefio y (1990), 'Simulaci6n de Circuitos deMolienda, Universidad de Concepción, Concepción,

Behzadi, S.S., Prakasvudhisarn, C., Klocker, J., Wolschann, P., Viernstein, H. 2009, 'Comparison between two types of Artificial Neural Networks used for validation of pharmaceutical processes', Powder Technology 195 150–157.

Bond F.C., Crushing and grinding calculations, Allis Chalmers Tech. Pub.07R9235B1961.

Biomine. 2006 [Online] Available at: http://www.campus.skelleftea.se/biomine/leaching/index.htm [Accessed 20/13/2008].

Blaskett, K.S. 1970, 'Estimation of power consumption in grinding mills', In: M.J. Jones (Editor), Proceedings of Ninth Commonwealth Mining and Metallurgical Congress, 1969. Instn. Min. Metall, London, no. 3, pp. 631-649.

Bond, F. C. Trans. A.I.M.E., 193, 4 84, (1952).

Breuer, P.L., Jeffrey, M.I., Hewitt, D.M. 2008, 'Mechanisms of sulphide ion oxidation during cyanidation'. Part 1: Effect of Lead (II) ions', Minerals Engineering, 22, pp 579-586.

Bwalya, M.M., Moys, M.H., Finnie, G.J., Mulenga, F.K. 2014, 'Exploring ball size distribution in coal grinding mills,' Powder Technology. 257 pp 68–73.

Chimwani, N., Glasser, D., Hildebrandt, D., Metzger, M.J., Mulenga, F.K 2013 'Determination of the milling parameters of a platinum group minerals ore to optimize product size distribution for flotation purposes' Miner. Eng. Vol. 43–44, pp 67–78.

Cho, H. Kwon, J. Kim, K. Mun, M. (2013), 'Optimum choice of the make-up ball sizes for maximum throughput in tumbling ball mills', Powder Technol. 246 pp. 625–634.

Cleary, P.W. 2009, 'Ball motion, axial segregation and power consumption in a full scale two chamber cement mill', Minerals Engineering, vol. 22, no. 9 – 10, pp. 809 – 820

Cohen, H.E. 1983, 'Energy usage in mineral processing' Trans. Inst. Min. Metall., 92: C160-C164.

Concha, F. Magne, L. Austin, L.G. (1992), 'Optimization of the make-up ball charge in a grinding mill', International Journal of Mineral Processing. 34 pp 231–241.

Crundwell, F.K. & Godorr, S.A. 1997, 'A mathematical model of the leaching of gold in cyanide solutions', Hydrometallurgy, vol. 44, pp. 147-162.

Cundall, P.A. 1971, A computer model for simulating progressive large scale movements in block rock systems. *Symp. Intl. Society of Rock.*

Cundall, P.A. & Strack, O.L., 1979, ‘A distinct element model for granular Assemblies’, Geotechnique, 29(1), pp. 47-65.

G. Danha, D. Hildebrandt, D. Glasser, C. Bhondayi, ‘A laboratory scale application of the Attainable Region technique on a platinum ore’, Powder Technology 274 (2015) 14-19.

Dahner, J & Van Den Bosch, A. 2010 ‘Total primary milling cost reduction by improved liner design’. The 4th International Platinum Conference, Platinum in transition ‘Boom or Bust’, The Southern African Institute of Mining and Metallurgy,

De Andrade Lima, L.R.P & Hodouin, D. 2005, ‘A lumped kinetic model for gold ore cyanidation’, Hydrometallurgy.vol. 79 pp 121-137.

De Andrade Lima, L.R.P. & Hodouin, D. 2006, ‘Simulation study of the optimal distribution of cyanide in a gold leaching circuit’, Minerals Engineering, vol. 19, no. 13, pp 1319-1327.

Deniz, V. & Onur, T. 2002, ‘Investigation of the breakage kinetic of pumice samples as dependent on powder filling in a ball mill’, International Journal of Mineral Processing, vol. 67, pp 71–78.

Deniz, V. 2004, ‘The effect of mill speed on kinetic breakage parameters of clinker and limestone’, Cement and concrete research, vol. 34, no. 8, pp. 1365-1371.

Deniz, V. 2010, ‘Influence of interstitial filling on breakage kinetics of gypsum in ball mill’, Advanced Powder Technology, vol. 22, no. 4, pp. 512-517.

Deschênes, G., Lacasse, S., Fulton, M. 2003, ‘Improvement of cyanidation practice at Gold corp Red Lake Mine’, Minerals Engineering, vol. 16, no. 6, pp. 503-509.

Dong, H. & Moys, M.H. 2003, 'Load behavior and mill power', International Journal of Mineral Processing, vol. 69, no. 1 – 4, pp. 11 – 28

Djordjevic, N. 2003, 'Discreet element modelling of power draw of tumbling mills', Trans Inst Min Metall, C, vol 112, pp. C109-C114.

Ellis, S. & Senanayake, G. 2004, 'The effects of dissolved oxygen and cyanide dosage on gold extraction from a pyrrhotite-rich ore', Hydrometallurgy, vol. 72, no. 1-2, pp 39-50.

Fuerstenau, D.W., Lutch, J.J. & De, A. 1999, 'The effect of ball size on the energy efficiency of hybrid high-pressure roll mill/ball mill grinding', Powder Technology, vol. 105, no. 1-3, pp. 199-204.

Gasparrini, C. 1983, 'The Metallurgy of gold and its significance in metal extraction', CIM Bull, vol.76, no. 851, pp 141-153.

Glasser, D., Hildebrandt, D., 1997, 'Reactor and process synthesis', Computers in Chemical Engineering, vol. 21, Suppl. 1, pp. S775 – S783

Glasser, D., Hildebrandt, D. & Crowe, C. 1987, 'A geometric approach to steady flow reactors: The attainable region and optimisation in concentration space', Industrial and engineering chemistry research, vol. 26, no. 9, pp. 1803-1810.

Gupta, D. & Yan, S. 2006, 'Mineral Processing Design and Operation: An introduction', Elsevier, Pert.

Habashi, F. 1969, 'Principles of Extractive metallurgy', General Principles, Gordon & Breach, New York, London, vol. 1.

Habashi, F. 1999, ‘Kinetics of Metallurgical Processes’, 2nd Ed., Metallurgies Extractive Quebec, pp.24.

Habashi, F. 1967, ‘Kinetics and mechanisms of gold and silver dissolution in cyanide solution’, Bur. Mines Geology, Montana Bull. 59.

Herbst, J.A. & Fuerstenau, D.W. 1980, ‘Scale-up procedure for continuous grinding mill design using population balance models’, International Journal of Mineral Processing, vol. 7, no. 1, pp. 1-31.

Herbst, J.A, Lo, Y.A, Flintoff, B, (2003). Size Reduction and Liberation, in Principles of Minerals Processing (ed: K.N Han, M.C. Fuerstenau) (pp. 61-115). Society for Mining, Metallurgy, and Exploration, INC (SME).

Hildebrandt, D. & Glasser, D. 1990, ‘The attainable region and optimal reactor structures’, Chemical Engineering Science, vol. 45, no. 8, pp. 2161-2168.

Hlabangana, N. Danha, G. Hildebrandt, D. & Glasser, D, (2016). Use of the attainable region approach to determine major trends and optimize particle breakage in a laboratory mill, Powder Technology 291 414–419.

Horn, F. 1964, ‘Attainable and non-attainable regions in chemical reaction technique’, Proceedings of the European Symposium on Chemical Reaction Engineering; Pergamon: New York, pp. 1.

Hukki, R.T. 1954, ‘Correlation between principal parameters affecting mechanical ball wear’, Mining Engineering, pp. 642-644.

Katubilwa, F.M., Moys, M.H., Glasser, D. & Hildebrandt, D. 2011, ‘An attainable region analysis of the effect of ball size on milling’, Powder Technology, vol. 210, no. 1, pp 36-46

Kavetsky, A., Whiten, W.J. & Narayanan, S. 1982, ‘Studies on the scale-up of ball mills’, Symposia Series - Australasian Institute of Mining and Metallurgy, pp. 113.

Kelly, E.G., Spottiswood, D.J., 1982, ‘Introduction to Mineral Processing’, John Wiley & Sons, New York

Kick, F. 1885, ‘Contributions to the knowledge of brittle materials’, Dinglers J., 247: 1-5.1.

King, R. 2001, ‘Modelling and simulation of mineral processing systems’, Butterwort-Heinemann, ISBN: 0-7506-4884-8.

Khumalo, N., Glasser, D., Hildebrandt, D., Hausberger, B., Kauchali, S. 2006, ‘The application of the attainable region analysis to comminution’, Chem. Eng. Sci, no. 61, pp 5969-5980.

Khumalo, N., Glasser, D., Hildebrandt, D., Hausberger, B. 2007, ‘An experimental validation of a specific energy-based approach for comminution’, Chemical Engineering Science, vol. 62, no. 10, pp 2765-2776.

Khumalo, N., Glasser, D., Hildebrandt, D., Hausberger, B. 2008, ‘Improving comminution efficiency using classification: An attainable region approach’, Powder Technology, vol. 187, no. 3, pp 252-259.

Klimpel, R.R. 1984, ‘Influence of material breakage properties and associated slurry rheology on breakage rates in wet grinding of coal/ores in tumbling media mills’, Reagents in the Minerals Industry, pp. 265-269.

Klimpel, R.R. 1982, ‘Influence of slurry rheology on the performance of mineral/coal grinding circuits’, Symposia Series - Australasian Institute of Mining and Metallurgy, pp. 1.

Klimpel, R.R. 1983,‘Slurry rheology influence on the performance of mineral/coal grinding circuits - 2’, Mining Engineering, vol. 35, no. 1, pp. 21-26.

Kokossis, A.C. & Floudas, C.A. 1991,‘Synthesis of isothermal reactor-separator-recycle systems’, Chemical Engineering Science, vol. 46, no. 5-6, pp. 1361-1383.

Kondos, P.D., Deschênes, G. & Morrison, R.M. 1995, ‘Process Optimization Studies in Gold Cyanidation’, Hydrometallurgy, vol. 39, pp. 235-250.

Koivistoinen, P., Virtanen, M., Eerola, P., Kalapudas, R., 1989. A Comminution Cost Comparison of Traditional Metallic Grinding, Semi autogenous Grinding (SAG) and Two Stage Autogenous Grinding. Proceedings of SAG 1989 Conference, Vancouver B.C.,

Levenspiel, O. (1999), ‘Chemical Reaction Engineering. 3rd Ed. Massachusetts: John Wiley & Sons.

Liddell, K.S., Moys, M.H., 1988,‘The effects of mill speed and filling on the behaviour of the load in a rotary grinding mill’, Journal of the South African Institute of Mining and Metallurgy, vol. 88, no. 2, pp. 49 – 57

Ling, P., Papangelakis, V.G., Argyropoulos, S.A. & Kondos, P.D. 1996, ‘An improved rate equation for cyanidation of a gold ore’, Canadian Metallurgical Quarterly, vol. 35, no. 3, pp. 225-234.

Maclaurin, J.S., 1893, ‘The dissolution of gold in solution of potassium cyanide’, J. Chem. Sot, no. 63, pp. 724-738.

Makokha, A.B., Moys, M.H., 2006, ‘Towards optimising ball-milling capacity: Effect of lifter design’, Minerals Engineering, vol. 19, no. 14, pp. 1439 – 1445

Makokha, A.B, Moys M.H, Bwalya M.M, Kimera, K. (2006). A new approach to optimising the life and performance of worn liners in ball mills: Experimental study and DEM simulation. Minerals Engineering, 1439-1445.

Marsden, J. & House, I. (1992), ‘The Chemistry of Gold Extraction', West Sussex, England: Ellis Horwood.

Mishra, B. K. & Rajamani, R. K. 1990,‘Study of media mechanics in tumbling mills by the Discrete Element Method’, Kona powder and particle., pp.92-98.

Morrell, S. 1993, ‘The prediction of power draw in wet tumbling mills’, PhD Thesis, University of Queensland (JKMRC), Australia.

Metzger, M.J, Glasser D., Hausberger B., Hildebrandt, D. & Glasser B.J 2009, ‘Use of the Attainable Region Analysis to Optimize Particle Breakage in a Ball Mill’, Chem. Eng. Sci, vol. 64, Issue 17. 1, pp. 3766 -3777.

Metzger, M.J., Desai, S.P., Glasser, D., Hildebrandt, D. & Glasser, B.J. 2012, ‘Using the attainable region analysis to determine the effect of process parameters on breakage in a ball mill’, AIChE Journal, vol. 58, no. 9, pp. 2665-2673.

Metzger, M.J., Glasser, B.J., Glasser, D., Hausberger, B. & Hildebrandt, D. 2007, ‘Teaching reaction engineering using the attainable region’, Chemical Engineering Education, vol. 41, no. 4, pp. 258-264.

Onur, M. 1999, ‘Ball size rationing affects clinker grinding’, World Cement Research. February. Pp. 101-106

Metzger, M.J. 2011, ‘Numerical and experimental analysis of breakage in a mill using the attainable region approach’, PhD Thesis, New Brunswick, the State University of New Jersey

Mills, T. 1951, ‘An electrochemical study of the dissolution of gold and silver in cyanide solutions’, Ph.D. Thesis, Univ. Melbourne.

Napier-Munn, T.J., Morrell, S., Morrison, R.D. & Kojovic, T. 1996, ‘Mineral comminution circuits – Their operation and optimization’, JKMRC Monograph Series, University of Queensland

Nicol, M.J. Fleming, C.A. Paul, R.L. 1987, ‘The chemistry of the extraction of gold in the extractive metallurgy of gold in South Africa’, Journal of the South Africa Institute of Mining and Metallurgy M7: pp. 831-906.

Norgate, T, Haque, N. 2010. ‘Energy and greenhouse gas impacts of mining and mineral processing operations’. Journal of Cleaner Production, 266-274.

Onur, M. 1999, ‘Ball size rationing affects clinker grinding’, World Cement Research. February, pp. 101-106

Parga, J.R., Valenzuela, J.L. & Francisco, C.T. 2007, ‘Pressure Cyanide Leaching for Precious Metals Recovery’, Aqueous Processing, Oct 2007.

Perry, R., Browner, R.E., Dunne, R. & Stoitis, N, N. 1999, 'Low pH cyanidation of gold', Minerals Engineering, 12(2), pp. 1431-1440.

Powell, M.S. Verneulen, L.A. 1993. 'The influence of liner design on the rate of production of fines in a rotary mill'. Minerals Engineering. 169-183.

Prasher, C.L. editor, 1987, Particle shape, size and surface, Grinding handbook, pp. 46-62.

Rose H, E., 1967, 'A comprehensive theory of the comminution process', 2nd European Symposium Zerkleinem, Amsterdam,

Rose, H.E & Sullivan, R.M.E. 1958, 'Treatise on the internal mechanics of ball tube and rod mills', Constable and Company Ltd, London.

Rumpf, H., 1973, 'Physical aspects of comminution and new formulation of a law of comminution', Powder Technol., no.7, pp. 145-159.

Schonert, K. 1979, 'Energy aspects of size reduction of brittle materials', Zem-Kalk-Gips, Transl. No. 1/79., 3: pp. 40-44.

Senanayake, G. 2005,'Kinetics and reaction mechanism of gold cyanidation: Surface reaction model via Au(I)-OH-CN complexes', Hydrometallurgy, vol 80, pp. 1-12.

Shoji, K., Austin, L.G., Smalia, F., Brame, K. & Luckie, P.T. 1982, 'Further studies of ball and powder filling effects in ball milling', Powder Technology, vol 31, pp. 121–126

M.S. Siraj, S. Radl, B.J. Glasser, J.G. Khinast, Effect of blade angle and particle size on powder mixing performance in arectangular box, Powder Technology 211 (2011) 100-113.

Stange, W. (January/February 1999), 'The process design of gold leaching and carbon-in-pulp circuits'. The Journal of the South African Institute of Mining and Metallurgy

Taggart, A.F., 'Handbook of Mineral Dressing', John Wile and Sons, Inc., N.Y., Sec. 5, p.126 (1945).

Tangsathitkulchai, C., 2002,'Acceleration of particle breakage rates in wet batch ball milling', Powder Technology, vol. 124, no. 1 – 2, pp. 67 – 75

Tangsathitkulchai, C. 2003, 'Effects of slurry concentration and powder filling on the net mill power of a laboratory ball mill', Powder Technology, vol. 137, no. 3, pp. 131-138.

Tavares, L.M. & King, R.P. 1998, 'Single- particle fracture under impact loading', International Journal of Mineral Processing, no.54, pp. 1-28.

Tsuji, Y., Kawaguchi, T. & Tanaka, T. 1993, 'Discrete particle simulation of two-dimensional fluidized bed', Powder Technology, 77, pp. 79-87.

Von Rittinger, P.R., Lynch, A.J., 1977, 'Mineral crushing and grinding circuits, their simulation, optimisation, design and control', Elsevier, Amsterdam, pp. 340

Walker, W. H., Lewis, W. K., McAdams, W. H. & Gilliland, E. R. 1937,'Principles of *Chemical Engineering',* McGraw-Hill New York, , p 255

WATES, J. A. (November/December 1983), 'The disposal of mine tailings: the real cost of excess water in residues'. The Journal of the South African Institute of Mining and Metallurgy.

Yagi, S. & Kunii, D. 1955, 'Studies on combustion of carbon particles in flames and fluidized beds', In: Fifth Symposium (International) on Combustion, Reinhold, New York, pp. 231–2

Yildirim, K., Cho, H., & Austin, L.G. 1999,'The modelling of dry grinding of quartz in tumbling media mills', Powder Technology, vol 105, no. 1-3, pp. 210-221.

Zhang, Y., Fang, Z. & Muhammed, M. 1997, 'On the solution chemistry of cyanidation of gold and silver bearing sulphide ores: A critical evaluation of thermodynamic calculations', Hydrometallurgy, vol. 46, no. 3, pp. 251-269.

PUBLICATIONS

- N. Hlabangana, G. Danha, D. Hildebrandt, D. Glasser, Use of the attainable region approach to determine major trends and optimize particle breakage in a laboratory mill, Powder Technology. Volume 291, (2016) 414–419
- G. Danha, N. Hlabangana, D. Legodi, D. Hildebrandt, D. Glasser, A fundamental investigation on the breakage of a bed of silica sand particles: An attainable region approach' Powder Technology. Volume 301, (2016) 1208–1212
- N. Hlabangana, G. Danha, D. Hildebrandt, D. Glasser, Application of the Attainable Region method to determine optimal conditions for milling and leaching, Powder Technology. (Accepted with minor corrections awaiting publication)
- N. Hlabangana, D. Hildebrandt, G. Danha, D. Glasser, Optimisation of the leaching parameters of a low grade Far West Rand gold ore in NaCN' International Journal of Minerals, Metallurgy and Materials (Under review)

APPENDIX A: LEACHING DATA UNDER DIFFERENT CONDITIONS

Table A. 1: Leaching data for cyanide concentration of 30ppm, particle size, -150 + 75µm; temperature, 25^{o}C.

Run No	Time (min)	Solution % Extraction	Film Xb	Reaction (1-(1-Xb)^(1/3)	Ash (1-3(1-Xb)^(2/3)+2(1-Xb))
0	0	0	0	0	0
1	60	0.096774	0.096774	0.033358151	0.003264123
2	120	0.152025	0.152025	0.053483975	0.008275779
3	180	0.193274	0.193274	0.069087156	0.013659852
4	360	0.262526	0.262526	0.096525159	0.026153128
5	1440	0.482361	0.482361	0.197071983	0.101206259

Table A. 2: Leaching data for cyanide concentration of 75ppm, particle size, -150 + 75µm; temperature, 25^{o}C.

Run No	Time (min)	Solution % Extraction	Film Xb	Reaction (1-(1-Xb)^(1/3)	Ash (1-3(1-Xb)^(2/3)+2(1-Xb))
	0	0	0	0	0
1	60	0.136226	0.136226	0.047642	0.006593
2	120	0.187648	0.187648	0.066928	0.012839
3	180	0.233806	0.233806	0.084946	0.020422
4	360	0.317263	0.317263	0.119455	0.0394
5	1440	0.574244	0.574244	0.247705	0.153679

Table A. 3: Leaching data for cyanide concentration of 210ppm, particle size, -150 + 75µm; temperature, 25^{o}C.

Run No	Time (min)	Solution % Extraction	Film Xb	Reaction (1-(1-Xb)^(1/3)	Ash (1-3(1-Xb)^(2/3)+2(1-Xb))
	0	0	0	0	0
1	60	0.138088	0.138088	0.048327	0.006781
2	120	0.221609	0.221609	0.080116	0.018228
3	360	0.363228	0.363228	0.139676	0.053079
4	1440	0.617834	0.617834	0.274308	0.184457

Table A. 4: Leaching data for cyanide concentration of 400ppm, particle size, -150 + 75µm; temperature, 25^{o}C.

Run No	Time (min)	Solution % Extraction	Film Xb	Reaction (1-(1-Xb)^(1/3)	Ash (1-3(1-Xb)^(2/3)+2(1-Xb))
	0	0	0	0	0
1	60	0.191974	0.191974	0.068587	0.013468
2	120	0.252875	0.252875	0.092601	0.024137
3	180	0.299297	0.299297	0.111798	0.034702
4	300	0.369715	0.369715	0.142607	0.055211
5	1440	0.657427	0.657427	0.300288	0.216366

Table A. 5: Leaching data for cyanide concentration of 500ppm, particle size, -150 + 75µm; temperature, 25^{o}C.

Run No	Time (min)	Solution % Extraction	Film Xb	Reaction (1-(1-Xb)^(1/3)	Ash (1-3(1-Xb)^(2/3)+2(1-Xb))
	0	0	0	0	0
1	60	0.191179	0.191179	0.068282	0.013351
2	120	0.26828	0.26828	0.098881	0.027399
3	180	0.29826	0.29826	0.11136	0.034442
4	360	0.394492	0.394492	0.153993	0.063839
5	1440	0.679078	0.679078	0.315351	0.235621

Table A. 6: Leaching data for stirring speed of 180rpm, cyanide concentration 500ppm, particle size, -150 + 75µm; temperature, 25^{o}C.

Run No	Time (min)	Solution % Extraction	Film Xb	Reaction (1-(1-Xb)^(1/3)	Ash (1-3(1-Xb)^(2/3)+2(1-Xb))
	0	0	0	0	0
1	60	0.138088	0.138088	0.048327	0.006781
2	120	0.221609	0.221609	0.080116	0.018228
3	360	0.363228	0.363228	0.139676	0.053079
4	1440	0.617834	0.617834	0.274308	0.184457

Table A. 7: Leaching data for stirring speed of 360rpm, cyanide concentration 500ppm, particle size, -150 + 75µm; temperature, 25^{o}C.

Run No	Time (min)	Solution % Extraction	Film Xb	Reaction (1-(1-Xb)^(1/3)	Ash (1-3(1-Xb)^(2/3)+2(1-Xb))
	0	0	0	0	0
1	60	0.157668357	0.157668	0.055588	0.008927
2	120	0.232586506	0.232587	0.084461	0.020196
3	180	0.256082686	0.256083	0.093902	0.024797
4	360	0.400205431	0.400205	0.156662	0.06594
5	1440	0.746934583	0.746935	0.367472	0.305868

Table A. 8: Leaching data for stirring speed of 720rpm, cyanide concentration 500ppm, particle size, -150 + 75µm; temperature, 25^{o}C.

Run No	Time (min)	Solution % Extraction	Film Xb	Reaction (1-(1-Xb)^(1/3)	Ash (1-3(1-Xb)^(2/3)+2(1-Xb))
	0	0	0	0	0
1	60	0.247416	0.247416	0.090397	0.023038
2	120	0.316813	0.316813	0.119261	0.039278
3	180	0.38422	0.38422	0.149236	0.060168
4	300	0.497785	0.497785	0.205127	0.108971
5	1440	0.833601	0.833601	0.44997	0.42521

Table A. 9: Leaching data for stirring speed of 900rpm, cyanide concentration 500ppm, particle size, -150 + 75µm; temperature, 25^{o}C.

Run No	Time (min)	Solution % Extraction	Film Xb	Reaction (1-(1-Xb)^(1/3)	Ash (1-3(1-Xb)^(2/3)+2(1-Xb))
	0	0	0	0	0
1	60	0.248828	0.248828	0.090966	0.023319
2	120	0.318675	0.318675	0.120062	0.039784
3	180	0.407396	0.407396	0.160046	0.068646
4	360	0.569365	0.569365	0.244842	0.15049
5	1440	0.884766	0.884766	0.513372	0.520059

Table A. 10: Leaching data for stirring speed of 990rpm, cyanide concentration 500ppm, particle size, -150 + 75µm; temperature, 25^{o}C.

Run No	Time (min)	Solution % Extraction	Film Xb	Reaction (1-(1-Xb)^(1/3)	Ash (1-3(1-Xb)^(2/3)+2(1-Xb))
	0	0	0	0	0
1	60	0.255248	0.255248	0.093563	0.024624
2	120	0.325737	0.325737	0.123113	0.041739
3	180	0.407396	0.407396	0.160046	0.068646
4	300	0.569558	0.569558	0.244955	0.150615
5	1440	0.872697	0.872697	0.496944	0.495422

Table A. 11: Leaching data for temperature 25^0 C, particle size -150 + 75µm; cyanide concentration 210ppm).

Run No	Time (min)	Solution % Extraction	Film Xb	Reaction (1-(1-Xb)^(1/3)	Ash (1-3(1-Xb)^(2/3)+2(1-Xb))
	0	0	0	0	0
1	60	0.138088207	0.138088	0.048327	0.006781
2	120	0.221608782	0.221609	0.080116	0.018228
3	360	0.363227836	0.363228	0.139676	0.053079
4	1440	0.617833986	0.617834	0.274308	0.184457

Table A. 12: Leaching data for temperature 40^0 C, particle size -150 + 75µm; cyanide concentration 210ppm).

Run No	Time (min)	Solution % Extraction	Film Xb	Reaction (1-(1-Xb)^(1/3)	Ash (1-3(1-Xb)^(2/3)+2(1-Xb))
	0	0	0	0	0
1	60	0.174102844	0.174103	0.061771	0.010976
2	120	0.28593439	0.285934	0.106187	0.031433
3	180	0.337420556	0.337421	0.128207	0.045097
4	300	0.418822623	0.418823	0.165479	0.073089
5	1440	0.720998909	0.720999	0.346563	0.277073

Table A. 13: Leaching data for temperature 80^0 C, particle size -150 + 75µm; cyanide concentration 210ppm).

Run No	Time (min)	Solution % Extraction	Film Xb	Reaction (1-(1-Xb)^(1/3)	Ash (1-3(1-Xb)^(2/3)+2(1-Xb))
	0	0	0	0	0
1	60	0.244270399	0.24427	0.089131	0.022417
2	120	0.318867561	0.318868	0.120145	0.039837
3	180	0.380432689	0.380433	0.147495	0.058848
4	360	0.474738396	0.474738	0.19315	0.097511
5	1440	0.797650382	0.79765	0.412912	0.370694

Table A. 14: Leaching data for temperature 100^0 C, particle size -150 + 75µm; cyanide concentration 210ppm).

Run No	Time (min)	Solution % Extraction	Film Xb	Reaction (1-(1-Xb)^(1/3)	Ash (1-3(1-Xb)^(2/3)+2(1-Xb))
	0	0	0	0	0
1	60	0.1728189	0.172819	0.061285	0.010807
2	120	0.272709764	0.27271	0.100703	0.028381
3	180	0.329460101	0.32946	0.12473	0.042792
4	300	0.440649676	0.44065	0.17606	0.082078
5	1440	0.761635745	0.761636	0.379966	0.323412

Table A. 15: Leaching data for temperature 120^0 C, particle size -150 + 75µm; cyanide concentration 210ppm).

Run No	Time (min)	Solution % Extraction	Reaction Xb	Reaction (1-(1-Xb)^(1/3)	Ash (1-3(1-Xb)^(2/3)+2(1-Xb))
	0	0	0	0	0
1	60	0.163253515	0.163254	0.05768	0.009597
2	120	0.264877704	0.264878	0.097487	0.026658
3	180	0.321114464	0.321114	0.121114	0.040453
4	300	0.425755922	0.425756	0.168811	0.075872
5	1440	0.726905052	0.726905	0.351207	0.283402

Table A. 16: Leaching data for particle size -1700+850µm, temperature 25^0 C, cyanide concentration 210ppm).

Run No	Time (min)	Solution % Extraction	Film Xb	Reaction (1-(1-Xb)^(1/3)	Ash (1-3(1-Xb)^(2/3)+2(1-Xb))
	0	0	0	0	0
1	60	0.060423	0.060423	0.020561	0.001251
2	120	0.09024	0.09024	0.031033	0.002829
3	180	0.109681	0.109681	0.037984	0.004219
4	300	0.157362	0.157362	0.055474	0.008891
5	1440	0.289636	0.289636	0.107734	0.03232

Table A. 17: Leaching data for -850+300µm particle size, temperature 25^0 C, cyanide concentration 210ppm).

Run No	Time (min)	Solution % Extraction	Film Xb	Reaction (1-(1-Xb)^(1/3)	Ash (1-3(1-Xb)^(2/3)+2(1-Xb))
	0	0	0	0	0
1	60	0.050740242	0.05074	0.017208	0.000878
2	120	0.065006729	0.065007	0.022156	0.001451
3	180	0.088021534	0.088022	0.030246	0.002689
4	300	0.114939435	0.114939	0.039882	0.004645
5	1440	0.220592194	0.220592	0.079716	0.018051

Table A. 18: Leaching data for -300+150µm particle size, temperature 25^0 C, cyanide concentration 210ppm).

Run No	Time (min)	Solution % Extraction	Film Xb	Reaction (1-(1-Xb)^(1/3)	Ash (1-3(1-Xb)^(2/3)+2(1-Xb))
	0	0	0	0	0
1	60	0.186691775	0.186692	0.066562	0.012702
2	120	0.294201108	0.294201	0.10965	0.033433
3	180	0.380043774	0.380044	0.147317	0.058714
4	300	0.471162598	0.471163	0.191323	0.095809
5	1440	0.771221758	0.771222	0.388391	0.335372

Table A. 19: Leaching data for -150+75µm particle size, temperature 25^0 C, cyanide concentration 210ppm).

Run No	Time (min)	Solution % Extraction	Film Xb	Reaction (1-(1-Xb)^(1/3)	Ash (1-3(1-Xb)^(2/3)+2(1-Xb))
	0	0	0	0	0
1	60	0.26751389	0.267514	0.098567	0.027231
2	120	0.362666837	0.362667	0.139423	0.052897
3	360	0.572067182	0.572067	0.246425	0.15225
4	1440	0.870936841	0.870937	0.494637	0.49196

Table A. 20: Leaching data for -75+25µm particle size, temperature 25^0 C, cyanide concentration 210ppm).

Run No	Time (min)	Solution % Extraction	Film Xb	Reaction (1-(1-Xb)^(1/3)	Ash (1-3(1-Xb)^(2/3)+2(1-Xb))
	0	0	0	0	0
1	60	0.313089812	0.31309	0.117664	0.038277
2	120	0.419785581	0.419786	0.165941	0.073471
3	360	0.483276626	0.483277	0.197546	0.101656
4	1440	0.615458689	0.615459	0.272808	0.182668

Table A 21: Combined leaching, milling and recovery data for Far west Witwatersrand gold ore

Recovery (%) ↘	Milling time (mins) →								
Leaching time (mins)		0	3	5	15	30	60	80	100
↓	0	0	0	0	0	0	0	0	0
	12.5	2	2.936782	3.837209	5.706667	6.4	6.810127	6.956522	7
	50	5	9.477011	13.56977	21.92	24.72857	26.26582	26.82609	27
	100	8	14.75862	20.68605	32.58667	36.25714	38.10127	38.78261	39
	250	13	23.05747	31.45349	48.16667	52.53571	54.22785	54.82609	55
	300	15	25.37356	33.97674	51	55.47143	57.21519	57.82609	58
	400	17	27.06897	35.85465	53.68	59.02857	61.49367	62.30435	62.5
	500	18	29.93103	39.73256	58.90667	64	66.05063	66.78261	67
	600	20.5	32.68391	42.61047	61.89333	67	69.05063	69.78261	70
	800	23	36.87356	47.82558	68.55333	73.93571	76.03797	76.78261	77
	1000	26.5	40.95977	52.33721	73.8	79.32857	81.48101	82.26087	82.5
	1200	28.5	43.98276	56.09884	78.84	84.65714	86.91139	87.73913	88
	1400	29	45.66092	58.68605	83.06667	89.31429	91.77215	92.69565	93
	1500	29	46.2069	59.54651	84.48	90.65714	92.91139	93.73913	94
	1600	29	46.68966	60.45349	86.32	92.65714	94.91139	95.73913	96
	1800	29	47.52299	61.7907	88.44667	94.82857	96.98101	97.76087	98
	2000	29	48.27586	62.80233	89.65333	95.6	97.24051	97.82609	98
	2200	29	48.98276	63.86047	91.21333	97.05	98.43671	98.8913	99
	2400	29	49.5	64.67442	92.50667	98.28571	99.51899	99.91304	100
	2500	29	50.4137	65.4883	93.2533	98.7571	99.6835	99.9565	100

			9	7	3	4	4	2	
	2600	29	50.03448	65.4186	93.58	99.03571	99.81013	100	100
	2800	29.5	50.58621	65.93605	93.96	99.22857	99.8481	100	100
	3000	29.5	51.06322	66.57558	94.66667	99.61429	99.92405	100	100
	3200	29.5	51.55747	67.20349	95.17333	99.87143	99.97468	100	100
	3400	29.5	51.93678	67.6686	95.45333	100	100	100	100
	3600	30	52.58046	68.24419	95.54667	100	100	100	100
	3800	30	52.71264	68.39535	95.57333	100	100	100	100
	4000	30	52.84483	68.54651	95.6	100	100	100	100
	4200	30	52.97701	68.69767	95.62667	100	100	100	100

APPENDIX B: BATCH GRINGING DATA

Table B.1: Measured particle size distribution for ball size 10 mm, feed size (-1700 +850 μm), U = 0.75, J = 5 %, ϕc = 75 of critical

Size x_i (mm)	Fraction Passing per Grinding time in %				
	3	5	15	30	60
1700	100	100	100	100	100
850	41.66667	53.94737	82.55034	88.07947	92.46575
300	16.66667	24.34211	58.38926	78.80795	89.0411
150	11.11111	15.78947	39.59732	65.56291	84.93151
75	7.638889	11.18421	25.50336	49.66887	74.65753
25	4.861111	7.236842	12.08054	31.12583	44.52055

Table B.2: Measured particle size distribution for ball size 20 mm, feed size (-1700 +850 µm), U = 0.75, J = 5 %, ϕc = 75 of critical

Size x_i (mm)	Fraction Passing per Grinding time in %				
	3	5	15	30	60
1700	100	100	100	100	100
850	42	67.76316	92	98.01325	100
300	20	36.84211	77.33333	93.37748	99.28058
150	11.33333	22.36842	56.66667	82.78146	96.40288
75	6.666667	14.47368	38	60.92715	78.41727
25	3.333333	8.552632	23.33333	37.74834	53.33333

Table B.3: Measured particle size distribution for ball size 10 mm, feed size (-1700 +850 µm), U = 0.75, J = 15 %, ϕc = 75 of critical

Size x_i (mm)	Fraction Passing per Grinding time in %				
	3	5	15	30	60
1700	100	100	100	100	100
850	34.52381	50	74.57627	80	92.30769
300	13.69048	21.875	47.45763	62	83.43195
150	7.738095	12.5	36.15819	54.5	78.10651
75	5.952381	8.125	27.68362	46	67.45562
25	3.571429	5.625	19.20904	31	43.19527

Table B.4: Measured particle size distribution for ball size 20 mm, feed size (-1700 +850 μm), U = 0.75, J = 15 %, ϕc = 75 of critical

Size x_i (mm)	Fraction Passing per Grinding time in %				
	3	5	15	30	60
1700	100	100	100	100	100
850	63.1016	81.02564	98.9011	99.47644	100
300	27.27273	43.58974	81.31868	98.42932	99.48718
150	18.71658	30.76923	64.83516	85.34031	97.4359
75	13.36898	21.02564	43.95604	61.7801	80
25	9.625668	15.38462	31.86813	41.88482	56.92308

Table B.5: Measured particle size distribution for ball size 30 mm, feed size (-1700 +850 μm), U = 0.75, J = 30 %, ϕc = 75 of critical

Size x_i (mm)	Fraction Passing per Grinding time in %				
	3	5	15	30	60
1700	100	100	100	100	100
850	63.1016	81.02564	98.9011	99.47644	100
300	27.27273	43.58974	81.31868	98.42932	99.48718
150	18.71658	30.76923	64.83516	85.34031	97.4359
75	13.36898	21.02564	43.95604	61.7801	80
25	9.625668	15.38462	31.86813	41.88482	56.92308

Table B.6 Measured particle size distribution for feed size -425+300 µm, ball size 20 mm, U = 0.75, J = 5 %, ϕc = 75 of critical.

Size x_i (mm)	Fraction Passing per Grinding time in %				
	0.5	1	3	5	9
425	84.29319	72.72727	47.56098	31.03448	11.41304
300	10.99476	15.15152	18.90244	22.41379	24.45652
212	2.617801	6.060606	18.29268	18.96552	23.36957
150	1.570681	3.636364	6.097561	14.36782	16.84783
106	0.52356	1.818182	6.707317	8.045977	11.41304
75	0	0.606061	1.829268	3.448276	5.978261
53	0	0	0.609756	1.724138	4.347826
45	0	0	0	0	1.630435
25	0	0	0	0	0.543478

Table B.7: Measured particle size distribution for feed size -600+425 µm, ball size 20 mm, U = 0.75, J = 5 %, ϕc = 75 of critical.

Size x_i (mm)	Fraction Passing per Grinding time in %				
	0.5	1	3	5	9
600	76.37131	67.66917	41.29353	23.88889	7.185629
425	14.76793	16.91729	24.87562	22.22222	25.7485
300	5.485232	8.270677	14.92537	19.44444	30.53892

212	2.109705	3.383459	9.950249	17.22222	12.57485
150	0.843882	2.255639	4.975124	9.444444	6.586826
106	0.421941	1.12782	2.487562	3.888889	8.982036
75	0	0.37594	0.995025	2.222222	4.191617
53	0	0	0.497512	1.111111	2.994012
45	0	0	0	0.555556	0.598802
25	0	0	0	0	0.598802

Table B.8: Measured particle size distribution for feed size -850+600 µm, ball size 20 mm, U = 0.75, J = 5 %, ϕc = 75 of critical.

Size x_i (mm)	Fraction Passing per Grinding time in %				
	0.5	1	3	5	9
850	75.75758	64.01869	34.30233	18.71658	4.790419
600	14.71861	20.56075	31.39535	34.2246	24.5509
425	4.761905	7.009346	15.69767	20.85561	22.75449
300	3.030303	4.672897	8.72093	11.22995	20.35928
212	1.298701	2.336449	5.813953	7.486631	15.56886
150	0.4329	0.934579	2.325581	5.347594	8.982036
106	0	0.46729	1.162791	1.604278	1.796407
75	0	0	0.581395	0.534759	1.197605
53	0	0	0	0	0

Table B.8: Measured particle size distribution for feed size -1180+850 μm, ball size 20 mm, U = 0.75, J = 5 %, ϕc = 75 of critical.

Size x_i (mm)	Fraction Passing per Grinding time in %				
	0.5	1	3	5	9
1180	74.66667	57.66423	25	12.92517	5.434783
850	17.33333	26.27737	42.30769	34.69388	23.36957
600	5.333333	8.759124	16.34615	22.44898	33.15217
425	2	5.109489	8.653846	18.36735	19.02174
300	0.666667	1.459854	3.846154	6.122449	11.41304
212	0	0.729927	2.884615	4.081633	4.347826
150	0	0	0.961538	1.360544	2.173913
106	0	0	0	0	0.543478
75	0	0	0	0	0.543478
53	0	0	0	0	0

APPENDIX C: AMOUNT OF GOLD ATTAINED DURING THE LEACH DURATION

Table C 1: Total amount of gold attained for ball size 10 mm, feed size (-1700+850µm), U = 0.75, J = 5 %, ϕc = 75 of critical

Time	M1	M2	M3	M4	M5	M6	Total amount of gold
0	0	0	0	0	0	0	0
3	1.742416	0.862625	0.441187	0.32831	0.264655	0.479664	4.118857
5	1.375591	1.021531	0.679188	0.43545	0.376089	0.714084	4.601932
15	0.521223	0.833679	1.492321	1.332644	1.278857	1.192031	6.650755
30	0.356065	0.319913	1.051825	1.502841	1.766684	3.071307	8.068636
60	0.225047	0.118169	0.326356	0.971448	2.871303	4.393016	8.905338

Table C 2: Total amount of gold attained for ball size 20 mm, feed size (-1700+850µm), U = 0.75, J = 5 %, ϕc = 75 of critical

Time	M1	M2	M3	M4	M5	M6	Total amount of gold
0	0	0	0	0	0	0	0
3	1.73246	0.75911	0.688249	0.441255	0.31758	0.32891	4.267564
5	0.962913	1.066933	1.1494	0.746475	0.564133	0.843919	5.333773
15	0.23896	0.506074	1.641205	1.765011	1.39737	2.30239	7.85101
30	0.059346	0.159958	0.84146	2.066411	2.20836	3.724776	9.060312
60	0	0.024823	0.228527	1.70061	1.987751	5.679083	9.620794

Table C 3: Total amount of gold attained for ball size 10 mm, feed size (-1700+850µm), U = 0.75, J = 15 %, ϕc = 75 of critical

Time	M1	M2	M3	M4	M5	M6	Total amount of gold
0	0	0	0	0	0	0	0
3	1.955774	0.718853	0.472698	0.168845	0.22685	0.352404	3.895424
5	1.4935	0.970453	0.744497	0.413674	0.238188	0.555041	4.415353
15	0.759406	0.935727	0.897319	0.801307	0.807418	1.895429	6.096606
30	0.5974	0.62109	0.595598	0.803709	1.429125	3.058894	7.105816
60	0.229769	0.306256	0.422906	1.007085	2.31141	4.262253	8.539679

Table C 4: Total amount of gold attained for ball size 20 mm, feed size (-1700+850µm), U = 0.75, J = 15 %, ϕc = 75 of critical

Time	M1	M2	M3	M4	M5	M6	Total amount of gold
0	0	0	0	0	0	0	0
3	1.102155	1.236276	0.679466	0.505637	0.356643	0.949806	4.829983
5	0.566765	1.291726	1.018114	0.921296	0.537446	1.51806	5.853408
15	0.032824	0.606681	1.309004	1.974202	1.151675	3.144553	8.218939
30	0.01564	0.03613	1.039437	2.227711	1.895525	4.132941	9.347383
60	0	0.017694	0.1629	1.648634	2.198652	5.61683	9.64471

APPENDIX D: MILL ENERGY CONSUMPTION DURING MILLING

Table D 1: Energy used for grinding with 10mm media (J=5%)

Grinding Times (mins)	0	3	5	15	30	60
Set	0	60	60	60	60	60
Actual Speed (RPM)	0	68.28553	68.28553	68.28553	68.28553	68.28553
Voltage	0	0.15206	0.15206	0.15206	0.15206	0.15206
Torque	0	-1.36958	-1.36958	-1.36958	-1.36958	-1.36958
Gross power	0	-9.79395	-9.79395	-9.79395	-9.79395	-9.79395
No load power	0	-0.2565	-0.2565	-0.2565	-0.2565	-0.2565
Net Power	0	9.537449	9.537449	9.537449	9.537449	9.537449
Energy used (kJ)	0	1.716741	2.861235	8.583704	17.16741	34.33482

Table D 2: Energy used for grinding with 20mm media (J=5%)

Grinding Times (mins)	0	3	5	15	30	60
Set	0	60	60	60	60	60
Actual Speed (RPM)	0	68.28553	68.28553	68.28553	68.28553	68.28553
Voltage	0	0.172555	0.172555	0.172555	0.172555	0.172555
Torque	0	-1.50646	-1.50646	-1.50646	-1.50646	-1.50646
Gross power	0	-10.7728	-10.7728	-10.7728	-10.7728	-10.7728
No load power	0	-0.2565	-0.2565	-0.2565	-0.2565	-0.2565

Net Power	0	10.51629	10.51629	10.51629	10.51629	10.51629
Energy used (kJ)	0	1.892933	3.154888	9.464664	18.92933	37.85866

Table D 3: Energy used for grinding with 10mm media (J=15%)

Grinding Times (mins)	0	3	5	15	30	60
Set	60	60	60	60	60	60
Actual Speed (RPM)	68.28553	68.28553	68.28553	68.28553	68.28553	68.28553
Voltage	0.315673	0.315673	0.315673	0.315673	0.315673	0.315673
Torque	-2.46231	-2.46231	-2.46231	-2.46231	-2.46231	-2.46231
Gross power	-17.6082	-17.6082	-17.6082	-17.6082	-17.6082	-17.6082
No load power	-0.2565	-0.2565	-0.2565	-0.2565	-0.2565	-0.2565
Net Power	17.35167	17.35167	17.35167	17.35167	17.35167	17.35167
Energy used (kJ)	3.1233	5.2055	15.6165	31.233	62.466	3.1233

Table D 4: Energy used for grinding with 20mm media (J=15%)

Grinding Times (mins)	0	3	5	15	30	60
Set	0	60	60	60	60	60
Actual Speed (RPM)	0	68.28553	68.28553	68.28553	68.28553	68.28553
Voltage	0	0.347618	0.347618	0.347618	0.347618	0.347618
Torque	0	-2.67567	-2.67567	-2.67567	-2.67567	-2.67567
Gross power	0	-19.1339	-19.1339	-19.1339	-19.1339	-19.1339
No load power	0	-0.2565	-0.2565	-0.2565	-0.2565	-0.2565
Net Power	0	18.87739	18.87739	18.87739	18.87739	18.87739
Energy used (kJ)	0	3.39793	5.663216	16.98965	33.9793	67.95859